Durham E-Theses

Chemistry of single-wall Carbon Nanotubes: Studies in purification, non-covalent modification by tertiary phosphines and covalent functionalisation via Nucleophilic reduction

Sun, Anil

Chemistry of Single-Wall Carbon Nanotubes:

Studies in Purification, Non-Covalent Modification by Tertiary Phosphines and Covalent Functionalisation via Nucleophilic Reduction

A thesis submitted for the partial fulfillment of the requirements for the degree of

Doctor of Philosophy

In the Faculty of Science,

Durham University

by

Anil Suri

1 3 NOV 2008

**Department of Chemistry
Durham University
University Science Laboratories
South Road
Durham**

2007

ABSTRACT

Carbon nanotubes (CNTs) have attracted considerable research interest owing to their exciting properties and potential for a wide range of applications. However, major challenges must be overcome before these applications can be realised. As-prepared CNT material contains a significant proportion of impurities, such as amorphous carbon, fullerenes and metal catalyst particles. The raw CNT material must be purified before the CNTs can be studied and utilised. Also, CNTs tend to aggregate into bundles or "ropes", and have poor solubility in common solvents, making their handling and processing extremely difficult. Also, many applications require individually separated CNTs. To improve the solubility of CNTs, and amenability to processing on a large scale, chemical modification of CNT surfaces is necessary. To this end, non-covalent as well as covalent strategies have been developed. However, chemical modification may perturb the electronic structure of CNTs, thereby compromising their interesting properties. The challenge, therefore, is to develop chemical modification routes that improve CNT solubility while not seriously affecting their properties.

In this work, we firstly study the problem of purification of as-produced CNT material. We have resolved a major controversy concerning the use of oxidising acids for purifying CNTs, which has profound implications for the spectroscopy and subsequent chemical modification of the CNTs. Secondly, we have developed a route for the non-covalent modification of CNTs by tertiary phosphines. This method has the advantages of significantly improving the solubility of CNTs in organic solvents while being extremely simple, not seriously perturbing the CNT electronic structure, as well as not rendering large areas of the CNT inaccessible. Thirdly, we describe a method for the covalent derivatisation of CNTs based on reduction, followed by electrophilic substitution. This route is considerably more facile and versatile than other covalent functionalisation methods reported to date, and does not cause significant disruption of the CNT electronic structure. Finally, we demonstrate the covalent attachment of formyl (–CHO) groups to CNT walls, which could potentially open the gateway for a plethora of of coupling and modification reactions.

ACKNOWLEDGEMENTS

CONTENTS

1. INTRODUCTION

1.1 Overview

Carbon nanotubes (CNTs) are materials related to both graphite and fullerenes. They have attracted considerable research interest across a range of disciplines, from physics and chemistry through materials science and medicine to engineering, owing to their extremely interesting properties and potential for a range of applications.

The discovery of CNTs is overwhelmingly attributed to Iijima (1991) [1]. However, these nanostructures may have been synthesised and observed on several earlier occasions [2-4]. But it was Iijima's report [1] which triggered the explosion of research on CNTs, thanks to the discovery of fullerenes in 1985 [5], and the burgeoning interest in nanoscience and nanotechnology in the early 1990s.

1.2 Structure of carbon nanotubes

Ideal CNTs, also called "buckytubes", can be thought of simply as sheets of graphite rolled into seamless cylinders, the ends of which are capped by fullerene hemispheres (Figure 1-1). It follows that the carbon atoms comprising CNTs are sp^2-hybridised. CNTs may consist of a single cylindrical shell or several coaxial cylindrical shells of increasing diameters, known as single-wall (SWNTs) or multi-wall carbon nanotubes (MWNTs) respectively (Figure 1-2). The spacing between the walls in MWNTs is approximately the same as that between the layers of graphite i.e., 3.4 Å. SWNTs [6,7] were discovered shortly after MWNTs.
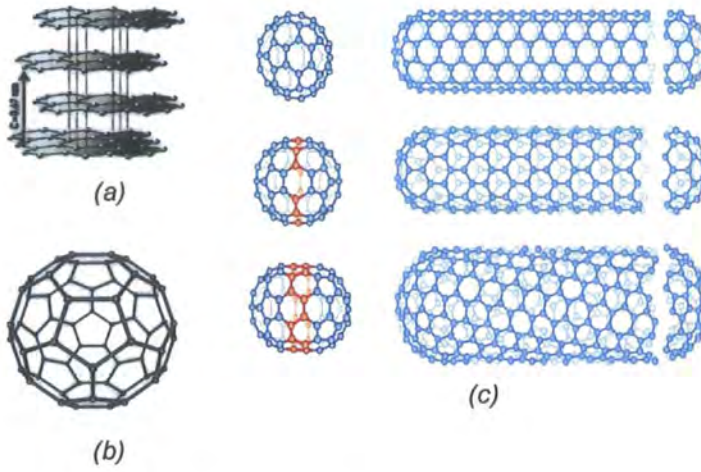
Figure 1-1

Equilibrium structure of (a) graphite, (b) fullerene and (c) carbon nanotubes.

CNTs are high aspect ratio materials with diameters of the order of nanometres, while their lengths could be of the order of microns. The smallest diameter for a CNT has been found to be 0.4 nm, for the innermost shell in an MWNT [8], while the smallest diameter for a single-wall carbon nanotube has been reported to be 0.43 nm [9].
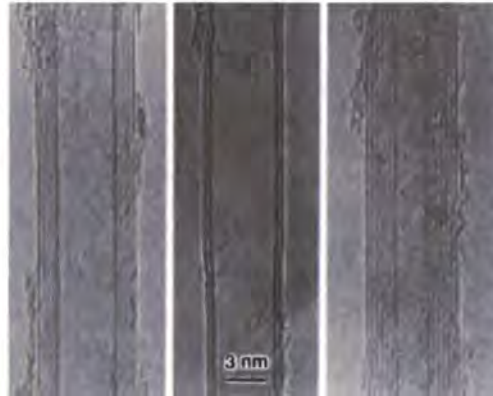
Figure 1-2

Transmission electron micrographs showing multi-wall carbon nanotubes (Ref. 1).

Depending on the "direction of rolling" of graphene into seamless cylinders, it is possible to obtain nanotubes of different "helicities" or "chiralities" (Figure 1-3).
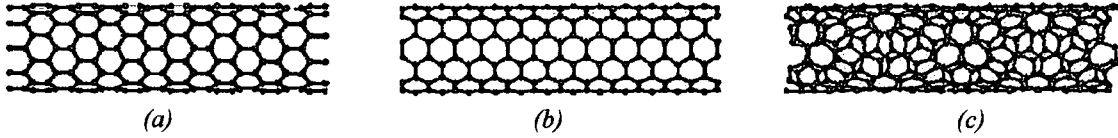
Figure 1-3

CNTs of different helicities: (a) zigzag, (b) armchair and (c) chiral.

The circumferential periodicity of a nanotube can be described by a chiral vector, C_h, which connects two crystallographically equivalent points on the graphene lattice, as shown in Figure 1-4. The chiral vector is determined in terms of the graphene lattice vectors, a_1 and a_2, as

$$C_h = na_1 + ma_2$$ Equation 1-1

where n and m are integers. The diameter, d, of the nanotube can be determined from the equation

$$d \, (/\text{nm}) = 0.0783 \times \sqrt{(n^2 + m^2 + nm)}$$ Equation 1-2

In other words, the structure of a CNT can be completely described by the indices (n, m). For example, Figure 1-4 illustrates the case of a (5, 2) nanotube. A zigzag nanotube will have the indices $(n, 0)$, and an armchair nanotube (n, n). Alternatively, the wrapping angle (also called chiral angle), θ, is a useful measure of the helicity of the nanotube. It is the angle between the zigzag direction of graphene and the chiral vector of the nanotube. The value of θ is 0° for a zigzag nanotube, 30° for an armchair CNT, and anything between 0 and 30° for a chiral nanotube.

tube axis

zigzag
(n, 0)

θ

C_h

C_h=5a_1+2a_2=(5, 2)

armchair
(n, n)
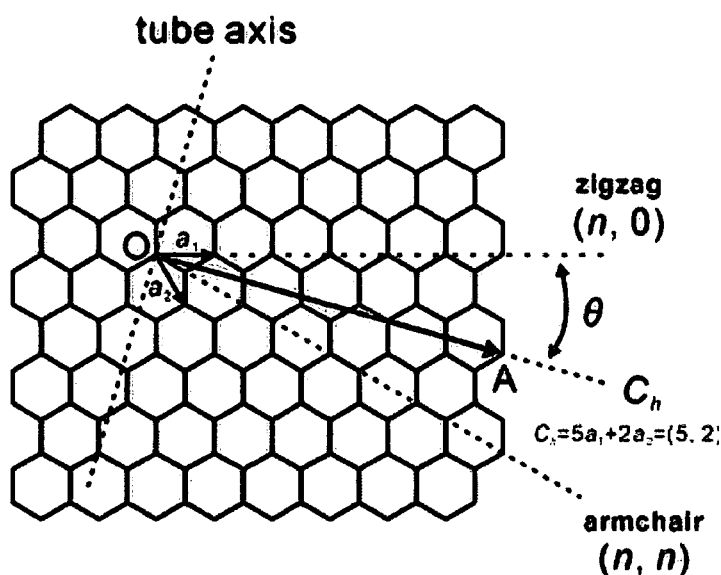
Figure 1-4

Schematic illustration of the roll-up of a graphene sheet to form a carbon nanotube, showing the graphene lattice vectors a_1 and a_2, chiral vector C_h, and nanotube indices *(n, m)*.

1.3 Synthesis

1.3.1 Arc-discharge

Iijima had observed CNTs in the soot discharged by arc evaporation [1], a process quite similar to that used for the large-scale synthesis of fullerenes [10]. Other methods have since been developed for the synthesis of CNTs, and are described in detail below.

In this method, an electric arc is struck between two pure graphite electrodes in an inert atmosphere, such as of helium or argon. The arc produces temperatures of around 3000°C, causing the graphite to evaporate. CNTs are one of the products in the soot collected at the cathode, along with other graphitic nanostructures such as fullerenes and multi-shell spherical polyhedra ("buckyonions"), and amorphous carbon. The optimisation of this process to maximise the yield of CNTs to gram scales was soon demonstrated [11]. The purification of this soot to obtain CNTs is dealt with in Chapter 2.

When the graphite anode is doped with metals such as cobalt, nickel or iron, the selective formation of single-wall CNTs is observed [6, 7].

1.3.2 Laser ablation

Large quantities of high-purity bundles or "ropes" of SWNTs can be synthesised by the laser ablation method [12, 13]. This process involves the evaporation of a graphite target impregnated with a suitable catalyst (iron, cobalt or nickel) by an intense laser beam at a temperature of around 1200°C in an inert atmosphere. The evaporated carbon nucleates and forms CNTs, which are deposited as a "felt" on a collector. By this method, high-purity bundles or "ropes" of single-wall carbon nanotubes are obtained. These ropes are of the order of 100 μm long, and consist of hundreds of tubes of a very narrow diameter distribution, arranged in a regular triangular lattice.

1.3.3 Chemical vapour deposition

The use of chemical vapour deposition (CVD) for growing carbon filaments has a history that extends for more than a century [3]. CNTs have been extensively synthesised by the thermal disproportionation of a gas / vapour carbonaceous precursor and growth over nanoparticles of transition metals, supported over a suitable support such as alumina, silica or magnesium oxide.

A variety of carbon-containing feedstocks have been employed, such as 2-methyl-1,2'-naphthyl ketone [14], methane [15, 16], carbon monoxide [17, 18, 19], ethylene [18], acetylene [20] and ethanol [21]. In a slight variation, the catalyst too may be introduced in the form of a gaseous precursor, such as iron pentacarbonyl, $Fe(CO)_5$ [19], or ferrocene [22] for iron catalyst. This has been used to advantage in developing a fully continuous process for spinning fibres of several metres length from CNTs, which has tremendous potential for industrial application [23].

The temperature, pressure in the chamber, flowrate of the feedstock, nature and size of the catalyst particles are all variables governing the quality and nature (i.e., whether single-wall, multi-wall or a mixture of both types) of the CNTs obtained. The range of temperatures employed by various groups is as wide as 600°C–1200°C. Also, if the catalyst particles are of a size less than around 5 nm, SWNTs can be selectively grown.

1.3.4 Comparison of the various methods of synthesis

Owing to the high temperature involved (~ 3000°C), the arc discharge method yields CNTs of the best level of crystallinity and structural perfection, followed by the laser ablation method (~ 1200°C). However, the high operating temperature also means a higher cost of production. While the low temperatures involved in CVD synthesis (600-1200°C) lead to CNTs with relatively higher levels of defects and by-production of greater amounts of amorphous carbon, they are also conducive for industrial scale-up.

CNTs can be grown by CVD in the form of high quality films with a high degree of alignment at desired locations on pre-patterned substrates. This has been exploited to grow individual CNTs in such a way as to directly yield device structures [24], or for growing CNTs that can be used as high-resolution atomic force microscopy (AFM) tips [25]. The obvious disadvantage of arc discharge or laser ablation methods for such applications would be that the CNTs would have to be first separated and then individually manipulated into position by procedures such as AFM, which would be prohibitively tedious.

Arc discharge synthesis of CNTs also leads to the formation of considerable amounts of by-products including fullerenes, buckyonions and metal nanoparticles enclosed in graphitic carbon polyhedra. Laser ablation CNTs also contain fullerenes, albeit to a much lesser extent. The presence of these by-products greatly complicates the purification of the as-produced raw material to yield a starting material enriched in CNTs, as shall be described in Chapter 2.

1.3.5 Growth mechanisms

All synthesis methods usually yield a mixture of CNTs of varying helicities. Identifying and understanding the mechanism by which CNTs grow may be the first step towards achieving rational synthesis of CNTs of a particular helicity (which ultimately corresponds to the electronic nature of the CNTs, as described in Section 1.4.1.1), which could be very important for many technological applications of CNTs.

It was recognised early on that the growth mechanism in the case of CVD may be different from that in the case of arc discharge or laser ablation [17]. For CVD synthesis, the mechanism that has come to be increasingly accepted as the most likely is the "yarmulke" (Yiddish for "skullcap") mechanism [17]. In CVD synthesis, a clear correspondence is observed between the diameters of carbon nanotubes and the size of the catalyst particle they have grown from and which can often be seen enclosed at the lower end of the nanotubes. The yarmulke mechanism explains this by postulating that the catalyst causes disproportionation of the precursor, leading to formation of carbon atoms. These carbon atoms first form a hemispherical cap on the catalyst particle. Thereafter, the tube grows by cap lift-off as the carbon atoms diffuse either over the surface of the catalyst particle, or dissolve in it and are precipitated out, thereby continuing to add to the end. Both root-growth (extrusion from catalyst particle) and tip-growth are possible, as shown in Figure 1-5. This mechanism appears to account for the fact that the metals that have been employed as catalysts for the growth of CNTs are those which are known to form stable interstitial carbides, which would be required for the carbon atoms to dissolve in the metal nanoparticle before crystallising as the CNT.
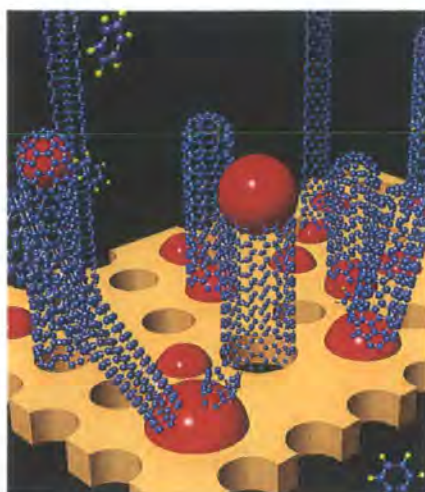
Figure 1-5

The *yarmulke* mechanism for the growth of SWNTs (Ref. 9). The red spheres denote the catalyst nanoparticles, and the beige base, the catalytic support. The SWNT appearing nearest in the picture is forming by root-growth (extrusion). The SWNT in the middle is being formed by tip-growth.

There is very little agreement on the growth mechanism of CNTs by the arc discharge and laser ablation methods. Among the models proposed include vapour phase growth [26], liquid phase growth [27], solid phase growth [28] and growth by crystallisation [29, 30]. These have been reviewed elsewhere [31]. None of these mechanisms appears to satisfactorily explain all aspects of CNT growth, and it is likely that the actual mechanism may be a combination of all of these.

It is interesting to note that fullerenes were believed to be occuring naturally in the universe from the condensation of carbon vapours [5, 32]. Fullerenes have been found to occur in geological samples on Earth, in contexts which seemed to suggest that they had been formed either as a result of lightning or by as yet unknown solid- or liquid-phase mechanisms quite different from the methods employed in their laboratory synthesis [33-35]. (There is also at least one report of fullerenes occurring in a structure resulting from the impact of a meteorite [36], but it is easy to rationalise their formation, as the temperature and pressure conditions during such an impact may have been extreme.) More recently, it was demonstrated that high-quality CNTs could be grown on minerals [37]. CNTs have also been grown by plasma-enhanced CVD at temperatures under 400°C [38]. In a

surprising development, it was also found that, by suitable activation, it may be possible to grow SWNTs on any metal [39]. Further, the synthesis of graphite structures including sheets and CNTs has been reported in the solution phase at temperatures as low as 110°C [40]. Thus, it may be reasonable to state that (a) CNTs, like fullerenes, may be expected to be naturally occurring in the geological environment, and that (b) it is entirely probable that they may be synthesised by new routes radically different and much gentler than those currently employed in laboratories.

To conclude this Section, it will suffice to say that a deeper understanding of the kinetics and thermodynamics of the fundamental processes involved in the nucleation and growth of CNTs is necessary before a complete picture of the growth mechanism can be constructed.

1.4 Properties

The exciting properties of CNTs have drawn the interest of theorists from very early on. In fact, attempts were being made to understand the electronic properties [41-43] of these as yet hypothetical materials from around the same time that these materials were being identified by Iijima [1]. CNTs are nanomaterials with extremely exciting electronic, and, consequently, thermal and mechanical, properties. They shall be briefly summarised in this section. The chemical nature of CNTs shall be described in detail in Section 1.7.

1.4.1 Electronic and electrical properties

1.4.1.1 Electronic structure

It was first theoretically predicted [41-43] and later experimentally confirmed by scanning tunnelling microscopy (STM) [44-46] that the electronic properties of SWNTs are sensitive functions of their diameters and helicities. Owing to curvature, quantum effects come into play as a result of the boundary conditions imposed by the confinement of the

electron wave to the circumference. Hence, the densities of state (DOS) in nanotubes are split into spikes or the so-called van Hove singularities, and are not continuous as is the case for graphene, or usually all bulk materials. Graphene has a zero band gap. However, owing to the splitting of the bands into spikes, SWNTs may be either metallic (i.e., zero band gap), semiconducting with a small band gap or semiconducting with a large band gap, depending on diameter and helicity. As a general rule, for a (n, m) SWNT, the nanotube is metallic if it is armchair i.e., (n, n), semiconducting with a small band gap if $n - m = 3j$ (j being a non-zero integer), and semiconducting with a large band gap for all other values of n and m. Further, the energy gap between the densities of state is inversely proportional to the diameter of the SWNT. It is worth mentioning that the band gap for $n - m = 3j$ is small enough for practically observed SWNTs that they can be regarded as metallic. Electronic transitions between the van Hove singularities have been observed in optical absorption spectroscopy in the visible and near-infrared region [47, 48]. The densities of state and the electronic transitions between them for the three different types of SWNTs are schematically illustrated in Figure 1-6.
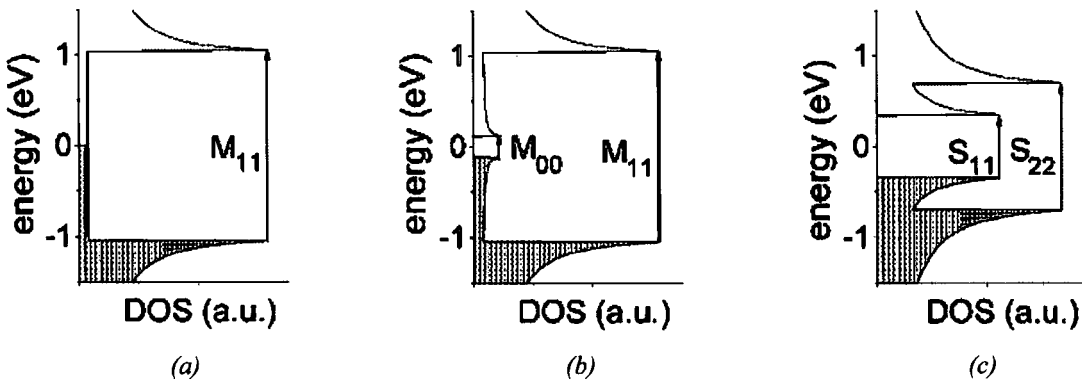
Figure 1-6

Schematic illustration of the densities of state (DOS) in (a) metallic, denoted by M, (b) semiconducting, denoted by S (with small bandgap) and (c) semiconducting (with large bandgap) SWNTs (Ref. 346). For preserving the wave vector, transitions can take place only between symmetrical singularities (for convenience, the Fermi level is taken as lying in the centre of the energy gap). Thus, we have the first and second metallic or semiconducting transitions, M_{11}, S_{11} and S_{22} respectively.

Thus, not only do the indices *(n, m)* completely specify the physical structure of a CNT, they also give its electronic structure. One-third of SWNTs will be metallic, whereas two-thirds will be semiconducting[43].

1.4.1.2 Electrical properties

Owing to their nanometre-scale diameters, extremely high aspect ratios and confinement of the electron wave to a single atom-thick circumferential layer, CNTs are one-dimensional (1-D) conductors. Also, the band gap in semiconducting nanotubes is of the order of 1 eV for a diameter of around 1 nm, implying that the 1-D nature is retained even at room temperature. In addition, CNTs also have high chemical and thermal stability.

CNTs show excellent field emission properties owing to their extreme aspect ratios and small tip diameters. CNTs have the advantage of a turn-on voltage as low as 1-2 V, and can operate stably at current densities as high as 10^9 A/m^2, at least an order of magnitude higher than the best field emitters currently available[49].

1.4.1.3 Electrical transport

Individual CNTs have been experimentally observed to behave like quantum conductors or, in other words, show ballistic conduction[50, 51], even at room temperature. This is remarkable as it implies that the nature of electrical transport may not be significantly perturbed by defects in the walls, which should always be expected to be present. An important consequence of ballistic conduction is that CNTs can be expected to carry extremely high currents without Joule heating which arises from scattering of electrons. Actual experimental observation shows that this is indeed the case. MWNTs have been observed to stably carry current densities as high as 10^{11} A/m^2 at room temperature without dissipation of heat[51]. The room temperature resistivity of ropes of SWNTs was measured by a four-point technique to be of the order of 10^{-4} Ω-cm[13].

1.4.2 Thermal properties

As in most other carbon materials, thermal conduction in CNTs is by phonons at all temperatures [52]. The thermal conductivity of bulk mats of SWNTs has been experimentally found to be as high as 200 W/mK at room temperature [53], but it has been theoretically predicted that the thermal conductivity of an individual ideal SWNT at room temperature could be as high as 6,600 W/mK [54], comparable with diamond and graphite, themselves among the best thermal conductors known. Practical values will be much lesser, owing to the presence of defects on the walls of nanotubes. Also, such unusually high values may be expected only in the tube axial direction; in the radial direction, it may only be a few hundredths of the axial value, identical with in-plane and out-of-plane graphite [55].

1.4.3 Physical and mechanical properties

Owing to their hollow tubular structure, CNTs can be expected to have very low densities. Recently, Lu and co-workers estimated the density of isolated as well as bundled CNTs to be in the region of 2 g/cm^3 from gradient sedimentation studies [56]. CNTs have outstanding mechanical properties, made further attractive by the fact that they would translate into superlative specific properties, given their low densities.

Treacy and co-workers attempted the estimation of the Young's modulus of arc discharge MWNTs by direct measurement of their intrinsic thermal vibrations in a transmission electron microscope, and arrived at values of the order of 1 TPa [57]. Similar results were obtained for SWNTs [58]. These values are comparable with the in-plane values for graphite and with that of diamond, and also broadly agree with theoretical estimates for CNTs [59, 60]. Direct measurements using an AFM set-up in a scanning electron microscope (SEM) also yielded similar values of Young's modulus, and tensile strengths of the order of 20 GPa [61, 62]. Similar values have been estimated for individual CNTs from direct measurements of the properties of ropes [63]. Typical values of the Young's modulus and tensile strength for steel are 200 GPa and 400 MPa respectively.

Clearly, therefore, CNTs are at least one order of magnitude stiffer and two orders of magnitude stronger than steel, but are less than one-third as heavy.

1.5 Applications

With such exciting properties, it is hardly surprising that a very wide range of applications has been envisaged for CNTs [64, 65]. While many applications are still at a very early stage of development, thanks to the enormous technological challenges involved in harnessing CNTs, some have already been realised. These are briefly described below, along with the technological challenges involved.

1.5.1 Nanoelectronics

Miniaturisation of microelectronic devices at the present rate cannot continue for more than a few years, as there shall be a dramatic change in the behaviour of traditional semiconductor materials (such as silicon), as quantum effects will come in to play. This has prompted the exploration of novel semiconductor nanowires, molecular wires etc. for future electronics applications. CNTs are excellent candidates for nanoscale electronics of the future owing to their nanoscale dimensions, quantum conducting behaviour, high current carrying capacity (for interconnects) and stability. Fig. 1-7 shows the schematic representation of an SWNT-based transistor device. CNT-based field effect transistor (FET) devices have been demonstrated and studied [66-69], and are ordinarily observed to behave as *p*- type semiconductors.
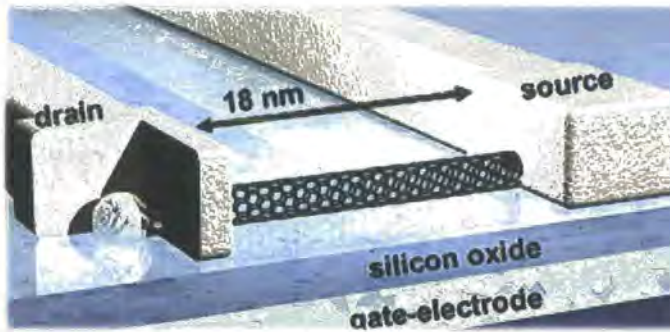
Figure 1-7

Schematic representation of a CNT-based field effect transistor.

However, the fabrication of CNT-based devices is as yet very tedious, and cannot be scaled up easily to match the throughput of silicon devices. Also, the current sizes of these devices are limited by available lithographic techniques, being no less than a few hundred nanometres. Most importantly, the success of these devices is a matter of chance, depending on whether the nanotube selected was semiconducting and not metallic. CNT electronics is unlikely to become a viable option before rational synthesis of tubes of a particular electronic type is achieved.

Samsung has demonstrated a CNT-based flat panel display [70], which exploits the favourable field emission properties of CNTs (see Section 1.4.1.2). Other applications based on field emission that are being explored include lamps [71] and X-ray generators [72].

1.5.2 Electrochemical devices

This category includes applications which exploit the exceptionally high specific surface of CNTs, such as lithium ion batteries [73], as catalytic support in enhanced-performance electrodes for fuel cells [74, 75], supercapacitors which have much higher energy storage abilities than batteries as well as much higher storage capacities and quicker discharge than ordinary capacitors [76, 77], and actuators in which stored charge is converted into mechanical energy for robotics and artificial muscles [78].

1.5.3 Sensors and detectors

CNTs have been observed to show large and rapid changes in electrical characteristics upon exposure to extremely small concentrations of gases such as ammonia and nitrogen dioxide [79-81], opening up the possibility that they may be used as chemical sensors and detectors. They have also been shown to be useful for detecting biomolecules [82, 83].

1.5.4 Polymer composites

CNTs combine superlative mechanical, thermal and electrical properties with low density, nanoscale diameter and extreme aspect ratios. Thus, they are ideal candidates for use as reinforcements in polymer composites with dramatically enhanced properties, which have become the goal of a considerable amount of research effort.

There are several reports of impressive enhancement of mechanical properties in polymer composites upon loading with extremely low loading of CNT fillers, indicating that the percolation thresholds are very low: upto 42% increase in elastic modulus, and 25% in break stress, were achieved in polystyrene composites upon 1 weight *per cent* loading with MWNTs [84]; the Young's modulus of poly(methyl methacrylate) almost doubled upon incorporation of 8 weight *per cent* of SWNTs [85]; 10 weight *per cent* of SWNTs in poly(*p*-phenylenebenzobisoxazole) (PBO) led to a 50% increase in tensile strength together with reduction in shrinkage and high-temperature creep [86]; addition of 0.1 weight *per cent* MWNTs increased the elastic modulus of epoxy by 20% [87].

CNTs have also been reported to enhance thermal transport properties in polymers. Epoxy loaded with 1 weight *per cent* SWNTs showed an enhancement in thermal conductivity of 125% at room temperature [88]. Choi and co-workers found a 300% enhancement in thermal conductivity of industrial epoxy with 3 weight *per cent* loading of SWNTs, which increased by a further 10% upon alignment of the tubes by a magnetic field [89].

Similar enhancement has been observed for electrical properties. Room temperature-resistivity of 3 weight *per cent* loaded epoxy showed six orders of magnitude reduction over pure epoxy [89].

However, such enhancement, while significant, is considerably short of what is predicted by theory [90]. In at least one case, very modest increase in moduli and strength, and a slight degradation in failure properties, was observed [91]. This has been attributed to nanotubes not having been dispersed individually in the matrix, being still in bundles in which there is a relative slipping of tubes, leading to ineffective load transfer from matrix to reinforcement and, thereby, premature failure [92]. Better separation of nanotubes in polymer matrices would also be helpful towards maximising thermal conductivity [88]. Suggestions to achieve individual nanotube dispersion in, and effective binding with, polymer matrices include ultrasonication [90] and chemical functionalisation [88, 92, 93]. Recent work suggests that functionalisation of CNTs might aid their better dispersion in, and improve their interaction with, polymers [93-96].

1.5.5 Hydrogen storage

It has been believed from very early on that CNTs would be very well suited for hydrogen storage on account of their high porosity. The United States Department of Energy has set a benchmark of 6.5 weight *per cent* capacity at room temperature for hydrogen storage materials. While there have been a few claims [97] of achieving more than 6.5 weight *per cent* hydrogen adsorption by CNTs, most reports in this area have not been as encouraging [98, 99]. At the present time, it will perhaps only be safe to say that the suitability of CNTs for hydrogen storage is not settled.

1.6 Chemistry of carbon nanotubes

1.6.1 Overview

One of the most significant hurdles in the way of widespread application of CNTs is their insolubility and the consequent difficulty in handling and processing them on large, industrial scales. CNTs aggregate into bundles or "ropes" owing to the van der Waals attraction between their smooth, highly polarisable graphitic walls [100]. It is extremely difficult to break these bundles to obtain individual CNTs, although single or singly dispersed nanotubes will be required for many applications such as nanoelectronics and polymer composites. Dispersion and solubilisation of CNTs will invariably require one or all of vigorous mechanical agitation (such as by ultrasonication) and chemical modification of the surfaces of CNTs (either by the use of surface active agents or long molecules, or outright chemical derivatisation of the tube walls).

Both mechanical and chemical treatments have their own advantages and disadvantages. Ultrasonication inflicts mechanical damage on the walls of nanotubes [101, 102]. Chemical modification may disrupt the intrinsic electronic structure of the pristine nanotubes [103], thereby compromising their exciting properties. For instance, it was found that ozonation of CNTs resulted in several orders of magnitude increase in their resistance [104]. Ultrasonication of itself cannot achieve the efficient and stable dispersion of individual nanotubes into solution without causing an unacceptable level of damage to the CNT walls. Chemical modification of CNT surfaces is inevitable for improving the solubility of CNTs in a variety of solvents and, consequently, enable inexpensive large-scale processing.

Fullerenes have a rich chemistry [105]. While the chemistry of CNTs may not be comparable with that of fullerenes, a large number of routes have been developed for the modification of CNTs by both covalent as well as non-covalent means. These are reviewed here. The purification of as-produced CNTs, which is the first step before any chemistry can be carried out on them, is dealt with separately in Chapter 2.

1.6.2 Reactivity

The reactivity of fullerenes can be thought of as arising from the strain induced by the curvature necessary to form a closed cage structure [106, 107]. The preferred geometry of the orbitals of sp^2-hybridised carbon atoms is planar, which is the case in graphene. However, in fullerenes, there is a deviation from planarity. Reaction at any of the carbon atoms, causing it to change to an sp^3-hybridised state (the preferred geometry of which is tetrahedral) reduces this strain. This also explains why fullerenes are particularly susceptible to addition reactions. A very good measure of the extent of curvature or deviation from planarity is the angle of pyramidalisation, θ_p, which is illustrated in Figure 1-8.

Pyramidalization Angle: $\theta_p = (\theta_{\sigma\pi} - 90)°$

TRIGONAL   TETRAHEDRAL

$\theta_{\sigma\pi} = 90°$ $\theta_{\sigma\pi} = 109.47°$

$\theta_p = 0°$ $\theta_p = 19.47°$
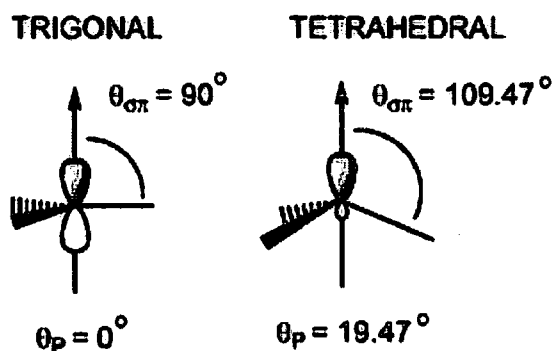
Figure 1-8

The angle of pyramidalisation, θ_p, which is a measure of deviation in fullerenes and CNTs, from the preferred trigonal planar geometry of sp^2-hybridised carbon atoms.

In addition to pyramidalisation, another effect that comes into play in the case of large, non-planar aromatic molecules is the misalignment of the π-orbitals causing torsional strain [107], Φ, which is shown in Figure 1-9. Such misalignment is either negligible or altogether absent in fullerenes, but is very pronounced in CNTs. Thus, the chemistry of CNTs can be expected to be slightly different from that of fullerenes. At the same time, it must be remembered that while the curvature of CNTs is only in two

dimensions, that of fullerenes is in three. Thus, the extent of pyramidalisation (and, consequently, the susceptibility for reaction) is considerably greater in a fullerene than in a nanotube of the same diameter. Hence, CNT walls can be expected to be less reactive than the hemispherical fullerene end-caps.

Also, as can be easily appreciated, for CNTs, both θ_p and Φ decrease with increasing nanotube diameter. This accounts for the lesser reactivity of larger diameter tubes as compared with the smaller diameter ones.
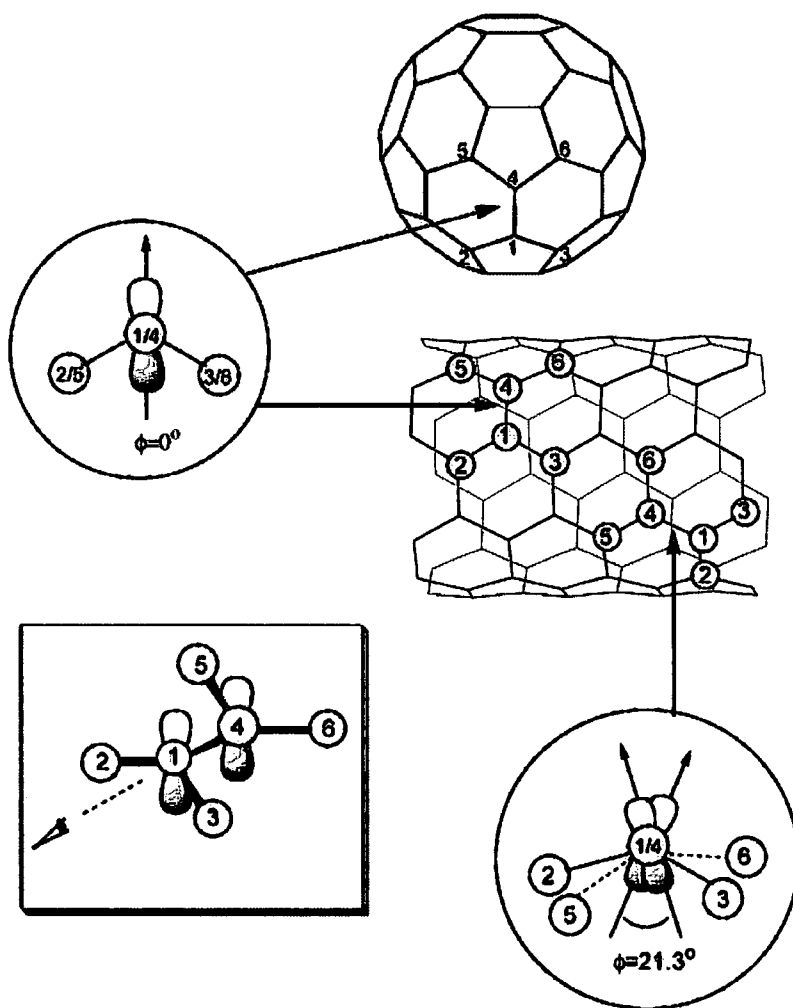
Figure 1-9

π-Orbital misalignment in fullerenes and a *(5, 5)* CNT.

19

1.6.3 Routes for the chemical modification of CNTs

The routes for the chemical modification of CNTs can be broadly classified into three categories:

1. Non-covalent modification by the adsorption or wrapping of molecules on their external surfaces;
2. Covalent modification by the creation of functional groups on, or attachment of species directly to, the walls of the CNTs; and
3. Endohedral filling of species into their hollow cavities.

The various routes for the modification of CNTs that have been reported to date are reviewed in the subsequent sections of this chapter. The work described in this thesis is exclusively concerned with the modification of the external surfaces of SWNTs, *i.e.* the first two routes mentioned above.

1.6.4 Non-covalent modification

Non-covalent modification of CNT surfaces is achieved by adsorption or wrapping of surfactants, or long chains such as polymers and biomolecules. The debundling and solubilisation of CNTs in solvents is thermodynamic, wherein the solubilising species both disrupt the affinity between the CNT walls in bundles as well as overcome the lack of affinity with solvents, including water. In particular, modification with surfactants such as sodium dodecyl sulphate (SDS) or biological polymers to yield water-soluble CNTs is of great importance to the potential biomedical applications of CNTs. The major advantages of non-covalent routes for the modification of CNTs are that they do not perturb their intrinsic electronic structure, thus leaving most of their properties intact, and are generally easily reversible. However, they can make large portions of the CNT surface inaccessible, which could be a disadvantage for applications such as electronics.

1.6.4.1 Surfactants

Surfactants adsorb non-specifically on the surface of CNTs, and have been extensively used to obtain stable dispersions of de-bundled CNTs by subjecting them to mild ultrasonic treatment in solutions of the chosen surfactant. Commonly used surfactants include anionic surfactants such as sodium dodecyl sulphate [108, 109], sodium dodecylbenzene sulphonate [110, 111]; cationic surfactants such as benzalkonium chloride [112]; and non-ionic surfactants such Triton-X [108]. A comparative study of the performance of a variety of surfactants has also been reported [113].

1.6.4.2 Polymers

Incubation of CNTs with a range of polymers, in particular polyvinyl pyrrolidone (PVP) and polystyrene sulphonate (PSS) led to soluble CNTs owing to the wrapping of the long polymer chains around the CNT backbone [114]. Solubilisation has also been demonstrated with other synthetic polymers such as polyethylene [115], polybutadiene, polystyrene, polyisoprenes, poly(dimethylsiloxane) (PDMS) [116], poly(acrylic acid) (PAA) [117], and natural polymers, such as Gum Arabic [118] and starch [119]. The wrapping phenomenon is robust, and the solubilised CNTs can even be passed, without separation, through filter membranes; however, it can also be easily reversed by changing the solvent.

The solubilisation of CNTs by conjugated polymers such as poly(*m*-phenylenevinylene-*co*-2,5-dioctoxy-*p*-phenylenevinylene) (PmPV) [120-123], substituted PmPV [124], poly{(5-alkoxy-*m*-phenylenevinylene)-*co*-[(2,5-dioctyloxy-*p*-phenylene)vinylene]} (PA*m*PV) and its derivatives [125], poly(phenylacetylene) [126] and poly{(2,6-pyridinylenevinylene)-co-[(2,5-dioetyloxy-p-phenylene)vinylene]} (PPyPV) [127] have been extensively studied. It is believed that π-π interactions aid the wrapping of the helical polymer molecules around the CNTs. There is also one report of CNT surfaces modified by the conjugated polymer with a rod-like backbone, poly-*p*-phenylenebenzobisoxazole (PBO) [128]. CNT-conjugated polymer composite materials are particularly interesting from the point of view of photovoltaic applications. Synergistic

interaction is observed between the conjugated polymer and the CNTs, leading to composites with enhanced electrical conductivities and, therefore lower "turn-on" fields, and high stabilities under irradiation as the CNTs act as "heat-sinks" preventing the build-up of pockets of heat.

1.6.4.3 Biomolecules

The assembly of biomolecules on the external surfaces of CNTs may have interesting applications like sensors and bionanoelectronics, stemming from the specific recognition properties of the biomolecules. CNTs modified in this way show significantly improved water-solubility.

It is now well known that proteins and DNA can be immobilised on CNT walls [129-132], resulting in water-soluble tubes. More recently, it has been shown that biomolecules organise themselves helically around CNTs [133-135].

CNT surfaces have also been modified by large aromatic molecules, such as pyrene derivatives, which adsorb on the CNTs by π-stacking [136-140].

1.6.5 Covalent derivatisation

Although the covalent chemistry of CNTs is not as rich as that of fullerenes, a wide range of routes have been developed for the covalent functionalisation of CNTs. In one of the first attempts at solubilising CNTs, it was shown that treatment with oxidising acids could etch and shorten CNTs; such treatment could lead to the creation of oxygen-containing functional groups, predominantly carboxylic acid, by rupturing the side-walls, and on opened end-caps, of the CNTs [108]. Subsequently, it was found that other oxidising media could similarly produce defects in CNTs. Derivatisation of oxidised CNTs via carboxylic group chemistry was demonstrated, and has gone on to become the most widely used route for the covalent attachment of functional moieties to CNTs. Many other routes have also been developed, such as radical additions, cycloadditions etc.,

22

which do not rely on the prior creation of carboxylic acid groups at "ruptures" or "defects" on the CNTs. Instead, they cause a local puckering of the tube surface, thereby releasing the strain engendered by curvature and π-orbital misalignment, as described in Section 1.6.2. Thus, we can classify the covalent functionalisation routes for CNTs into two broad categories:

1. Defect-based chemistry, and
2. Non-defect chemistry.

1.6.5.1 Defect-based covalent chemistry

1.6.5.1.1 Carboxylation of CNTs

One of the first attempts at the solubilisation of SWNTs involved their sonication in oxidising acids, such as sulphuric and nitric acids [108], which resulted in the etching of the SWNTs into short pipes and the creation of oxygen-contaning functional groups, predominantly carboxylic acids, at their cut ends and ruptures in their side-walls ("defects"). Subsequently, other routes for the oxidative etching and creation of oxygen-containing functional groups on CNT walls have been developed, including refluxing in sulphuric or nitric acids or mixtures of the two acids [141-155], $KMnO_4$ [156-158], and H_2O_2 [152, 159-162]. Other groups such as quinoidal, and ester groups are also formed as a result of oxidising treatment [104, 163-167].

1.6.5.1.2 Ozonation

In addition to the oxidising media mentioned in Section 1.6.5.1.1, CNTs have also been oxidised by treatment with ozone at room temperature, producing predominantly quinoidal and ester groups on the walls [165]. Liquid-phase ozonation at low temperatures leads, in the first instance, to the formation of primary ozonide by 1,3-dipolar

cycloaddition similar to alkenes and fullerenes. The ozonide can then be cleaved by hydrogen peroxide, dimethyl sulphide or sodium borohydride to produce preferentially carboxylic acid, aldehyde/ketone or alcohol groups respectively on the CNT walls [168].

1.6.5.1.3 Derivatisation via carboxylic group chemistry

Haddon and co-workers converted oxidatively etched CNTs to acid chlorides using thionyl chloride ($SOCl_2$) followed by derivatisation with octadecylamine via amide linkages resulting in highly soluble CNTs, as shown in Figure 1-10 [163, 164]. Subsequently, attachment of molecules via esterification of acid chlorides [166, 169, 170], as well as direct diimide-activated amidation of carboxylic acid groups without the intermediate acid chloride formation step has also been shown [171, 172]; this is particularly helpful for the attachment of delicate biomolecules to CNTs at ambient conditions. Alternatively, oxalyl chloride [$(COCl)_2$] can be employed for the conversion to acid chlorides [167] and the conversion to amide achieved simply by ammonia [167, 173] (Figure 1-10). Amines (R–NH_2) may also react directly with the carboxylic acid group (CNT–COOH), forming a zwitterion (CNT–$COO^-.NH_3^+$–R) [164].

Derivatisation via carboxylic acid chemistry has been used for attachment of functional molecules to CNTs. For example, poly(ethylene oxide) has been grafted onto CNTs for the synthesis of composites [174]. Biomolecules have also been tagged to CNTs, such as glucosamine by amidation via thionyl chloride [175], proteins like bovine serum albumin [171], Knob protein [176] and antibodies [177]. Significantly, biological molecules attached to CNTs by this route have been found to retain their activity and specificity, which is of great importance to applications such as biosensors.

Coleman and co-workers have demonstrated iodination via a modified Hunsdiecker reaction on oxidised CNTs [178].
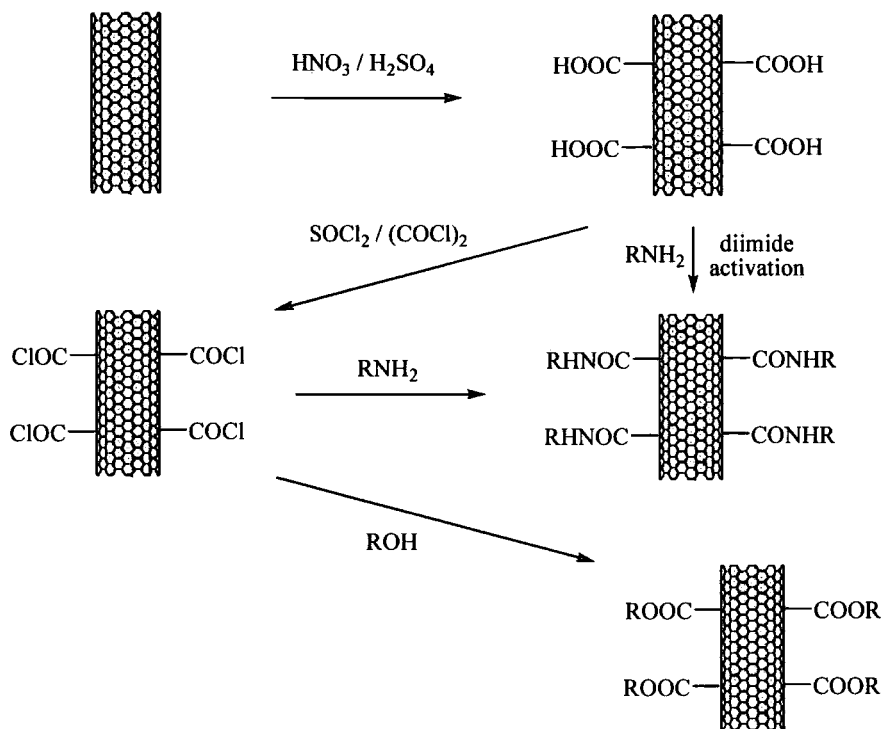
Figure 1-10

Carboxylation of CNTs and subsequent derivatisation via amidation / esterification.

1.6.5.2 Non-defect covalent chemistry

1.6.5.2.1 Fluorination

This approach to the functionalisation of CNTs has been pioneered by Margrave's group. Analogous with graphite [179] and fullerenes [180], the fluorination of CNTs was achieved by gas-phase treatment with fluorine at elevated temperatures in the range, 250-500°C [181, 182], to yield a grey to white powder of fluorinated CNTs having the stoichiometry CF (MWNTs) and C_2F (SWNTs). Although treatment with hydrazine [182] or, better still, annealing at temperatures in the range 100-350°C [183, 184] can be used to reverse fluorination, the damage caused may not be completely recoverable. At temperatures above 400°C, fluorination causes SWNTs to be converted into MWNTs.

Fluorination is observed to lead to increased solubility over pristine CNTs in alcohols [185], and greater uniformity of dispersion in polymer composites [186].

Fluorinated CNTs have been used as a starting point for further derivatisation by nucleophilic substitution by Grignard and alkyllithium reagents [187]. The functionalisation was reversible upon annealing, and the extent of functionalisation, as estimated from the weight loss profile in thermogravimetric analysis (TGA) was of the order of 10 atomic *per cent*. Fluorinated CNTs have also been subjected to nucleophilic substitution by diamines [188] and radicals generated thermally from peroxides [RC(O)OO(O)CR] [189]. Figure 1-11 shows the reaction scheme for the fluorination of CNTs and the subsequent derivatisation of fluorinated CNTs.

Fluorinated SWNTs were also produced by the treatment of nanotubes by CF_4 plasma [190, 191].
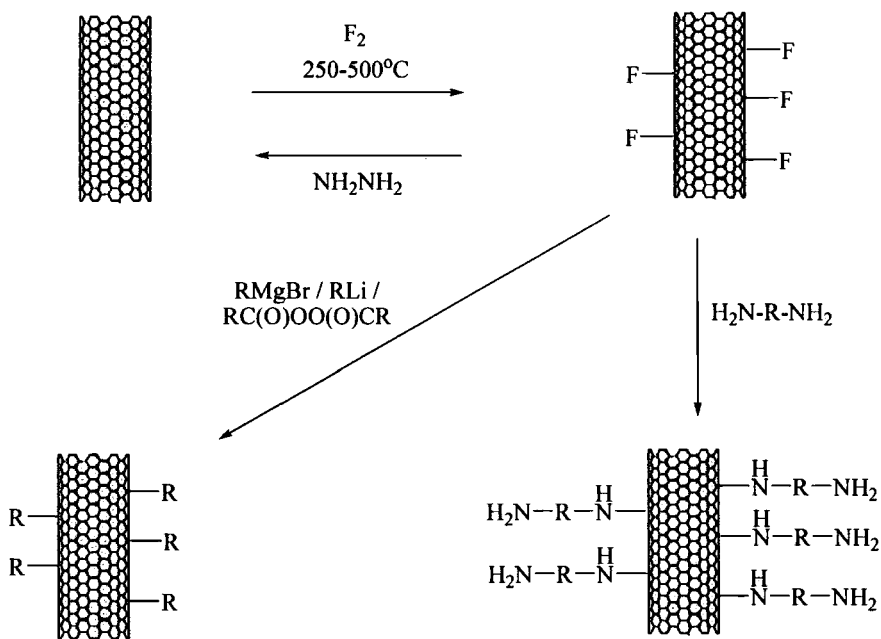
Figure 1-11

Fluorination of CNTs and further derivatisation of fluorinated CNTs.

1.6.5.2.2 Radical additions

1.6.5.2.2.1 Radicals from aryl diazonium salts

Radicals generated by the electrochemical reduction of aryl diazonium salts in non-aqueous media was demonstrated by Tour and co-workers [192]. They estimated that one in every twenty CNT carbon atoms was functionalised, and the functionalisation was reversible upon annealing the modified CNTs. Later, a more facile route via the decomposition of diazonium salts in aqueous solution was developed [193-195] (Figure 1-12). The reaction has a strong selectivity for metallic over semiconducting SWNTs [195, 196]. Very recently, Strano and others functionalised SWNTs with the radical generated from p-hydroxybenzene diazonium salt, deprotonated the hydroxyl group and, exploiting the differences in mobilities between metallic and semiconducting SWNTs induced by the selectivity of the reaction, achieved the enrichment of metallic and semiconducting fractions by electrophoresis [197].
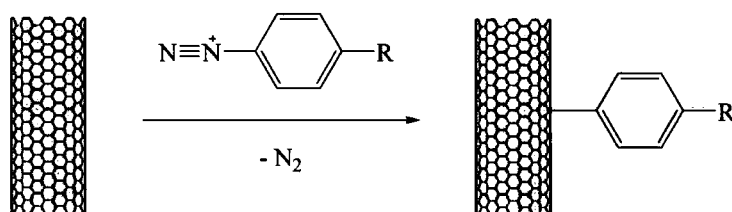
Figure 1-12

Functionalisation of CNTs by radicals derived from aryl diazonium salts.

1.6.5.2.2.2 Radicals from organic peroxides

Radicals generated by the decomposition of a range of organic peroxides either in the presence of alkyl halides [198] or simply upon mild heating [173, 189] have also been used to derivatise the sidewalls of CNTs (Figure 1-13). Ying and co-workers estimated the

degree of functionalisation to vary from as low as one in every thirty, to one in every five CNT carbon atoms [198].
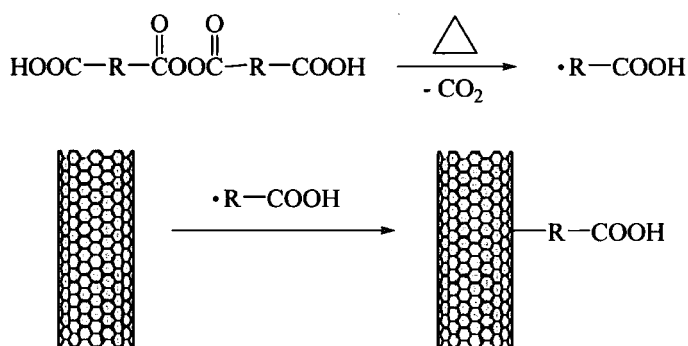
Figure 1-13

Functionalisation of CNTs by radicals derived from organic peroxides.

1.6.5.2.2.3 Other radical additions

Perfluoroalkyl radicals have been added to CNT sidewalls in a photoinduced reaction [199]. Plasma treatment of a CNT/sulphur mixture resulted in the formation of thiolated CNTs [200]. In what could be of significance to nanoelectronics, the thiolated CNTs are seen to self-assemble on gold electrodes.

1.6.5.2.2.4 Polymer grafting onto CNTs via radical chemistry

Radical addition has been exploited for the grafting of polymers onto CNTs, such as polystyrene [201], poly(methyl methacrylate) (PMMA) [202] and poly(4-vinylpyridine) [203], leading to highly soluble CNTs.

1.6.5.2.3 Nucleophilic additions – CNTs as nucleophiles

1.6.5.2.3.1 [2+1] cycloadditions

1.6.5.2.3.1.1 Cycloaddition of carbenes

Cycloaddition of dichlorocarbene (Figure 1-14), generated from chloroform in NaOH or $PhHgCCl_2Br$ precursor, to CNTs was reported by Haddon's group [103, 163, 204]. The disruption of the electronic structure was followed in terms of the features in UV-visible-IR spectroscopy. It was seen that 12% functionalisation led to a 50% suppression, while a 23% functionalisation led to a near-complete suppression of the features.
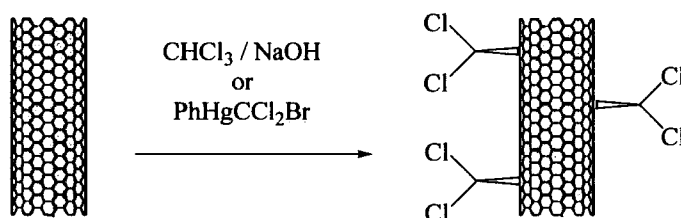
Figure 1-14

Cycloaddition of dichlorocarbene to CNTs.

1.6.5.2.3.1.2 Nitrene addition

Holzinger and co-workers demonstrated the *[2+1]* cycloaddition of nitrenes generated thermally from alkyl azidoformates to CNTs [199, 205] (Figure 1-15). UV-visible-NIR spectroscopy shows that, in general, this route does not cause a significant disruption of the electronic structure of the CNTs. Also, Raman spectroscopy reveals that the reaction has a greater selectivity for metallic over semiconducting SWNTs. This reaction was also employed by the same group to cross-link SWNTs [206].
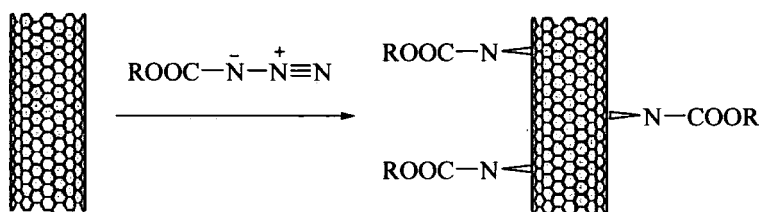
Figure 1-15

Cycloaddition of nitrenes to CNTs.

1.6.5.2.3.2 Carbene addition

Addition of the nucleophilic carbene derived by the deprotonation of dipyridyl imidazolidene was shown by Holzinger and co-workers [199].

1.6.5.2.3.3 *1,3*-Dipolar cycloaddition

Extending their reaction demonstrated previously for fullerenes [207], Prato's group showed the cycloaddition of azomethine ylides formed by the *in situ* condensation of an aldehyde and an α-amino acid to CNTs [208, 209] (Figure 1-16). The reaction occurs over several days. It has been shown that, by a careful choice of the decorating chains, CNTs of high solubility in water or several organic solvents can be obtained. Although only one pyrrolidine moiety is introduced for every hundred CNT carbon atoms, significant disruption of the CNT electronic structure is indicated by the UV-visible-NIR spectra of the modified nanotubes.

This route has subsequently been used for tagging molecules with several functionalities. Ferrocene was attached to CNTs to study photo-induced electron transfer processes [137]. The covalent tagging of the amino acid, glycine, has also been achieved by the same group [210].
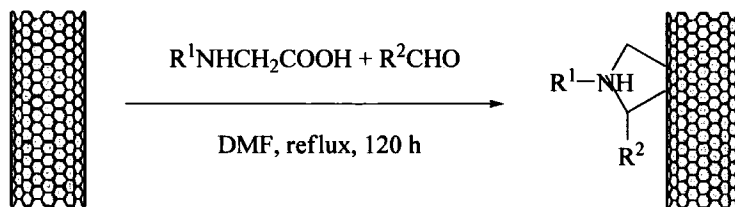
Figure 1-16

1,3-Dipolar cycloaddition of azomethine ylides.

1.6.5.2.3.4 Bingel Reaction

This is also an instance of *[2+1]* cycloaddition. The cyclopropanation of fullerenes by bromomalonates has been extensively studied [211]. This route has been extended to SWNTs by Coleman *et al.* [212] (Figure 1-17).
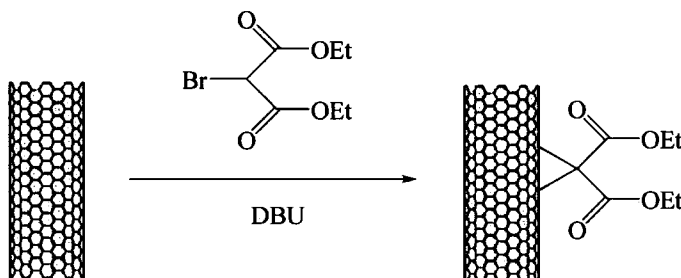
Figure 1-17

Cyclopropanation of CNTs via the Bingel reaction. (DBU = 1,8-diazabicyclo[5.4.0]undecene)

1.6.5.2.4 Reduction chemistry of CNTs – CNTs as electrophiles

1.6.5.2.4.1 Birch reduction

The Birch reduction, which is employed to reduce aromatic species to non-conjugated ones, has been shown for fullerenes [213]. Fullerenes (C_{60}) were reduced via the formation of anionic species to $C_{60}H_{36}$ by lithium and *t*-butanol in liquid ammonia. In an

analogous procedure, CNTs (and, simultaneously, graphite) were reduced using lithium and methanol in ammonia [214]. The stoichiometry of the products was found to be $C_{11}H$ for both SWNTs and MWNTs, and C_5H for graphite.

1.6.5.2.4.2 Reduction by alkali metals and nucleophiles

The reduction of graphite by alkali metals to give intercalation compounds, and their subsequent chemistry, is well-known [215]. The stoichiometry of these intercalation compounds is C_8M (M = Li, Na, K, Rb, Cs). For the case of fullerenes, intercalation compounds have been found to have a stoichiometry of up to M_6C_{60} [216]. Alkali metal-intercalated SWNTs synthesised by a vapour-phase reaction were also found to have the stoichiometry C_8M; also, the intercalation was found to be reversible [217]. Recently, Billups and co-workers reduced SWNTs by alkali metals in liquid ammonia, resulting in the formation of the salt, [(SWNT)x^-.Mx^+, M = Li, Na, K]. This salt was then subjected to electrophilic substitution with alkyl and aryl halides, resulting in highly soluble nanotubes [218-220]. The functionalisation ratio ranged from 1 in 17 to 1 in 54 CNT carbon atoms. Alkali metal naphthalenide solutions in THF have also been employed to reduce CNTs [221]. Interestingly, although elemental analysis indicated a stoichiometry of $C_{10}M$, only 20% of the metal atoms were dissociated into ions; in other words, the actual stoichiometry of the salt was $C_{50}M$.

It has been demonstrated that fullerenes can be reduced by t-butyllithium, followed by electrophilic substitution [222, 223]. Reduction by butyllithiums to generate charged CNT anionic species has been used for grafting polymers by anionic polymerisation onto CNTs for use in composites [224, 225]. Hirsch and co-workers have recently carried out a detailed investigation into the reduction of CNTs by t-butyllithium, which can be carried out in repeated steps on the same CNT backbone [226]. They have also found that the extent of functionalisation in the first reduction step is around 2 atomic *per cent*, which agrees well with the figure given by Pénicaud and group [221] for the reduction of CNTs by alkali metal naphthalenides.

The reduction chemistry of CNTs is discussed in greater detail in Section 4.1.

1.6.5.3 Characterisation

CNTs are materials. Although a CNT is a single molecule, any sample of CNTs will contain a mixture of tubes of varying diameters and helicities. Besides, their solubility, even when enhanced by suitable chemical modification, is low (generally less than the order of 1 mg/L). Thus, they are not easily amenable to conventional molecular spectroscopy, and it is extremely difficult to establish their chemical modification, or its result on their properties. Nevertheless, several techniques have been employed for their characterisation with increasing success over the years, such as Raman spectroscopy, optical absorption spectroscopy including the electronic ultraviolet-visible-near infrared (UV-vis-NIR) and vibrational mid-infrared (IR) spectroscopy, microscopic techniques for direct visualisation such as atomic force microscopy (AFM), transmission (TEM) and scanning (SEM) electron microscopy, X-ray photoelectron spectroscopy (XPS), thermal analysis, etc. In general, no single method of characterisation is able to furnish the entire picture regarding the modification of CNTs, and a combination of techniques will have to be employed. Often, the techniques used will be dictated by the specific modification route; also, the groups attached to the CNTs can be innovatively tailored to suit one or more spectroscopic methods. These are described in detail below.

1.6.5.3.1 Raman spectroscopy

The use of resonant Raman spectroscopy for characterising CNTs was placed on a firm experimental footing by Rao and co-workers [227]. The Raman spectra of CNTs consists of bands corresponding to low-energy radial breathing modes (RBM) of the tubular cages having Raman shifts below 500 cm^{-1}, a tangential mode corresponding to in-plane vibrations of sp^2-hybridised carbon commonly denoted as the "graphitic" or "G-band" at around 1580 cm^{-1}, a band arising from defects or amorphous carbon corresponding to vibrations of sp^3-hybridised carbon and denoted as the "disorder" or "D-band" at around 1350 cm^{-1}, and an overtone at around 2700 cm^{-1}. However, these features are very prone to resonance-enhancement, and are therefore strongly dependent

on the wavelength of the laser used for excitation. Further, Kataura and others demonstrated that the G-band may have a Breit-Wigner-Fano (BWF) line shape arising from metallic CNTs [47]. The presence of amorphous carbon or covalent derivatisation of CNTs leads to an increase in the proportion of sp^3-hybridised carbon, resulting in an enhancement of the intensity of the D-band (I_D) relative to the G-band (I_G). This observation has been extensively used to obtain proof of functionalisation [104, 163, 168, 182, 188, 190, 198, 218, 224].

Raman spectroscopy is also helpful in deducing chemoselectivity of reactions. It was found that nitrene cycloaddition shows a preference for metallic over semiconducting SWNTs, as spectra recorded using a 633 nm laser (which probes predominantly metallic SWNTs) showed greater change in the I_D/I_G ratio over pristine SWNTs than that recorded using a 1064 nm laser (which probes predominantly semiconducting SWNTs) [205]. Similarly, the functionalisation of SWNTs by radicals generated from aryl diazonium reagents also showed a high level of selectivity for metallic over SWNTs: the RBM bands corresponding to semiconducting SWNTs (recorded predominantly by a 532 nm laser) were largely unchanged, whereas those corresponding to metallic SWNTs (633 nm laser) decayed upon reaction [196]. The shape of the G-band, which results from the superimposition of the contributions of metallic and semiconducting SWNTs, was seen to be greatly affected owing to the chemoselectivity of the aryl diazonium reaction; also, beyond a certain level of functionalisation, the D-band intensity was seen to reduce sharply, underscoring the fact that it is strongly dependent on resonance enhancement and that a simple comparison of the I_D/I_G ratio may not always reveal if functionalisation has occurred [195].

Besides an increase in D-band intensity and change in the shape of the G-band, the intensity of the G-band relative to the RBM, and the intensities of the RBM in general may change upon modification [192-194, 220, 226]. The fact that the D-band is highly sensitive to resonance enhancement was also observed by Coleman and group for the iodination of SWNTs; when a He/Ne laser (632.8 nm) was used for excitation, the intensity of the D-band for derivatised SWNTs was found to reduce for the second step of the reaction; also, the RBM features were observed to change for the different chemical steps, indicating a change in the electronic properties of the SWNTs at each step [178].

Many times, it is of interest to know if a route for chemical modification is reversible, and if the electronic structure of pristine CNTs can be recovered. Thermal annealing was unable to restore the D-band intensity of SWNTs cyclopropanated by carbenes down to the level of that in pristine CNTs, indicating that this form of modification was not entirely reversible [204]. In contrast, Raman spectra indicated that modification by aryl diazonium radicals was completely reversible [194].

The low-energy RBMs are dependent on the state of aggregation of the CNTs. Thus, cross-linking of SWNTs achieved via the nitrene cycloaddition route caused a shift in the position of the RBMs owing to change in size of bundles [206].

The alteration in the electronic structure of CNTs upon chemical modification may also manifest as a shift in the position of the G-band, as was observed for functionalisation by nitrenes [205].

1.6.5.3.2 Ultraviolet-visible-near infrared (UV-vis-NIR) spectroscopy

Kataura's group demonstrated that the transitions between the electronic densities of state in SWNTs (see Figure 1-6) could be observed as bands in UV-vis-NIR absorption spectroscopy [47]. Approximately, the metallic transitions (M_{11}) can be observed in the 400-600 nm region, the first semiconducting transitions (S_{11}) in the 600-800 nm range, and the second semiconducting transitions (S_{22}) in the 800-1400 nm range. Later, Haddon and co-workers observed that the perturbation of the electronic structure of pristine SWNTs upon chemical modification leads to a suppression of these bands [163], and followed the extent of suppression of the bands with degree of functionalisation for the cyclopropanation of SWNTs with dichlorocarbene [103, 204]. Thereafter, UV-vis-NIR spectroscopy has become a common tool for characterising functionalised SWNTs [104, 178, 188, 192-194, 208, 224]. Chemically modified CNTs can be expected to have higher solubilities than pristine CNTs. Thus, a dispersion of modified CNTs will have a higher absorbance than that of pristine CNTs, and this can also be taken as proof of CNT derivatisation [104].

The degree of functionalisation can be qualitatively estimated from the extent of suppression of the absorption bands. For instance, carbene addition led to a very little

suppression of bands, indicating low extent of functionalisation, whereas cycloaddition of some nitrenes resulted in highly dispersed SWNTs even with a small extent of functionalisation, leading to an *enhancement* in the intensity of the bands [199].

By following the progress of the functionalisation of SWNTs by radicals derived from aryl diazonium salts by UV-vis-NIR spectroscopy, Strano and group observed that the reaction showed a remarkable selectivity for metallic over semiconducting SWNTs [195].

The restoration of UV-vis-NIR absorption bands can be used to judge if a chemical modification route is reversible. Margrave's group demonstrated the reversibility of fluorination of SWNTs, as well as the possibility of restoring pristine SWNTs from alkylated SWNTs synthesised from the fluorinated SWNTs by thermal annealing [187]. The reversal of fluorination has also been studied by other groups [183, 184]. UV-vis-NIR spectroscopy confirmed the Raman evidence that the disruption of the electronic structure of SWNTs by dichlorocarbene cyclopropanation could not be reversed completely by thermal annealing [204].

1.6.5.3.3 Mid-Infrared Spectroscopy

While CNTs have great polydispersity in terms of the range of helicities and diameters present in any sample, many groups have nevertheless successfully employed Fourier-transform infrared (FTIR) vibrational spectroscopy to obtain evidence of attachment of groups to CNTs. FTIR was first used to observe the effect of oxidising acid treatments on CNTs, with characteristic bands appearing for carboxylic acid and various oxygen-containing functional groups including ester and quinoidal groups [104, 163-167]. FTIR has now become fairly common for probing the attachment of groups to CNT walls [188, 189, 192, 198, 204, 218].

1.6.5.3.4 Nuclear magnetic resonance (NMR) spectroscopy

Even after chemical modification, the solubility of CNTs in most organic solvents is low as compared to ordinary molecular species. Also, one-third of any sample of CNTs consists of metallic nanotubes. Hence, it is not easy to characterise CNT samples by NMR. Nevertheless, there are a few reports where the organic moieties attached to CNTs have been successfully probed by NMR. SWNTs derivatised by addition of nitrenes, dissolved in $CDCl_3$ and *1,1,2,2*-tetrachloroethane (TCE-d_2), were characterised by ^{1}H NMR [205]. Fluorinated alkyl chains attached to CNTs via a radical reaction were detected by ^{19}F NMR for a dispersion of modified CNTs in DMSO [199]. Coleman *et al.* further derivatised SWNTs cyclopropanated via Bingel reaction with a fluoroalkyl chain, and were able to obtain an ^{19}F NMR of the tagged SWNTs suspended in d_7-DMF [212].

1.6.5.3.5 Atomic Force Microscopy (AFM)

Methods for the direct visualisation of CNTs prove to be very useful in observing the effects of chemical modification. AFM has been used by several groups to show the shortening of CNTs caused by oxidative treatments, or exfoliation of CNT bundles as a result of higher solubility conferred by chemical derivatisation, and AFM height images are often employed to determine the reduction in average bundle diameter upon modification [104, 150, 166, 171, 172, 176, 187, 194, 199, 204, 205, 218, 220, 224, 228]. Coleman *et al.* used gold colloid tagging to provide direct evidence of the successful cyclopropanation of SWNTs via the Bingel reaction. In their procedure, a thiolated moiety was attached to SWNTs, following which gold colloids were tagged to the thiol groups, whereupon AFM height images showed an increase equal to the diameters of the gold colloids [212]. Holzinger and group used AFM imaging to show the bundling of SWNTs brought about by cross-linking via nitrene addition to the side-walls [206].

1.6.5.3.6 Transmission electron microscopy (TEM)

TEM is also very helpful in directly observing the effect of chemical modification of CNTs and attachment of groups to their walls. Fluorination was observed to cause damage to SWNT walls, and formation of MWNTs if carried out above 500°C [182]. When organic chains are attached to CNT walls, they may be seen as hazy coatings on the sharply delineated CNT walls [172, 188, 189, 194, 205, 218, 220]. In addition to AFM images, Holzinger and co-workers also used TEM images to observe the cross-linking of SWNTs via nitrene addition to the nanotube walls [206]. Hydrogenation of CNTs by Birch reduction was seen to cause corrugation of the CNT walls [214]. TEM contrast images were used for showing the presence of iodine atoms attached to SWNT walls by the Hunsdiecker reaction [178].

1.6.5.3.7 Scanning Electron Microscopy (SEM)

Although to a lesser extent than TEM, SEM has been used by some groups to observe changes in the morphology of CNTs as a result of chemical modification [108], [188, 190, 206]. For instance, just as is the case with graphite [179], SEM images indicated that the fluorination of CNTs led to a change in their colour from black to white, which was reversed upon defluorination by hydrazine [182].

1.6.5.3.8 X-ray photoelectron spectroscopy (XPS)

XPS is a surface analysis technique for studying the elemental composition and chemical state of the elements present in a sample, that has been commonly used for polymers and carbon materials such as carbon fibres. XPS has also been used to characterise chemically modified CNTs. One of the first reports was for the study of CNTs that had been subjected to oxidising treatments; the C1s peak was deconvoluted to determine the oxygen-containing functional groups present on the CNT walls [168]. XPS

data was useful in observing the fluorination and defluorination of CNTs [184], and understanding the nature of the bonds between carbon and fluorine: the F1s peak of fluorinated CNTs showed the presence of both ionic and covalent C-F bonds [190], and the shape of the C1s peak upon deconvolution showed the contribution of C–F covalent bonds [191]. Other instances of the use of XPS in characterising modified CNTs include the detection of nitrogen introduced by *1,3*-dipolar cycloaddition [205] and by nitrene addition [206], fluorinated chains introduced via the Bingel reaction [212], iodine by the Hunsdiecker reaction [178], and sulphur covalent attached to SWNTs via a plasma-induced radical reaction [200].

A lesser used method for obtaining the elemental composition of modified CNTs is energy-dispersive X-ray analysis (EDAX) [103, 188].

1.6.5.3.9 Thermal analysis

Thermogravimetric analysis (TGA) of modified CNTs in an inert atmosphere, such as argon or helium, helps in following the thermal defragmentation of the groups attached to CNTs. The weight loss corresponding to the attached groups is used to quantitatively estimate the degree of functionalisation; often, this technique is coupled with gas-phase mass spectrometry (MS), which helps in exactly identifying the attached groups [167, 178, 187-189, 192, 194, 198, 218, 220, 224]. There is one report of TGA being coupled with infrared spectroscopy (TGA-FTIR) [189]. The temperature at which the groups evolve indicates if the attachment was covalent or non-specific adsorption, as the former takes place at higher temperatures. For instance, the high temperature of evolution of hydrogen, 500°C, and detection of methane was adduced as proof of covalent C-H bond formation in the Birch reduction of CNTs [214].

1.6.5.3.10 Electrical measurements

Owing to the presence of metallic tubes, any bulk sample of CNTs ordinarily behaves like a conductor. Chemical modification perturbs the intrinsic electronic structure of CNTs, and therefore shall alter their electrical properties. Based upon this principle, bulk electrical measurements have been used to probe CNT chemical modification. Electrical measurements on "buckypaper" showed that the resistance measured by a four-point apparatus increased by orders of magnitude owing to chemical functionalisation, and ideally returned to the value of pristine tubes if the modification was completely reversible [182-184, 187].

1.6.6 Endohedral filling

Incorporating molecules and chemical species within the cavities of CNTs may have implications for their potential use as nanoscale reactors, and biomedical applications such as drug-delivery. Also, from a more fundamental point of view, it would be interesting to study the formation and properties of 1-D crystals of dimensions where quantum effects would come into play, as well as the properties of the filled CNTs themselves.

The end-caps of CNTs can be opened by heat treatment or oxidation with acids, thereby making the cavity accessible for filling [156, 229-231]. CNTs have been filled by metals such as lead [229], ruthenium [232], metal oxides [233, 234] and mixtures of metal halides [235-237]. The filling can take place either in solution or by capillarity of molten species. For a review of the filling of CNTs by metal halides, see Ref. 238.

In the laser ablation method of synthesis, some CNTs were observed to have fullerenes encapsulated within them [239, 240]. Later, the targeted high-yield synthesis of these so-called "peapod" structures of CNTs encapsulating fullerenes (C_{60}@SWNTs), endohedral metallofullerenes [such as (Gd@C_{82})@SWNTs] has been achieved [241], as well as functionalised fullerenes [242, 243]. In an interesting report, Khlobystov and co-

workers have demonstrated the use of CNTs as nano-reactors for carrying out the polymerisation of C_{60} molecules encapsulated within the CNTs [244].

The encapsulation of proteins inside the hollow cavities of CNTs has been demonstrated [245, 246]. Significantly, it was found that the proteins retain most of their activity, which could pave the way for using such systems as nanoscale biological reactors.

For an exhaustive, in-depth review on the filling of CNTs, the reader is referred to Ref. 247.

2. PURIFICATION OF CARBON NANOTUBES: IMPLICATIONS FOR CHEMISTRY AND SPECTROSCOPY

2.1 Introduction

2.1.1 Overview

Purification of as-produced CNTs is the first step before any chemical modification can be carried out, or before they can be employed for any of their potential applications (see Chapter 1, Section 1.5). As-produced CNTs contain a very large amount (30-70% by weight) of impurities including metal catalyst particles, amorphous carbon, fullerenes and multi-shell graphitic carbon "buckyonions". Thus, the initial purification step is of great importance and criticality. The impurities associated with CNTs must be removed before commencing any investigations on their electronic, electrical, thermal, mechanical or chemical properties, or for their application in any of the areas ranging from electronics to polymer composites. The metal catalyst may be enclosed by the graphitic or amorphous carbon, as has been shown by transmission electron microscopy (TEM) imaging [144, 160, 161, 248-259]. As-produced CNT samples synthesised by laser ablation methods contain a significant amount of fullerenes [248], while arc-discharge CNTs have a considerable content of multi-layer graphitic carbon enclosing metal catalyst. A wide range of physical and chemical methods have been developed for the removal of these impurities from as-produced soot to yield a material considerably enriched in CNTs. The various routes for the purification of CNTs that have been reported to date, and their respective advantages and disadvantages, are reviewed in Sections 2.1.2 to 2.1.5. To the best of our knowledge, there is no comprehensive review in the published literature of what is a very important aspect of CNT research. This review shall provide the necessary background for appreciating the importance of the

present study into some fundamentally important aspects of the purification and chemistry of CNTs.

The initial purification step is of great importance to any subsequent chemistry that is carried out on the CNTs. Species of the highest purity possible are desirable for chemistry. The purity levels possible for molecular species are extremely difficult to achieve for heterogeneous materials such as CNTs. Amorphous carbon likely present in CNT material is more reactive than the CNTs, and will invariably be the preferred site of attack for any chemical reagents with which the CNTs are sought to be modified; besides, the reactivity of fullerenes and buckyonions, occurring as by-products in the CNT material, is almost identical with that of the end-caps, and quite similar (if not identical) with that of the side-walls, of CNTs. In addition, a great complication is introduced by the fact that the characterisation of chemically modified CNTs is extremely challenging, as, unlike molecular species, they are not easily amenable to standard techniques such as nuclear magnetic resonance (NMR) spectroscopy, mass spectrometry or infra-red (IR) spectroscopy.

Many groups have made use of previously reported recipes for the purification of CNTs, if the source of the CNTs was the same as, or if they were produced by processes identical with, that in the original report on the purification of the CNTs [166, 169, 182, 187, 189, 204, 260]. However, we find that, even for different batches of CNT material which have been made by the same synthesis method and while keeping the macroscopic synthesis conditions identical, it is not advisable to rely entirely on previously reported purification recipes without careful re-evaluation. This is an aspect of the purification of CNTs that has not been critically examined previously. Even though characterisation methods such as Raman spectroscopy and thermogravimetric analysis (TGA) show virtually identical spectra for the different batches of the CNT material, and the steps involved in the purification process may broadly be the same, they have to be fine-tuned and re-adapted afresh for each batch of material produced, if the removal of amorphous carbon and metal catalyst is to be ensured. This probably underscores the high inherent heterogeneity in the material, and the difficulty involved in characterising CNTs.

The elimination of amorphous and non-nanotube carbon is integral to any purification process for as-produced CNT material. The elimination of non-nanotube

carbon is generally achieved by exploiting its greater reactivity to oxidation as compared to the relatively stable nanotubes. An extensively employed purification route involves the treatment of as-produced CNT material with liquid-phase oxidising media, such as sulphuric or nitric acids, which selectively oxidise away the non-nanotube impurities. However, such oxidising treatments do cause some chemical modification of the CNTs, such as the formation of carboxylic acid and other oxygen-containing functional groups on the CNT backbones. Even very mild treatment with oxidising acids causes some amount of damage to the CNT structures [261, 262]. However, this may in fact be preferable, as the carboxylic acid groups lead to enhanced solubility or can be exploited for the further derivatisation of the CNTs, as described in Section 1.6.5.1.

One consequence of such oxidising treatments that was surprisingly not taken note of till very recently, is the effect of the amorphous carbon that may be formed as a result of chemical etching, on the subsequent chemistry carried out on the CNTs. In recent publications, it has been argued that the vast majority of carboxylic acid groups that were believed to have been created on the CNT walls may actually be associated with this amorphous carbon debris [263, 264], and not covalently attached to the CNT walls as previously assumed. This could potentially cast doubt over a great deal of the literature based on the carboxylation of CNTs and subsequent derivatisation via amidation / esterification, which is among the most commonly employed chemical modification routes for CNTs (see Section 1.6.5.1.3 and references therein). Also, their conclusions could have profound implications for the spectroscopy of chemically modified CNTs, and could call into question the currently accepted interpretations of the effect of chemical modification on CNT spectra. The evidence for the formation of carboxylic acid groups on the CNT walls was adduced from an increase in the disorder (D-) band corresponding to defects and sp^3 carbon atoms in the Raman spectra [149, 158, 265, 266], and the appearance of bands ascribable to oxygen-containing functional groups in the mid-infrared (IR) spectra [155, 158, 163-166, 262, 265, 267] of CNTs. However, Verdejo et al. [263] and Salzmann et al. [264] reported that washing the acid-treated CNTs was able to reverse the changes in the Raman and IR spectra that were attributed to the carboxylic acid groups on the CNT walls, which implied that the groups were not covalently attached to the CNT walls. Given how extensively this method is used for the purification and

modification of CNTs, this is a question of great importance, and has been investigated in great detail herein.

Our findings underscore the great difficulty in characterising CNTs, and the limitations in employing molecular spectroscopic methods for these materials. It has been suggested that ultraviolet-visible-near-infrared (UV-vis-NIR) spectroscopy has the potential to obviate the need for other characterisation methods for CNTs, such as Raman spectroscopy or transmission electron microscopy (TEM) [47]. Our findings however indicate that exclusive reliance on any one spectroscopic method may be very misleading. Accurate evaluation of the purity and characterisation of CNTs may be achieved only if multiple spectroscopic methods such as Raman spectroscopy, UV-vis-NIR spectroscopy, TEM and thermal analysis methods, such as thermogravimetric analysis (TGA) and thermogravimetric analysis-mass spectrometry (TGA-MS), are used in conjunction to complement each other. Our results especially bring to the fore the usefulness of thermal analysis in characterising CNTs.

2.1.2 Physical purification methods

Many research groups have attempted to develop purely physical or physico-chemical purification routes, which avoid the need for outright chemical treatments.

A common strategy is the use of surfactant or dispersing agent to assist in the debundling of CNTs [112, 122, 123, 145, 153, 160, 251, 255, 256, 268-272], thereby separating them from the amorphous carbon, non-CNT graphitic carbon and metal particles. However, mild sonication will invariably be required to achieve this dispersion, and the dispersion may be used for acid treatment as the non-CNT impurities can now be more easily removed. Chemical treatment can also be completely avoided and methods like centrifugation, microfiltration or even decantation can be employed for separating the CNTs from the impurities.

In an interesting procedure, CNTs have been mixed with inorganic nanoparticles such as ZrO_2 and $CaCO_3$ and subjected to sonication, whereupon it was found that these nanoparticles ejected the metal catalyst particles enclosed within amorphous or graphitic

carbon by mere elastic impact [257]. The catalyst paraticles (typically Fe, Co or Ni) could easily be separated by a magnet, leaving behind purified CNTs.

It has been shown that, under an electric field, CNTs migrate towards, accumulate on electrodes and align themselves [273, 274]. This is owing to the high aspect ratio of the CNTs and the polarization induced by the field in CNTs in the axial direction. As higher AC frequencies are applied, the non-CNT impurities become increasingly harder to mobilise. This has been exploited to electrophoretically separate CNTs from the impurities and obtain films of purified CNTs on electrodes [275-277]. The high power requirement for applying high-frequency AC voltages may be a drawback of this method.

Size-exclusion chromatography has been shown to be capable not only of purifying CNTs while causing virtually no damage to the tubes, but also of sorting them length-wise within very narrow ranges [109, 271, 278, 279]. Typically, surfactant-stabilised dispersions of CNTs are eluted through columns of carefully chosen packing, such as controlled pore glass (stationary phase). The successively collected fractions will consist of CNTs of decreasing lengths and, finally, impurities, in that order. This method has also been applied to oxidatively shortened CNTs [280-284]. However, as can be expected of chromatographic procedures, this method has a very low throughput.

Many proposed applications of CNTs require aligned films and arrays, which can be obtained by CVD growth of CNTs on substrates. The majority of the purification methods described above will be inapplicable for such films. While *in situ* methods for minimising the formation of amorphous carbon by the incorporation of water vapour or hydrogen in the feedstock have been mentioned above, post-synthesis purification processes have also been developed. Laser irradiation has been found to be useful in eliminating amorphous carbon and trimming the surfaces of CNT films [285]. Plasma etching has also been employed for the same purpose [286], although prolonged exposure to plasma was found to open the end-caps of the CNTs.

2.1.3 Chemical purification methods

For CNTs synthesised by chemical vapour deposition (CVD), the first step in the purification process is the removal of the catalyst support. This is generally done by washing the as-prepared sample with HF [157, 249, 250, 287-290], HCl [146, 154, 249] or NaOH [291, 292]. Along with the support, these treatments also dissolve away some of the metal catalyst as well. It must be kept in mind that carrying out this step with HCl or NaOH (or both in succession) is more environmentally benign than the use of HF.

Fullerenes and carbon onions are soluble and, hence, are easily removed by either washing or Soxhlet extraction of the raw sample with CS_2 [112, 151, 293], toluene [160] or benzene [294].

A far greater challenge is posed by the metal catalyst nanoparticles enclosed in either amorphous or graphitic carbon layers. A variety of strategies have been devised for the removal of these impurities from the raw soot. The most commonly adopted strategy for removing amorphous / graphitic carbon and the metal enclosed by them is to exploit their greater ease of oxidation than CNTs. In this step, the more reactive amorphous carbon, fullerenes and buckyonions are selectively oxidised, whereas the more stable CNTs are relatively unharmed. The oxidation can be carried out either in the gaseous phase or in the liquid phase.

The gas-phase oxidation can be carried out by simply heating the raw soot in air or oxygen-containing atmosphere [69, 147, 149, 157, 158, 249, 251, 252, 268, 287, 288, 290, 292, 295-302]. In a slight modification of this procedure, some groups have subjected the raw soot to microwave treatment in air [253, 303]. It is important to choose the proper temperature for oxidation, so as to minimise the burning of the CNTs themselves in the process. This can be done by carrying out a thermo-gravimetric analysis (TGA) of the raw material: initially, the non-CNT carbon gets oxidised and only at a slightly higher temperature does the degradation of the more stable CNTs begin. The temperature for carrying out the oxidation, then, would be slightly below this cross-over temperature at which the gradient of the curve changes. Once the carbon covering the metal particles is consumed, the exposed metal can be removed by subjecting the material to an acid treatment, such as with HCl, HNO_3, H_2SO_4 or HF. If the metal catalyst-free CNT material is now subjected

to TGA, the degradation temperature for the CNTs may be observed to be noticeably higher than before the purification [143, 145, 154, 162, 249-251, 253-256, 261, 268, 297, 300, 302, 304-307]. This is owing to the fact that the metal catalyst nanoparticles present in as-prepared material catalyze the oxidation, causing it to begin at a lower temperature [300, 301], and that purification by oxidation can lead to the loss of small-diameter CNTs, which would burn at lower temperatures (more below).

A variation of this method is the vapour-phase sulphidation of non-CNT impurities [308], which has been shown to be suitable for employing directly on CNT devices as it is less corrosive than oxidation.

Liquid-phase oxidation methods include stirring at a slightly high temperature, refluxing or sonicating the raw soot in oxidising acids like HNO_3 [69, 99, 108, 141-149, 151, 153, 154], H_2SO_4, or a mixture of the two [149, 151, 155], or in oxidising media such as acidic $KMnO_4$ [156-158], or H_2O_2 [69, 159-162]. While treatment with oxidising acids simultaneously removes the exposed metal catalyst particles, the $KMnO_4$ method necessitates washing the material with HCl to remove the MnO_2 formed during the oxidation, as does the H_2O_2 method for eliminating the exposed metal.

The fact that metals can catalyse oxidation has, in fact, been used to advantage by some groups who have resorted to the external addition of gold nanoparticles [309] or iron particles [161] to assist the oxidation.

Although they are inexpensive and can purify gram-scales of CNTs at a time, a major disadvantage of the above methods of oxidation from the industrial processing point of view is that the time period required for them is very long, being anywhere between three hours to two days. Considerable reduction in processing time – as low as one hour – is one of the benefits claimed for a purification procedure based on microwave treatment, as is low power consumption. In this method, the as-prepared CNT material is subjected to microwave irradiation in oxidising acid, most commonly HNO_3 [259, 310-314], but HCl [310, 311] and H_2O_2 [312] have also been used. Once again, it is very important to determine the optimum processing temperature at which maximum removal of metal catalyst and minimum damage to the CNTs can be ensured. It is observed that, below this temperature, the dissolution of metal particles is ineffective while, above this

temperature, considerable etching of the CNTs takes place. Very high levels of purity in the final CNT product ($\geq$ 99%) [314] have been reported using this method.

Electrochemical routes have also been proposed for the selective oxidation of amorphous carbon in as-produced CNT soot [258]. Once again, the principle is the higher reactivity of the amorphous carbon compared to the CNTs. A major drawback, however, is that the electrochemical oxidation potential of the graphitic layers enclosing the metal catalysts is quite similar to the CNTs and, hence, a significant amount of metal remained behind in the material.

As an alternative to oxidation for the selective removal of amorphous carbon, high-temperature reductive treatments such as by hydrogen [151, 305], ammonia [153] and water vapour [315] have also been used. With the aim of minimising the production of amorphous carbon by *in situ* etching during the synthesis of CNTs itself, small amounts of hydrogen [159, 252, 299] or water vapour [316, 317] have been included in the gaseous feed to, or atmosphere within, the reactor. While hydrogen reduces the more reactive amorphous carbon into volatile hydrocarbons, water vapour removes the carbon via the water gas shift reaction, leaving the stable CNTs in a highly pure state. For CVD synthesis of CNTs, the incorporation of controlled amounts of water vapour or hydrogen in the feedstock has been reported to yield thick forests of aligned, very high quality CNTs, which is of great relevance to applications such as optoelectronics.

Carbon nanotubes were first reported to be synthesised by the arc-discharge method [1, 6, 7]. Arc-discharge also leads to the by-production of a considerable amount of multi-layer graphitic "buckyonions", either empty or enclosing metal catalyst particles. Unsurprisingly, the problem of purification of arc-discharge CNTs by eliminating graphitic impurities has been the focus of researchers from the very outset, and has proved a major challenge, given that the reactivity of graphite is not very different from that of the CNTs themselves. To this end, graphite intercalation has been attempted. Copper iodide [318], bromine [319-321] and potassium [304] have been used as intercalating agents. The more rigid structures of CNTs (if multi-wall) cannot be intercalated. The exfoliated graphite can then be either selectively oxidised or washed away.

The importance of eliminating the carbon covering on the metal nanoparticles before attempting the removal of the latter can hardly be overstated: if due attention is not given, it may not be achieved at all [258].

2.1.4 Damage to pristine CNTs by purification procedures

It is now well-documented that chemical purification methods such as oxidative treatments inflict damage on CNTs including opening of end-caps [151, 155-157, 229-231, 259, 262, 289, 305, 311, 314, 315, 319, 320, 322], shortening [108, 143, 158, 289, 297], creation of defect sites such as vacancies and oxygen-containing functional groups on the CNT walls [142, 149, 155, 158, 165, 262, 265, 267, 323-325] and burning away of small diameter (and hence, more reactive) tubes [149, 262, 326-329]. While liquid-phase oxidising treatments carried out even under very mild conditions will cause some modification of the pristine CNTs [261, 262], gas-phase oxidation will cause damage to CNTs only above a threshold temperature, and the extent of side-wall modification will be much lesser than in the former instance [328]. Although opening of CNT tips is a modification from their pristine structure, it may, however, be necessary if the metal catalyst enclosed within the tip of the CNT (as frequently occurs for CVD-grown CNTs) is to be removed. Liquid-phase oxidation treatments can also lead to the formation of fragments of carbon, possibly attached to carboxyl groups [141], which may remain as a disordered coating on the CNTs [143, 144, 148, 248, 261, 310, 311, 329].

Even ultrasonication, which is often used to assist in the dispersion of CNT bundles and to separate them from metal catalyst particles for their efficient removal, can lead to damage of the CNT walls [101, 102].

While some amount of damage to CNTs as a result of purification may be inevitable, attempts have been made to reverse this, with varying degrees of success. Amorphous carbon produced as a result of oxidising acid treatments can be removed by air oxidation [99, 143, 145-148, 311]. Alternatively for this purpose, or for removing the defects and functional groups introduced during the purification, the CNTs can be annealed at high temperature (though under 1000°C) in an inert gas [148, 153, 304, 330], or in vacuum [254, 267, 305]. In fact, vacuum annealing at temperatures as low as 800°C has been reported to re-seal open tips of SWNTs [331, 332].

Further, annealing in vacuum or in an inert atmosphere at or above 1600°C has been found to be effective in purifying MWNTs by removing non-CNT carbon and even metal catalyst, although the mechanism for this is not known at present. Annealing at such high temperatures is also capable of producing re-graphitisation and re-ordering of defects, leading to MWNTs of high crystallinity [256, 333]. For, SWNTs, however, it has been reported that vacuum annealing at such elevated temperatures (> 1600°C) can lead to enlargement of diameters and even coalescence of SWNTs into MWNTs [334, 335]. The coalescence is believed to start from vacancies in the SWNT walls, triggering off a continuous re-organisation [336].

2.1.5 Choice of purification method

The choice of purification method will be governed by the cost, scale and the targeted end-application of the purified CNTs. Chemical purification routes have the advantage of low cost, low power consumption and applicability to large scales, but invariably produce some defects on the CNTs, although these may be reversed to some extent. Indeed, for some applications such as polymer composites, a small amount of defects on the CNTs may prove to be advantageous, as they ensure better dispersion in the polymer matrix. Most physical purification routes do not cause damage to the CNTs, but may not match the scalability of chemical routes.

2.2 Results and discussion

2.2.1 Impossibility of devising standard recipes for purification

The thermogravimetric analysis (TGA) in air of as-received SWNT material shows that there is a residual content of metal (iron) catalyst particles of around 15-20 weight %. For example, Curve 1A in Figure 2-1 shows the TGA profile of one batch (Batch 1) of as-received SWNTs (1A-SWNTs) obtained from Carbon Nanotechnologies,

Inc. (CNI), Houston TX, USA (see Section 7.1). The metal nanoparticles can be expected to be enclosed by a layer of amorphous carbon. This is confirmed by the fact that, upon soaking the as-received material in 6M HCl, the acid is not observed to turn yellow, which would have been the case upon dissolution of metal in the acid. Further, after this SWNT material was filtered and washed to remove the acid, TGA in air does not show a change in the residual weight *per cent*, indicating that virtually no removal of metal has taken place.

From Figure 2-1, it can be seen that there is a rapid weight loss of the as-received material after and above 350°C. Thus, the procedure employed for purification of the 1A-SWNTs involved heating in air at 350°C for 1h to remove the amorphous carbon, followed by soaking the material for 6h in 6M HCl (such that the overall concentration of the solids in the suspension was 0.25 g/mL) to dissolve the metal catalyst nanoparticles, and finally filtering the suspension over a polycarbonate membrane filter (pore size 0.2 μm) and washing with copious amounts of deionised water to remove the acid.

The yield at the end of the air oxidation step was around 90% by weight. The SWNTs subjected to all three steps described above are referred to as 1B-SWNTs. The TGA of the 1B-SWNTs is shown by Curve 1B in Figure 2-1. It can be seen that the residual weight in the purified SWNTs is around 3.5 weight %, indicating a significant reduction in the content of metal by the purification process. Also, as a result of the removal of amorphous carbon, the burning of the purified material begins at a higher temperature than the as-received 1A-SWNT material. The thermal degradation of the SWNTs also continues up to a much higher temperature (over 700°C, compared to the 600°C for as-received sample). This can be explained in terms of the higher content of metal nanoparticles in the 1A-SWNT material, which catalyse the oxidation of the nanotubes.
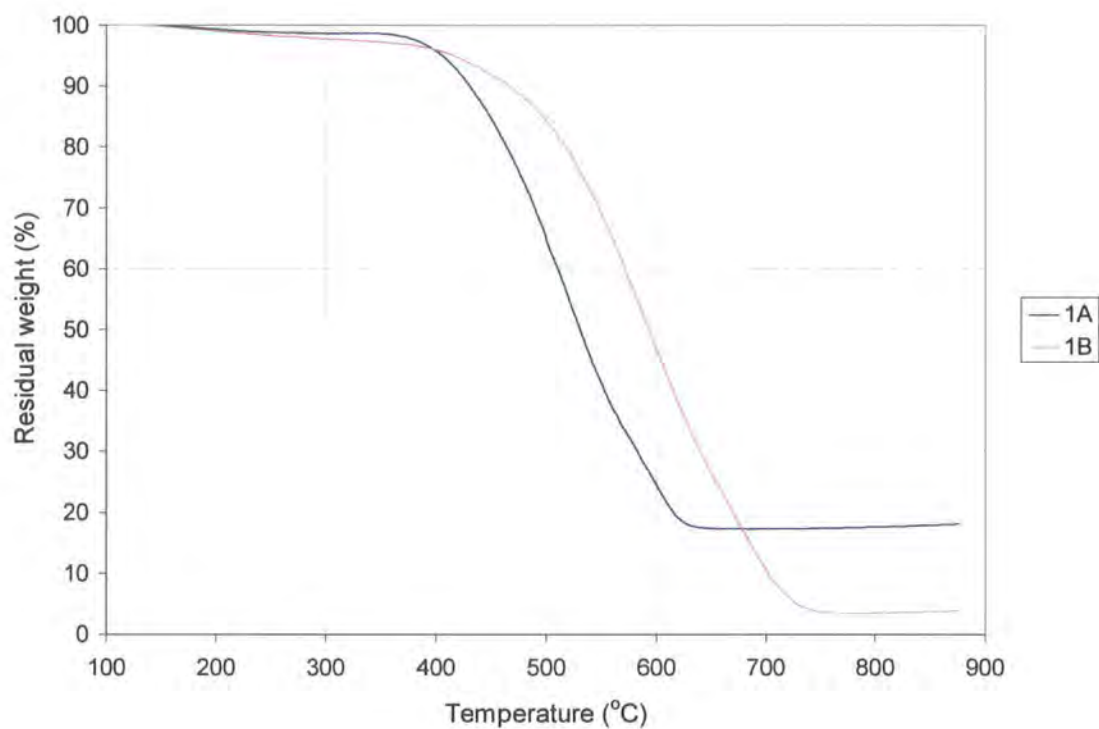
Figure 2-1

TGA in air of (1A) as-received SWNT material of Batch 1, and (1B) the SWNTs labelled 1A subjected to a
purification process. The samples were heated from room temperature to 1000°C at a rate of 10°C/min.

However, when the similar procedure was attempted for another batch (Batch 2)
of SWNTs, the TGA curves shown in Figure 2-2 were obtained.
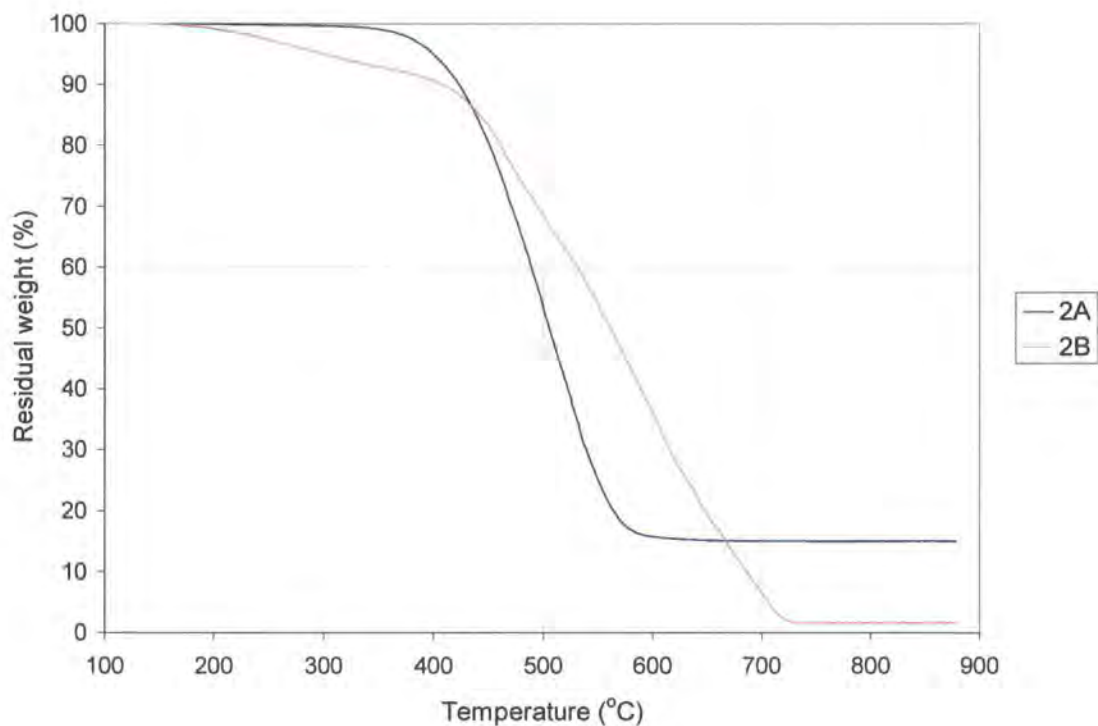
Figure 2-2

TGA in air of (2A) as-received SWNT material of Batch 2, and (2B) the SWNTs labelled 2A subjected to a purification process. The samples were heated from room temperature to 1000°C at a rate of 10°C/min.

The TGA profile of the as-received 2A-SWNTs is quite similar to that of 1A-SWNTs. In particular, the thermal degradation begins at around the same temperature *i.e.*, 350°C, justifying the choice of temperature for the initial air oxidation step in the purification process for this batch too. The yield after the air oxidation was around 90%, similar to that for the 1A-SWNTs. Once again, there is a considerable reduction in the metal content present in the as-received material, with the residual weight in the purified material being only 1.7%. It can, therefore, be safely concluded that the air oxidation step was able to crack open the carbon layers enclosing the metal nanoparticles, enabling their efficient leaching by the HCl.

However, it is clear from the considerable weight loss of over 10% before 400°C in Curve 2B of Figure 2-2 that the amorphous carbon has not been eliminated by the

purification. This would suggest that, for this batch of SWNT material, the air oxidation is able to crack the carbon coating on the metal nanoparticles into smaller fragments, thereby exposing the metal, but the duration of the step was insufficient to effect the complete burning of all the amorphous carbon. In order to address this issue, two approaches were tried: a) refluxing the SWNT material in NaOH solution to exfoliate the amorphous carbon, followed by washing in HCl to neutralise the NaOH; and b) increasing the duration of the air oxidation step.

Treatment with strong bases has been previously reported to exfoliate non-nanotube carbon and remove metal catalyst from SWNT material [291, 292, 304]. 2A-SWNTs were first heated in air at 350°C for 1 h, then refluxed in 6M NaOH solution at 120°C for 12 h, and then stirred in 6M HCl at room temperature for 6 h to neutralise the base. They were then filtered and washed as above to yield 2B'-SWNTs. As a control, as-received 2A-SWNTs were refluxed in 6M NaOH solution and stirred in 6M HCl without the air oxidation step (2B''-SWNTs). The TGA profiles of these materials are shown in Figure 2-3.
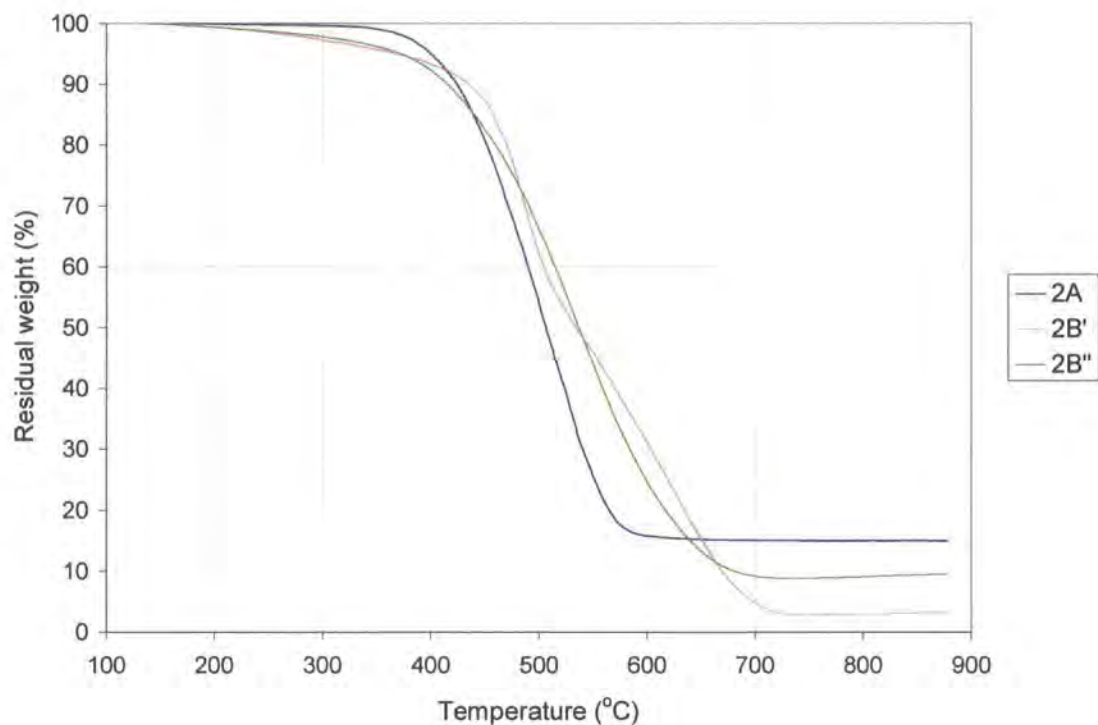
Figure 2-3

TGA in air of 2A-, 2B'- and 2B"-SWNTs. The samples were heated from room temperature to 1000°C at a rate of 10°C/min.

Alkali treatment is able to exfoliate the amorphous carbon to some extent, enabling a partial removal of metal catalyst from the as-received SWNT material. It can be seen from Curve 2B" in Figure 2-3 above that not only is the residual metal content lower than in case of the as-received 2A-SWNTs but the thermal degradation continues up to a much higher temperature, indicating reduced catalytic enhancement of the oxidation process by the metal catalyst. It has been previously reported [258] for arc-discharge CNTs that chemical treatment with alkali solutions fails to remove a considerable portion of the metal content in as-synthesised CNT material. Also, it can be seen from Curve 2B" that a significant amount of amorphous carbon does remain behind after the purification. If the alkali treatment is carried out after the air oxidation step (Curve 2B'), then a greater reduction in metal content is achieved, but a considerable

amount of amorphous carbon nevertheless remains behind after the purification process, as evident from the weight loss of around 8% before 400°C. In view of the fact that, even after a tripling in the processing time the amount of amorphous carbon has not been reduced to acceptable levels, it would appear that no purpose is served by an alkali treatment step in the purification process for CVD CNTs.

A far more satisfactory reduction in amorphous carbon content (together with efficient removal of metal catalyst) was observed upon increasing the duration of the air oxidation to 2 h for the SWNT material of Batch 2. However, the yield at the end of the air oxidation step was only around 75% (compared to around 90% when the duration is only 1 h), suggesting that some small-diameter SWNTs as well as the end-caps of many remaining SWNTs may have been burned away as a result of the prolonged oxidation. The SWNTs thus purified are labelled 2C-SWNTs, and their TGA profile is shown in Figure 2-4 (the 2B-SWNTs are also shown for comparison).
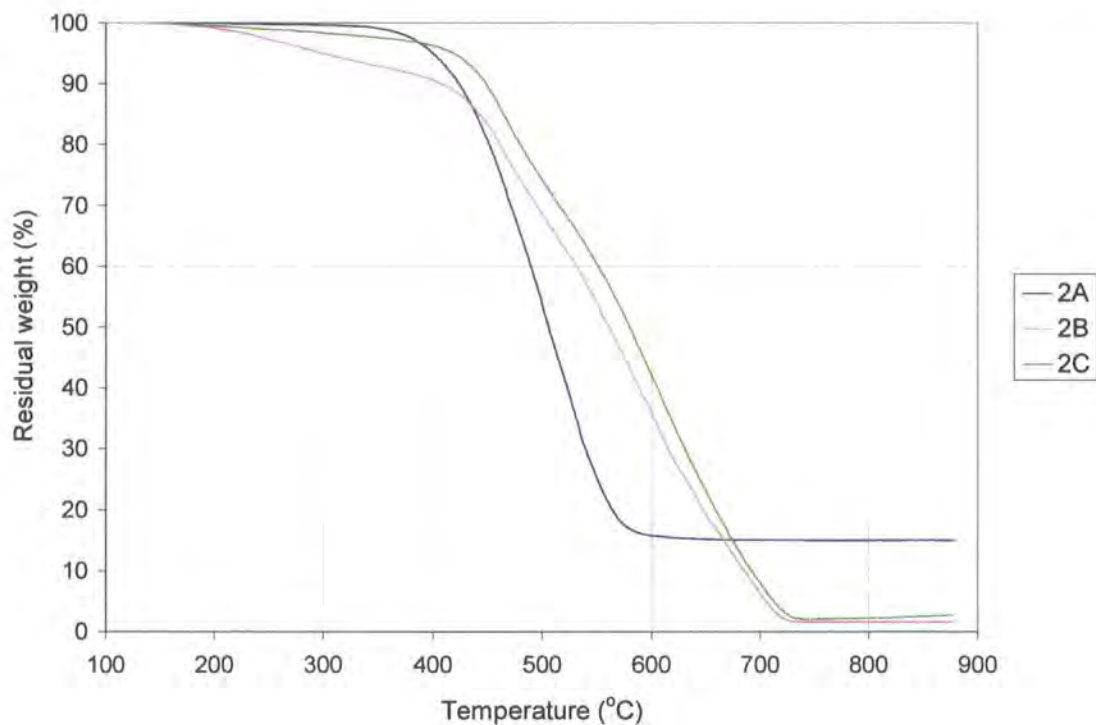
Figure 2-4

TGA in air of 2A-, 2B- and 2C-SWNTs. The samples were heated from room temperature to 1000°C at a rate of 10°C/min.

These results clearly illustrate that there is no "standard" procedure that can be applied to different batches of CNTs, even when they have been synthesised by the same process, and even when TGA analysis gives almost identical burning profiles for material from different batches. The purification process must be re-evaluated for each individual batch, and the purity of the SWNT material must be rigorously evaluated before further studies are carried out on them.

The purified 1B- and 2C-SWNTs, which have an amorphous carbon content of less than 3 weight *per cent* and a residual metal catalyst content of less than 4 weight *per cent* have been used in the remainder of the studies described in this thesis, and are hereafter referred to as Pur-SWNTs.

2.2.2 Amorphous carbon debris from liquid-phase oxidative purification

Purification by treatment with oxidising acids may be regarded as having the two-fold advantage of removing non-nanotube carbon and also providing a useful starting point for further chemistry by creating carboxylic acid groups on the CNT walls. 1B-SWNTs were refluxed in a mixture of sulphuric and nitric acids to give 1B-ox-SWNTs. Some 1B-ox-SWNTs were further refluxed in NaOH solution, then washed and filtered, whereupon a reddish-brown filtrate was obtained. The base-treated SWNTs were stirred in HCl solution to neutralise the base, and then filtered and washed to yield 1B-ox'-SWNTs. Refluxing the 1B-ox'-SWNTs once again in NaOH solution did not result in a reddish-brown filtrate. As a control, purified 1B-SWNTs that had not been subjected to any oxidising acid treatment were refluxed in NaOH solution, then washed and filtered, to yield a colourless filtrate. The SWNTs were then stirred in HCl solution to neutralise the base, and then washed and filtered, whereupon they are labelled as 1B-nox-SWNTs. The SWNTs were characterised by Raman spectroscopy and thermogravimetric analysis-mass spectrometry (TGA-MS).
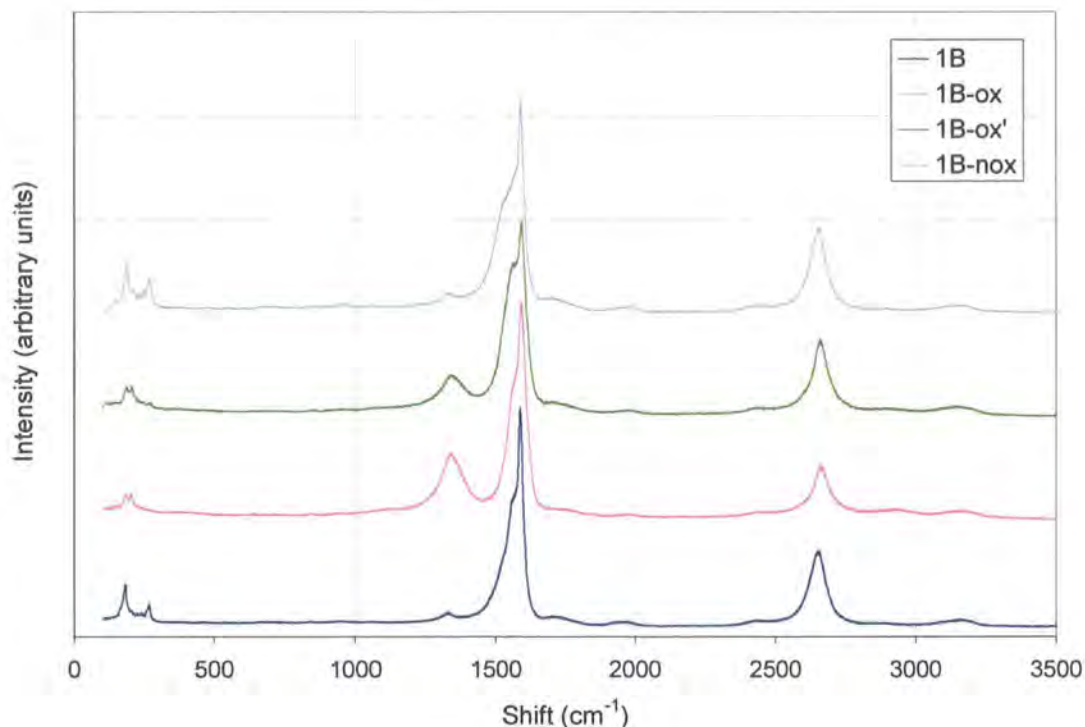
Figure 2-5

Raman spectra of the various SWNT samples. The wavelength of the laser used for excitation was 532 nm.

The Raman spectra of the SWNT samples are shown in Fig. 2-5. The low-energy features in the range 100-250 cm^{-1} correspond to the radial breathing of the nanotubes. The diameter, d (nm), of a nanotube is inversely related to the frequency of its radial breathing mode (RBM) peak, ω_r (cm^{-1}), as $d = 223.75 / \omega_r$ [355]. It can be seen from Figure 2-5 that some RBM peaks, especially that located at approximately 270 cm^{-1} (corresponding to nanotubes of diameter around 0.83 nm), present in the spectrum of 1B-SWNTs are absent in those of the 1B-ox-SWNTs and 1B-ox'-SWNTs, but present once again in the spectrum of the control 1B-nox-SWNTs. Thus, as expected, treatment with oxidising acids has led to the degradation of small diameter SWNTs, although refluxing in alkali does not appear to have done so. The band at around 1590 cm^{-1} is owing to the in-plane vibrations of sp^2-hybridised graphitic carbon, and hence is called the tangential or G-band. Defects and functional groups on the walls or ends of the CNTs, or

60

amorphous carbon give rise to the so-called disorder (D-) band corresponding to sp^3-carbon, which is located around 1340 cm^{-1}. The areal ratio of the intensities of the D-band to the G-band (I_D/I_G) is, therefore, a measure of the extent of defects or functional groups present on the CNTs. The ratios for the four samples are given in Table 2-1.

Sample	I_D/I_G
1B-SWNTs	0.02
1B-ox-SWNTs	0.25
1B-ox'-SWNTs	0.14
1B-nox-SWNTs	0.02

Table 2-1

The areal ratios (I_D/I_G) of the intensities of the disorder (D-) band to the graphitic tangential (G-) band of the SWNT samples.

The I_D/I_G ratio increases upon acid treatment (0.24 for 1B-ox-SWNTs as against 0.02 for 1B-SWNTs). However, this could be owing either to the formation of functional groups on the CNT walls or the presence of amorphous carbon debris. Additionally, the I_D/I_G ratio for 1B-ox-SWNTs is 0.25, whereas it is only 0.14 for 1B- ox'-SWNTs. Thus, there is a clear decrease in the intensity of the D-band of the oxidised SWNTs following the NaOH treatment, which may be the result of the removal of the amorphous carbon debris by the NaOH. But the I_D/I_G ratio of the oxidised SWNTs after base-treatment (1B-ox'-SWNTs) is nevertheless an order of magnitude higher than that for the starting 1B-SWNTs. This is very different from the recent reports of Verdejo *et al.* [263] and Salzmann *et al.* [264], who had found a near-complete reversal in the increase of the D-band upon

alkali treatment, which had led them to conclude that the carboxylic acid groups were mostly associated with the amorphous carbon debris. Further evidence that the oxygen-containing functional groups may be attached directly to the CNT walls is provided by thermogravimetric analysis-mass spectrometry (TGA-MS).

It has been reported that the thermal defragmentation of oxygen-containing functional groups, produced by the treatment with oxidising media, shall occur in the range 350-800°C, leading to the evolution of carbon dioxide (CO_2) as one of the defragmentation products [267, 324]. Thus, TGA-MS may be a useful tool to probe the effect of oxidising acid treatment on CNTs. A slight weight loss corresponding with the evolution of CO_2 (44.01 amu) can be observed in the TGA profile for the 1B-SWNTs (Fig. 2-6(i)), as some residual functional groups can be expected to be present on purified SWNTs as a result of the oxidation step in the purification process. For the 1B-ox-SWNTs that have been oxidised by acid treatment, two distinct regions for the evolution of CO_2 can be seen (Fig. 2-6(ii)). The peak at a temperature as low as 250°C can be explained in terms of the carboxylic acid groups associated with the amorphous carbon produced by the degradation of the SWNTs by the acid, which decompose at a much lower temperature than the groups directly on the SWNT walls, which are relatively stabler to thermal degradation than the amorphous carbon. The weight loss for the 1B-ox-SWNTs (~27%) is much higher than for the purified 1B-SWNTs (~17%), indicative of the introduction of functional groups introduced by the acid treatment. When the 1B-ox-SWNTs are refluxed in NaOH, it is this carboxylated amorphous carbon which dissolve in the base and results in a reddish-brown filtrate. After refluxing in NaOH, it can be seen that this low-temperature evolution of CO_2 is almost completely reduced, as a result of the removal of the amorphous carbon. When the alkali treatment was repeated, no further formation of coloured filtrate was observed, indicating that the amorphous carbon debris had been almost entirely removed. Significantly, the weight loss of the 1B-ox'-SWNTs (Fig. 2-6(iii)) is approximately the same as for the 1B-ox-SWNTs (~27%), which clearly suggests that most of the functional groups are associated with the SWNT backbone rather than the carbon fragments. The weight loss of the control 1B-nox-SWNTs (Fig. 2-6(iv)) is almost identical with that of the starting 1B-SWNTs, thus ruling out any oxidation being caused during the alkali treatment.
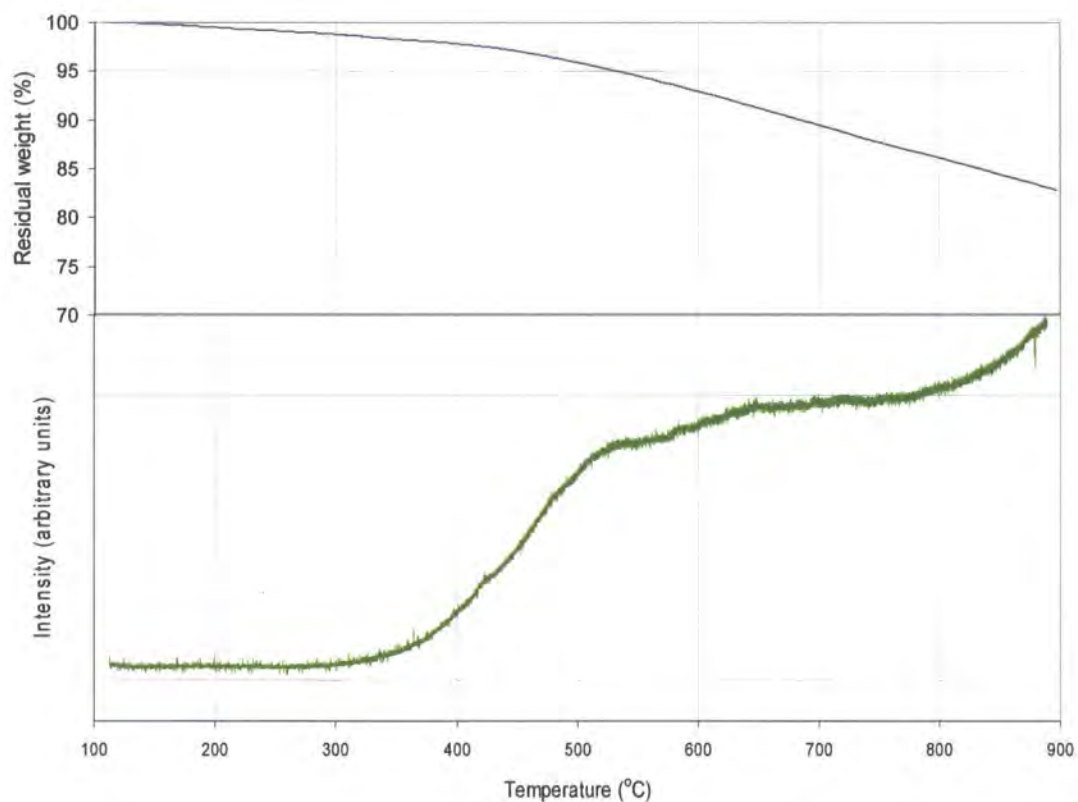
Figure 2-6

(i) (Above) TGA in helium and (below) the corresponding mass spectrometry data for the thermal evolution of CO_2 for purified 1B-SWNTs.
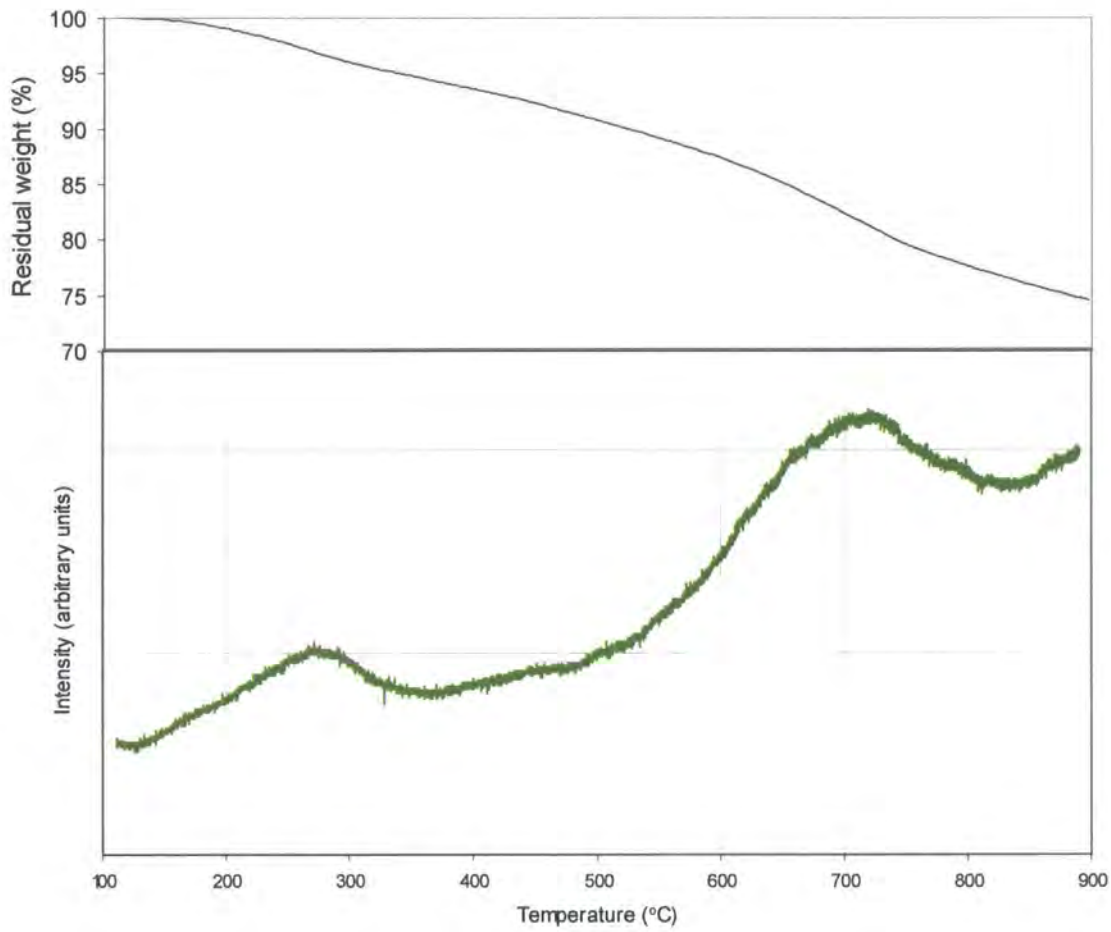
Figure 2-6

(ii) (Above) TGA in helium and (below) the corresponding mass spectrometry data for the thermal evolution of CO_2 for 1B-ox-SWNTs.
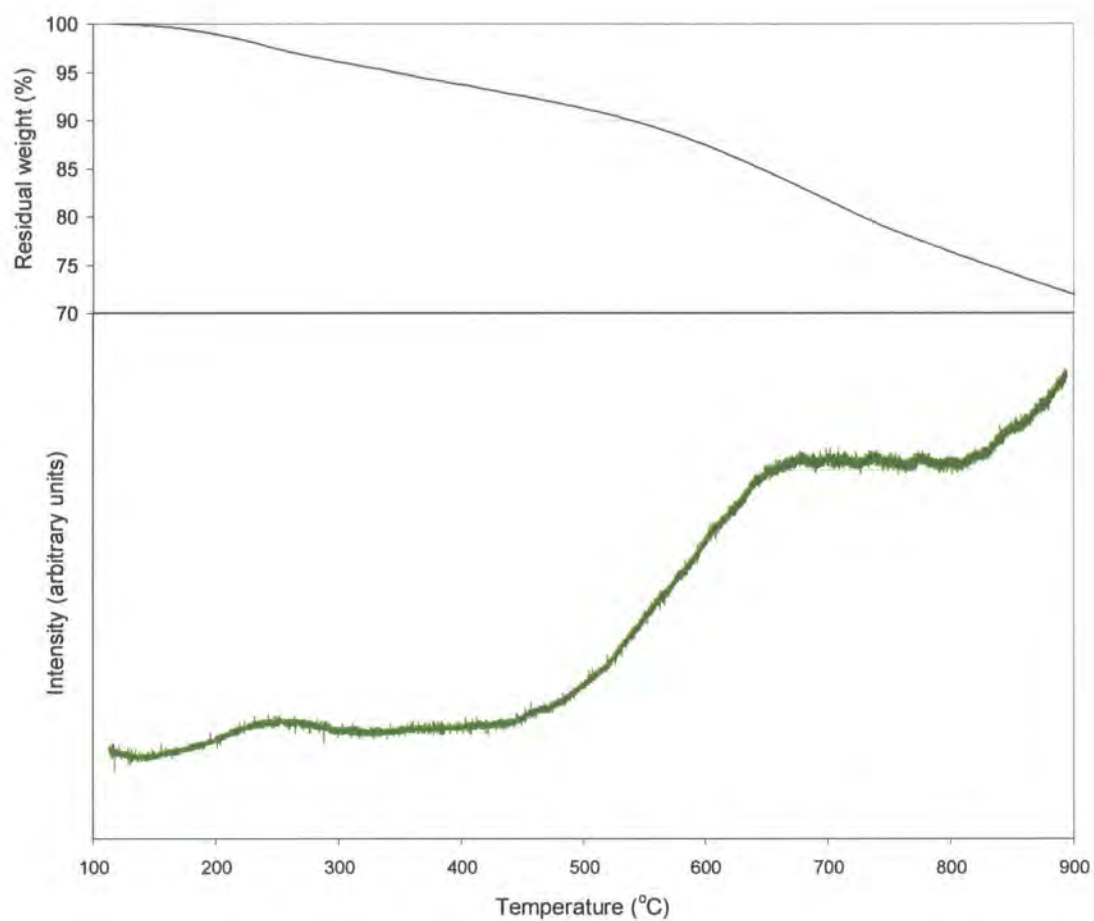
Figure 2-6

(iii) (Above) TGA in helium and (below) the corresponding mass spectrometry data for the thermal evolution of CO_2 for 1B-ox'-SWNTs.
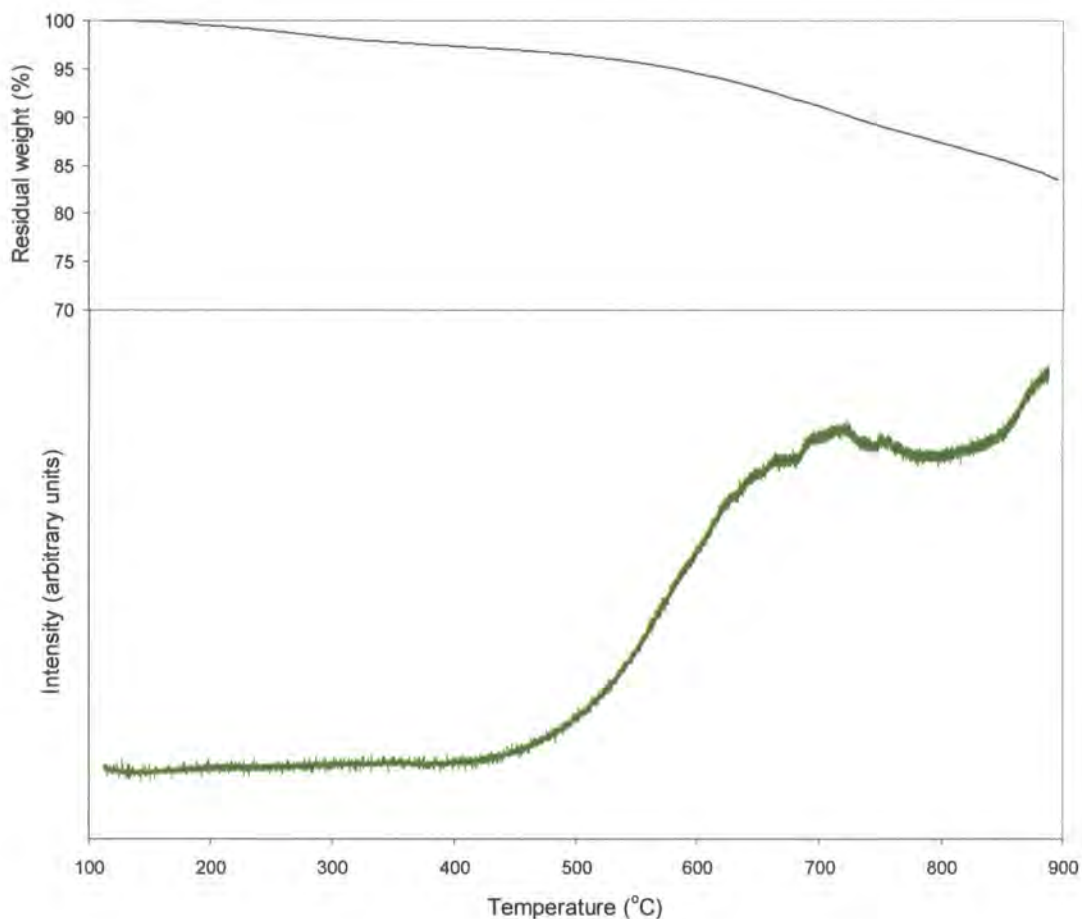
Figure 2-6

(iv) (Above) TGA in helium and (below) the corresponding mass spectrometry data for the thermal
evolution of CO_2 for 1B-nox-SWNTs.

Thus, our findings differ greatly from those of Verdejo and co-workers [263], and
Salzmann and co-workers [264], who had concluded that the enhancement in the I_D:I_G ratio
upon liquid-phase oxidation treatments is almost entirely owing to the formation of
amorphous carbon debris, and that very few, if any, functional groups are created directly
attached to the CNT walls, contrary to what was thought previously. We suggest that this
may be attributed to the difference in the purification procedures employed in the
aforesaid reports [263, 264], and in our study. Amorphous carbon is formed as a by-product

of CNT production, and is already present as a coating on nanotubes (and metal catalyst particles) in raw CNT material. As it is more reactive than the CNTs, it shall be the preferred site of chemical attack. Unlike Verdejo *et al.* [263] and Salzmann *et al.* [264], we have included a separate step in our purification procedure involving the heating of raw CNT material at high temperature in air, in order to oxidise and remove amorphous carbon (see Figure 1 *(a)* in Ref. 263) before *any* subsequent chemistry is carried out on the CNTs. Thus, when subjected to acid treatment, the CNT walls were accessible for oxidation, and functional groups were created directly on the walls. At the same time, some amorphous carbon is also generated from the degradation of the SWNTs by the oxidising acid, which remains as debris and must be removed by treatment with NaOH. Thus, unlike what has been suggested recently [263, 264], we are able to confirm that oxidising acid treatment does lead to a significant functionalisation of CNT walls, and this route can be safely used for the carboxylation of CNTs and subsequent covalent derivatisation.

2.3 Conclusion

Some very important aspects of the purification of SWNTs have been studied. The significance of these results stems from the fact that purification processes constitute the starting point of most studies into the properties and applications of CNTs. From the point of view of the chemistry and spectroscopy of CNTs, the implications of these studies could potentially be profound.

Firstly, it was found that heating raw CNTs in air may be an extremely important, and perhaps unavoidable, step for the elimination of amorphous carbon in any purification process for SWNTs. That it is extremely simple to carry out and easily scalable makes it attractive. If non-nanotube carbon in any as-produced CNT material is not eliminated, the metal catalyst nanoparticles present in the material cannot be efficiently removed in a subsequent chemical step, as the metal particles are enclosed by carbon layers. Also, it is very likely that the amorphous carbon that was not satisfactorily eliminated from the raw CNTs will be the preferred target of chemical attack in any

subsequent chemical modification, and the CNT walls may not be derivatised as intended.

Secondly, we are able to resolve a recent major controversy about the exact location of the oxygen-containing functional groups created by liquid-phase oxidising acid treatment of CNTs. Such treatments have been extensively used in the purification and chemical modification of CNTs as they are commonly regarded as having the two-fold advantage of removing non-nanotube carbon as well as creating carboxylic acid groups on the CNT walls, which are the starting point for the chemical derivatisation of the CNTs via amidation / esterification (see Chapter 1, Section 1.6.5.1). There is a great deal of published literature on the purification of CNTs by treatment with oxidising acids, and their carboxylic acid-based modification and spectroscopy. However, oxidising acid treatments inevitably cause some degradation of the nanotubes themselves, leading to generation of amorphous carbon debris, which may remain coating the nanotubes. In what could call a vast volume of literature into serious question, it has been very recently suggested [263, 264] that the carboxylic acid groups that were believed to have been created directly on the CNT walls, were actually associated with this debris. This could cast a doubt on the exact location of any further chemical derivatisation and, consequently, have serious implications for the spectroscopy of modified CNTs. We have been able to establish that treatment with oxidising acids, such as nitric, does indeed lead to creation of oxygen-containing functional groups directly attached to the CNT backbone, and not associated with the carbon debris. However, it is important to note that carbon debris is indeed generated by acid treatment of CNTs, which will remain on the surface of the CNTs if no attempt is made to expressly remove them, such as with alkali treatment.

Thirdly, there are numerous instances in the published literature of groups using previously reported recipes for the purification of CNTs, wherein the implicit assumption appears to be that the same purification process would be valid if the CNTs have been produced by identical methods or are from the same source. However, based on our study, we emphasise that, although the steps involved in the purification process may broadly be the same, previously reported recipes should not be treated as "standard"; the processing conditions in the purification procedure – such as temperature and time duration of the oxidation step – should be re-evaluated for the batch of CNTs being

studied at present. This is true for different batches of CNT material, even if the method used for synthesising the CNTs is the same, the macroscopic parameters of the synthesis process are kept the same, and analyses such as Raman spectroscopy and TGA yield very similar spectra for the different batches. This only underscores the inherent heterogeneity in CNT material, and the fact that present spectroscopic methods, or the models currently proposed to explain the growth of CNTs, do not yield an outright molecular-level picture of the CNTs and impurities present in the as-synthesised material.

3. MODIFICATION OF SINGLE-WALL CARBON NANOTUBES BY TERTIARY PHOSPHINES

3.1 INTRODUCTION

In attempts to realize the full potential of CNTs in nanoscale materials and devices, a problem of solubility is frequently encountered. CNTs have a tendency to aggregate together into bundles resulting in very low solubility in common solvents making their handling and processing difficult. It is no surprise therefore that considerable efforts have focused on producing stable dispersions of CNTs in both aqueous and organic solvents. Non-covalent routes for solubilising CNTs has been reviewed in depth in Chapter 1, Section 1.6.4. Briefly, CNTs can be solubilised in water by wrapping the nanotube in water-soluble polymers such as poly(vinyl pyrrolidone) [114] and poly(acrylic acid) [117], or by the π-stacking of ionic pyrenes (or other polycyclic aromatic compounds) onto the nanotube surface [138, 140]. The same methodology, using appropriate polymers, can be used to solubilise CNTs in organic solvents [116]. Similarly, stable CNT dispersions in aqueous media can be achieved using anionic (sodium dodecyl sulphate, SDS), cationic (dodecyltrimethylammonium bromide, DTAB) or non-ionic (Triton X) surfactants [113]. Alternatively CNTs can be solubilized in both organic and aqueous solvents by employing synthetic strategies that use covalent chemistry (Chapter 1, Section 1.6.5).

However, whilst non-covalent routes, such as the use of surfactants, polymer-wrapping and π-stacking of molecules, can have a dramatic effect on solubility they have the obvious disadvantage of rendering the CNT surface inaccessible therefore inhibiting further chemistry or interactions. On the other hand, covalent functionalization can disrupt the intrinsic electronic structure of the CNTs, thereby compromising their exciting properties [103, 104, 163, 178, 188, 192-194, 204, 208, 224]. The challenge, therefore, is to achieve sufficient modification of the CNT surface to ensure ease of processing, while avoiding significant degradation of electronic structure.

The chemistry of fullerenes and CNTs suggests that they can behave as electron-deficient systems, susceptible to nucleophilic reactions. Amines are nucleophilic species, as they have a lone-pair of electrons on the nitrogen atom. It was observed that there is indeed an interaction between SWNTs and ammonia [79]. Subsequently, there have been several studies on the non-covalent modification of CNTs by alkylamines, leading to enhanced solubility of the nanotubes [228, 260, 337-339]. However, the adsorption of amines could be easily reversed, and the amines desorbed with time.

Tertiary phosphines have been extensively used for capping nanoparticles and improving their solubility by preventing aggregation. Similar to the nitrogen atom in amines, these molecules also have a lone-pair of electrons on the phosphorus atom. Here we report a simple, solvent-free, low level non-covalent and non-destructive modification of SWNTs by triphenyl- $[P(C_6H_5)_3]$ and trioctyl- $[P(C_8H_{17})_3]$ phosphines [356]. The choice of these tertiary phosphines is governed by their stability (many other phosphines such as PH_3 or trimethylphosphine, $P(CH_3)_3$, are highly pyrophoric). Besides, they are inexpensive and very commonly used in the laboratory. The modified SWNTs showed greater ease of exfoliation and solubility in organic solvents as compared to pristine SWNTs.

3.2 Results and discussion

SWNTs produced by the HiPCO process [19] were purified as described in Chapter 2 (Pur-SWNT). In order to remove the oxygen-containing functional groups from the CNT walls that may have been introduced during the purification process, the material was annealed under vacuum at 900°C for 8 hours (Ann-Pur-SWNT). The purified, annealed SWNTs were then treated at 90°C with either molten triphenylphosphine (PPh₃) or tri-*n*-octylphosphine (POc₃) 90°C under nitrogen to produce SWNT-PPh₃ and SWNT-POc₃ respectively, as shown in Figure 3-1.
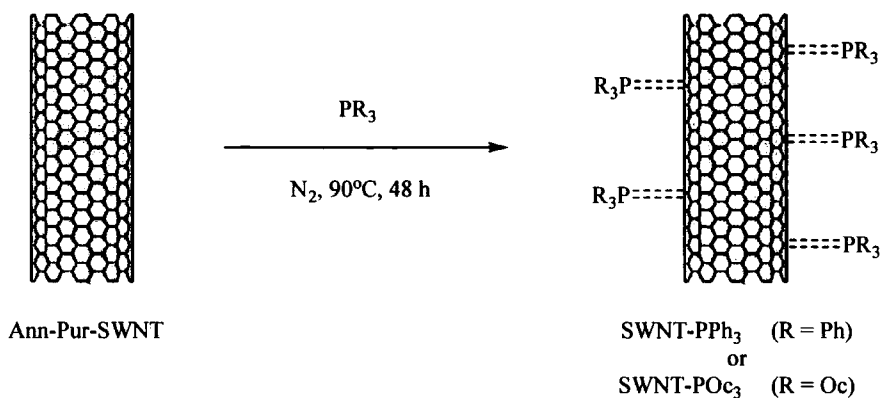
Figure 3-1

Modification of SWNTs by triphenylphosphine (PPh$_3$) or tri-n-octylphosphine (POc$_3$).

X-ray photoelectron spectroscopy (XPS), Ultraviolet-visible-near infrared (UV-vis-NIR) spectroscopy, Raman spectroscopy, thermogravimetric analysis (TGA), and atomic force microscopy (AFM) have been employed to characterize the functionalized material. Significantly, Raman spectroscopy and Ultraviolet-visible-near infrared (UV-vis-NIR) spectroscopy show minimal perturbation of the electronic structure of the SWNTs upon modification. AFM analysis shows considerable debundling of the SWNTs as a result of the modification. XPS suggests that the interaction between the phosphine molecules and the SWNTs may be via the lone-pair of electrons on the phosphorus. Bulk electrical transport properties of films of nanotubes measured by a four-point apparatus also show a significant change in the resistance of the modified SWNTs.

3.2.1 Enhancement of solubility

Interestingly, the treatment of SWNTs with the tertiary phosphines resulted in significant improvements in the dispersion of the carbon nanotubes in organic solvent. Ann-Pur-SWNTs, SWNT-PPh$_3$ and SWNT-POc$_3$ were suspended under mild bath sonication (Ultrawave U50, 30–40 kHz) for 15 min in absolute ethanol such that the

overall concentration of the suspensions was 0.1 mg/mL, and the suspensions were allowed to stand for 48 h. The improved solubility of SWNT-PPh$_3$ and SWNT-POc$_3$ in ethanol can be readily observed in the optical photographs taken after 48 h, displayed in Figure 3-2. It is clear that while the Ann-Pur-SWNT material starts aggregating shortly after sonication, the phosphine-treated samples form stable suspensions for several days.

Figure 3-2

Optical photographs of suspensions in absolute ethanol of (from left) Ann-Pur-SWNTs, SWNT-PPh$_3$ and SWNT-POc$_3$. The suspensions were obtained by mild bath sonication of SWNTs in ethanol, and allowed to stand for 48 hours.

In order to further support the enhanced dispersion properties of the phosphine-treated SWNTs in organic solvents, an AFM analysis of suspensions of the nanotube samples on a mica surface was carried out. The nanotube samples were suspended under mild bath sonication for 5 min in DMF, while maintaining an overall concentration of 0.03 mg / mL. The suspensions were allowed to stand for 1 h, after which 2 μL of clear supernatant was pipetted, drop cast onto freshly cleaved mica, and the solvent evaporated under a gentle stream of nitrogen. Figure 3-3 shows three representative AFM images of *(i)* Ann-Pur-SWNT, *(ii)* SWNT-PPh$_3$, and *(iii)* SWNT-POc$_3$ samples. It is evident that the untreated nanotubes, Ann-Pur-SWNT, are present as larger bundles when compared with SWNT-PPh$_3$ and SWNT-POc$_3$. Histograms showing the diameter distribution,

73

determined by measuring the heights of the individual bundles observed in the AFM height images are also shown. The mean diameter of the bundles in the two samples are calculated to be 16.0 nm, 6.1 nm and 5.6 nm for Ann-Pur-SWNT, SWNT-PPh$_3$ and SWNT-POc$_3$ respectively, clearly demonstrating a significant debundling in phosphine treated SWNTs which is presumably responsible for the improved dispersion of the material in common organic solvents.
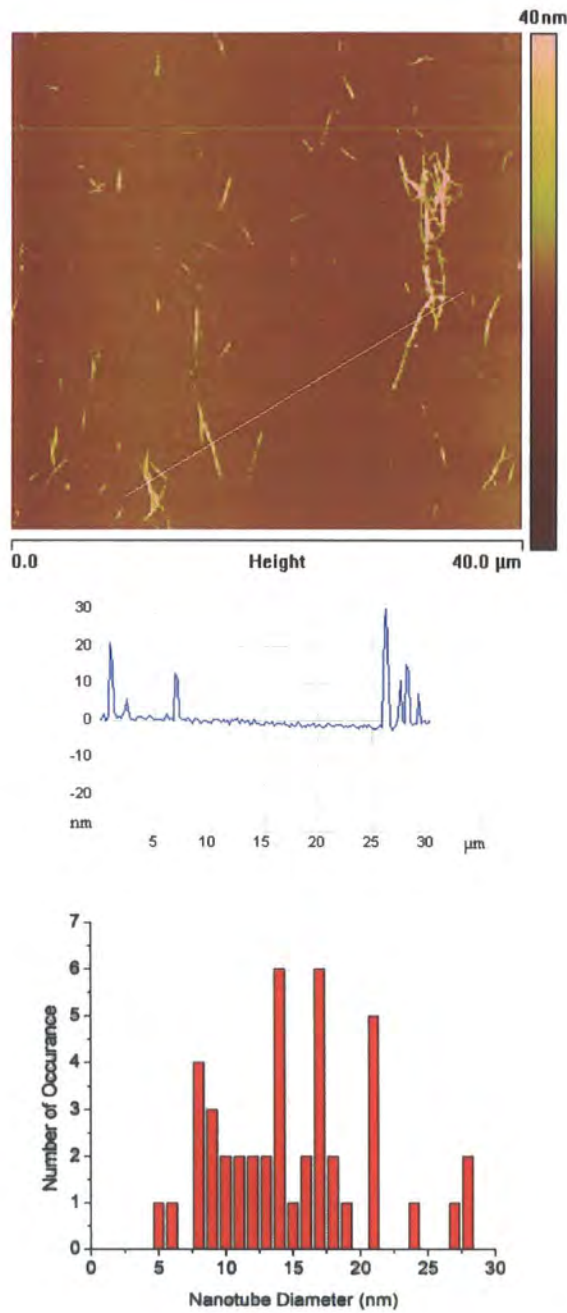
Figure 3-3

(i) (From top to bottom) A representative tapping mode AFM height image of pristine Ann-Pur-SWNT, diameters of nanotube bundles along the section marked by the white line, and histogram showing the diameter distributions.
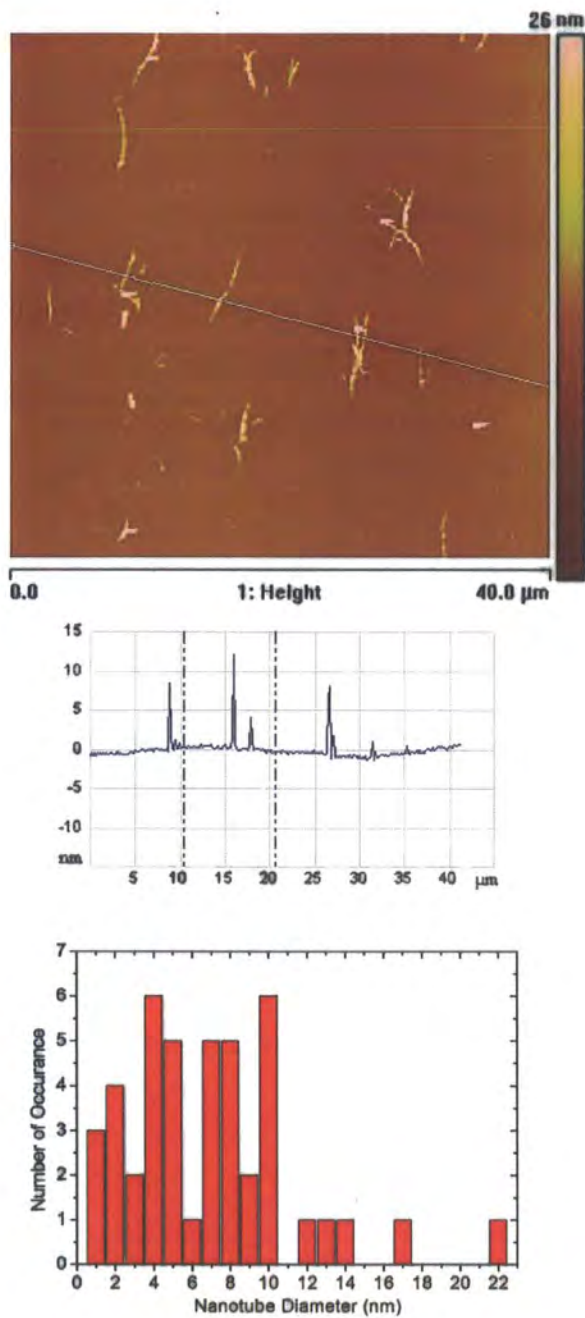
Figure 3-3

(ii) (From top to bottom) A representative tapping mode AFM height image of phosphine-modified SWNT-PPh$_3$, diameters of nanotube bundles along the section marked by the white line, and histogram showing the diameter distributions.
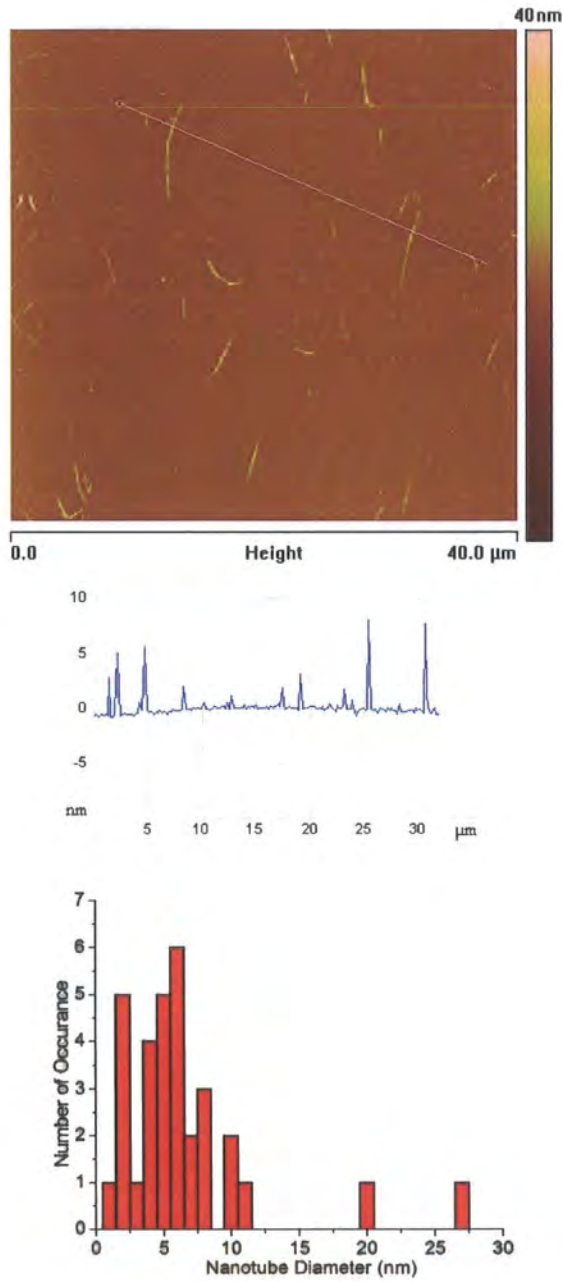
Figure 3-3

(iii) (From top to bottom) A representative tapping mode AFM height image of phosphine-modified
SWNT-POc₃, diameters of nanotube bundles along the section marked by the white line, and histogram
showing the diameter distributions.

3.2.2 X-ray photoelectron spectroscopy (XPS)

In order to probe the interaction of the tertiary phosphines with SWNTs the reacted material was studied by XPS. The XPS spectra are shown in Figure 3-4.
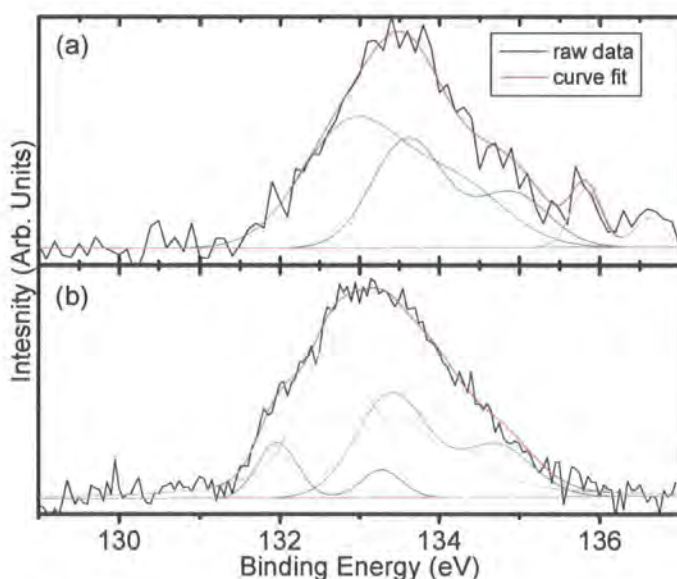
Figure 3-4

P 2p photoelectron spectra of SWNT samples treated with (a) triphenyl phosphine (SWNT-PPh₃) and (b) trioctyl phosphine (SWNT-POc₃). The red line represents the fitted curve to the experimental data (black), while the coloured peaks within the fitted curve represents the deconvoluted components.

XPS data recorded on SWNT-PPh₃ shows the presence of a broad peak associated with P 2p core electrons at a binding energy of approximately 133.5 eV (Figure 3-4 (a)). This value is approximately 2.6 eV shifted from the P 2p peak position expected for pure triphenylphosphine (130.9 eV) [340, 341]. This indicates that the phosphorus atoms present in the nanotube material are in a different chemical environment than those in the pure phosphine reagent. The binding energy is in line with that expected for a simple phosphine adduct such as PPh₃.BF₃, where the 2p₃/₂ binding energy has been reported to

have values between 132 – 133.2 eV [340, 341]. The broad nature of the P 2p peak can be understood by considering that the P 2p peak consists of two closely spaced (~1.3 eV apart) lines due to $2p_{3/2}$ and $2p_{1/2}$ electrons (which are unresolved in the current data) and may contribute, along with other factors such as inhomogeneity and the presence of more than one phosphorus environment, to the peak broadening. Deconvolution of the peak into its components shows the presence of two main doublets at 132.7 eV and 133.4 eV respectively, indicating signatures of a simple phosphine adduct or phosphorus (V)-like state [341]. While it is not possible to comment on the exact chemical nature of the interaction, the upward shift in the $2p_{3/2}$ binding energy of the phosphorous indicates that charge transfer between the electron donating phosphorus atoms and the carbon nanotubes may have taken place. Similar results were found for SWNT-POc₃, with the presence of a broad peak associated with P 2p core electrons at a binding energy of approximately 133.0 eV (Figure 3-4 (b)). Elemental composition analysis of the XPS data for SWNT-PPh₃ and SWNT-POc₃ show that the phosphorus content is approximately 0.1 atomic *per cent* for both materials.

Thermogravimetric analysis (TGA)

In order to follow the thermal desorption of the organic molecules from the CNTs, TGA was performed under helium. TGA data for SWNT-PPh₃ and SWNT-POc₃ (Figure 3-5) show a weight loss of up to ca. 20 wt.%, and 25 wt.% respectively, when compared to Ann-Pur-SWNTs, indicating the desorption of organic groups could correspond to as many as 0.9 and 0.8 tertiary phosphines per 100 carbon atoms for SWNT-PPh₃ and SWNT-POc₃ respectively.
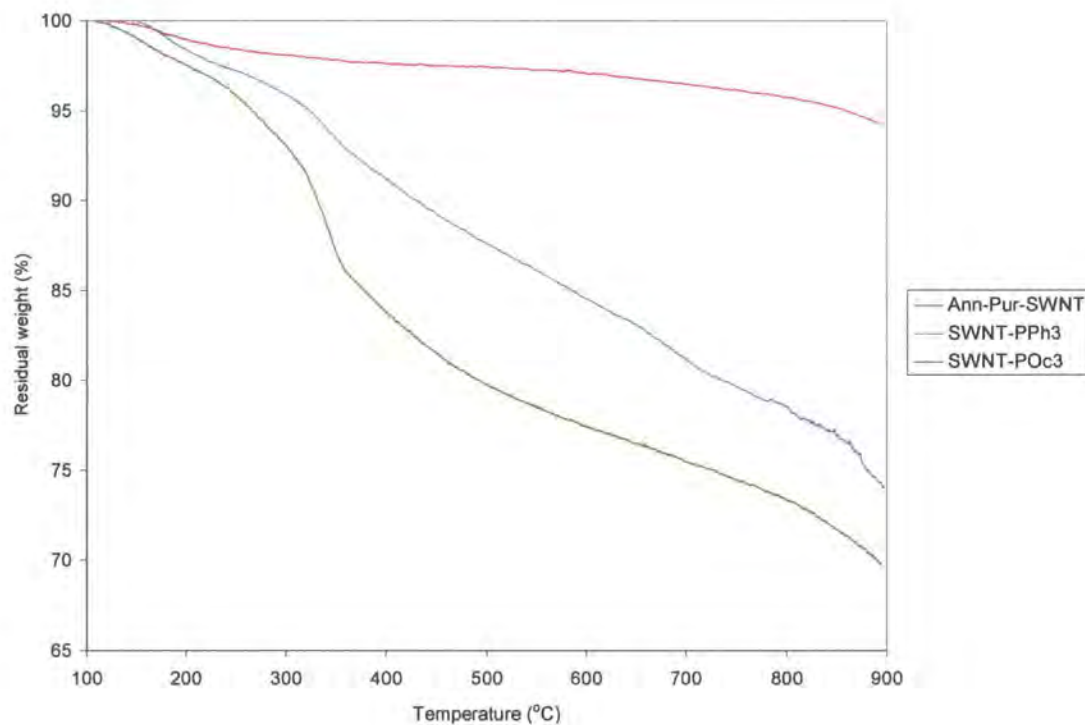
Figure 3-5

Thermogravimetric analysis (TGA) data under helium for pristine (Ann-Pur-SWNT), triphenyl phosphine-treated (SWNT-PPh₃), and trioctyl phosphine-treated (SWNTs-POc₃) nanotube samples.

3.2.3 Ultraviolet-visible-near infrared spectroscopy

UV-vis-NIR spectroscopy has been used extensively to follow functionalization of SWNTs with the loss of the characteristic absorption bands corresponding to the electronic transitions between the van Hove singularities, a consequence of their chemical modification . The absorption spectra obtained from the Ann-Pur-SWNT, SWNT-PPh₃ and SWNT-POc₃ samples are shown in Figure 3-6. Only a small suppression of the absorption bands of the phosphine-treated SWNTs can be seen which is indicative of a low level of functionalization. Importantly, the electronic structure of the SWNTs has not been perturbed significantly by the tertiary phosphine treatment.
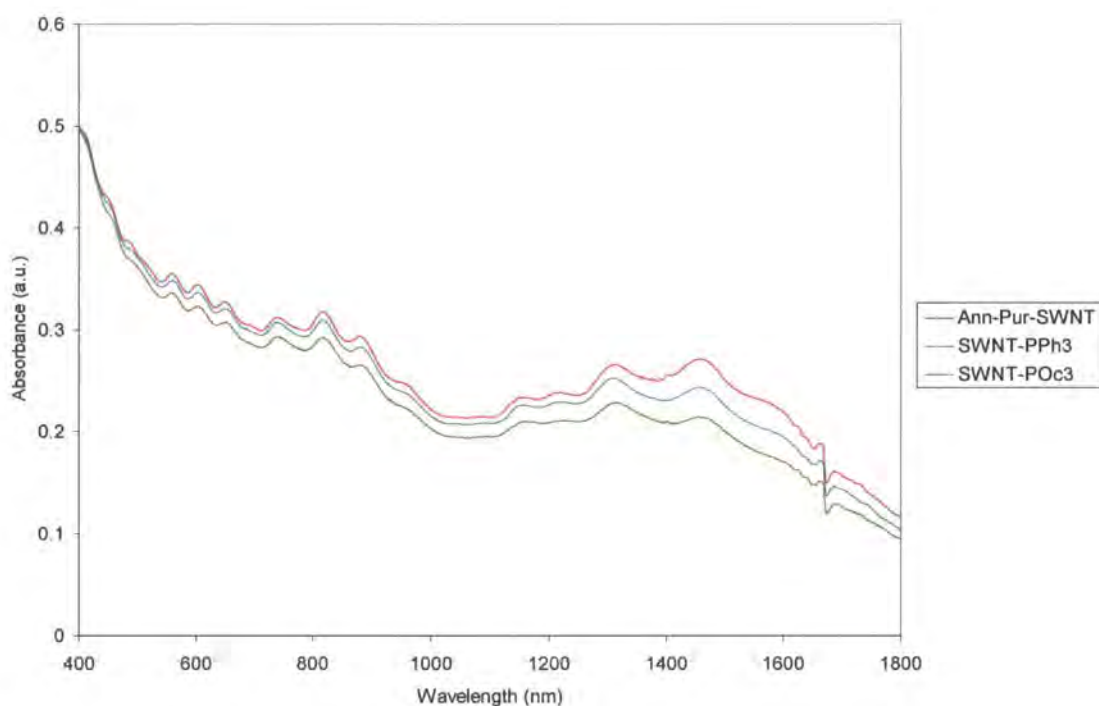
Figure 3-6

UV-vis-NIR spectra in DMF of Ann-Pur-SWNT, SWNT-PPh$_3$ and SWNT-POc$_3$. The spectra have been normalised to have an absorbance of 0.5 units at 400 nm.

3.2.4 Raman spectroscopy

Raman spectra of SWNT-PPh$_3$ and SWNT-POc$_3$ (Figure 3-7) show an expected enhancement in intensity of the disorder related D band (ca. 1330 cm^{-1}) compared to the Ann-Pur-SWNT sample. This Raman mode, linked to an increase in scattering sites and a lowering of the symmetry of the SWNT structure [342], indicates that groups have been introduced on to the walls of the nanotube material. Importantly however, the increase in the D band intensity reported here is well below those reported for other functional groups covalently attached to carbon nanotubes [104, 163, 168, 182, 188, 190, 198, 218, 224], which is in keeping with the low levels of functionalization determined by XPS and TGA, thus confirming the integrity of the samples. Similarly, only a small variation in the relative

intensities of the radial breathing modes (RBMs) of SWNT-PPh₃ and SWNT-POc₃ were evident upon comparison with the Ann-Pur-SWNT material, indicating that there is little perturbation of the electronic structure upon modification, which agrees with the UV-vis-NIR data.
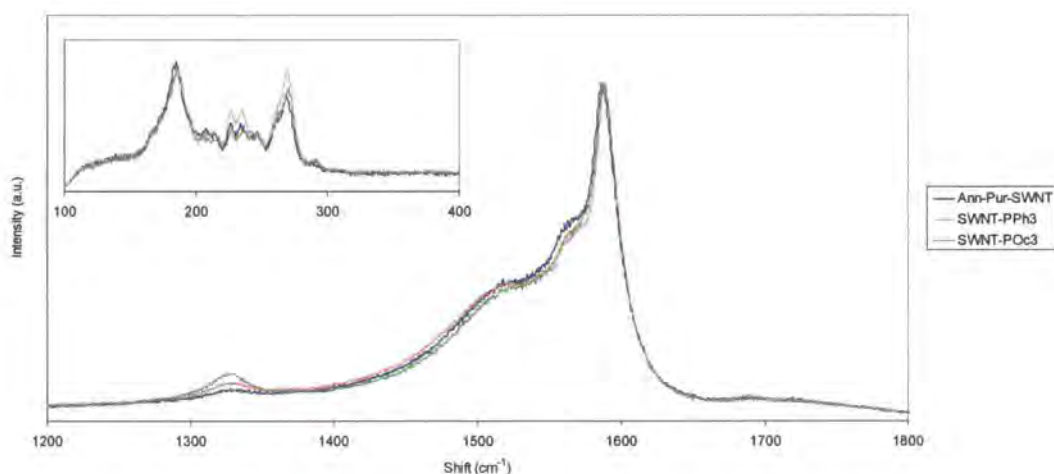
Figure 3-7

Raman spectra of unmodified (Ann-Pur-SWNT) and modified samples, SWNT-PPh₃ and SWNT-POc₃ obtained using an excitation wavelength of 633 nm (normalised to have the same maximum intensity of the G-band). Inset: radial breathing modes (RBMs).

3.2.5 Bulk electrical properties

It is normally observed that pristine SWCNTs behave as p-doped in air and as n-doped in ultra-high vacuum even if they are not intentionally doped [66, 67, 343-345]. The actual physical origin of such doping character of CNTs is not beyond debate. But it is thought that ordinarily used purification methods involving oxidising treatment steps (such as heating the CNTs in air in our case) lead to hole-doped (*i.e. p*-type) CNTs [346]. The electrical properties of individual semiconducting SWNTs has been observed to be extremely sensitive to adsorption of electron-donating species, such as NH₃ [79] and amines [337], and electron-accepting ones, such as O₂ [347] and NO₂ [79]. Electron-donating species

caused a few orders of magnitude increase in the resistance, while electron-accepting ones had the opposite effect. The former reduce the concentration of charge carriers (holes) in pristine tubes, thereby reducing the conductivity, whereas the latter increase it. Individual metallic tubes show a very small change (< 30%), as the concentration of charge carriers does not change significantly. Thus, it was observed that the bulk resistance of mats of tubes increased by < 50% owing to the averaging of metallic and semiconducting tubes [79, 347]. Also, these changes were reversible as the adsorbed species could be easily desorbed with time.

For measuring the bulk electrical resistance, films were made by filtering suspensions of pristine and phosphine-modified SWNTs in ethanol over polycarbonate membrane filters (Whatman Cyclopore™, 25 mm diameter, 0.2 micron pore size), followed by drying in a vacuum oven at 80°C for 1 hour and lift-off of the SWNT films from the membrane filter. The films were around 100 microns thick, as measured by a screw gauge. The electrical resistances, as measured by a four-point apparatus, are summarised in Table 3-1.

Sample	Electrical resistance (Ω)
Pur-SWNT	0.02
Ann-Pur-SWNT	0.631
SWNT-PPh$_3$	0.191
SWNT-POc$_3$	0.205

Table 3-1

Four-point electrical resistances of the pristine and modified SWNTs.

Just as has been observed in this study, Rinzler and co-workers have previously reported an increase in the resistivities of films upon annealing [141]. They had advanced a tentative explanation for this phenomenon, based on greater compaction of the annealed films. What is significant in this study is that, contrary to the trend expected from electron-donating species like amines, we find a *decrease* in the bulk resistance of mats of phosphine-treated CNTs. However, a closer inspection of the purification process employed in the current work can explain this apparent conundrum. The step in which the CNTs were annealed under vacuum at 900 °C after their purification employed in this study can be expected to nullify the hole-doping induced by the purification process. Thus, as the phosphines are electron-donating groups, one would expect that the SWNTs should be *n*-doped as a result of phosphine treatment. The increased charge carrier (electron) concentration will in turn increase the conductance, or in other words, *decrease* the resistance. This is exactly what we observe in the phosphine-treated CNTs as listed in Table 3-1.

3.2.6 Nature of interaction between SWNTs and tertiary phosphine molecules

The best comparison for the phosphine treated SWNTs discussed here is the interaction of amines, particularly octadecyl amine (ODA) with carbon nanotubes which is well documented [79, 228, 260, 337-339]. The nature of this amine interaction is predominantly physisorption although some degree of non-covalent functionalization, with the formation of zwitterions from the interaction of the amine with residual carboxylic acid groups, is possible [164, 338, 348]. In addition, yet another mode of interaction is possible: nucleophilic amines react with electron deficient fullerenes to form addition products (adducts) of the type $C_{60}H_n(NRR')_n$. Here, n is generally 6, or the number of pyracyclene rings in C_{60}. It has been suggested that the hydrogen atoms behave as "fullerene globe-trotters" [349]. Analogously, it has also been shown that, under suitable conditions, amination of the nanotubes (the activation of an N–H bond over a nanotube π-bond) can occur [339].

In the case of the phosphine-treated SWNTs described here the physisorption of the phosphine can be ruled out, as the attachment of the tertiary phosphines to the

SWNTs is not reversed even after repeated ultrasonication, washing with solvents and filtration. It is worth noting that a tertiary amine (triethylamine) has been shown to untangle bundled SWNTs and stabilise nanotube dispersions [228]. XPS suggests interaction of the tertiary phosphine molecules with the SWNTs via the lone pair of electrons on the phosphorus, similar to what has been observed with amines by Chattopadhyay and co-workers [338]. They also found that amines preferentially interact with the semiconducting SWNTs as compared to the metallic ones, and argued that this could be exploited to achieve a separation of SWNTs by electronic type. This throws up exciting possibilities for the modification of SWNTs by tertiary phosphines. However, considerable work is first required to determine the exact nature of the interaction between the phosphines and SWNTs. An effective way for probing the interaction between phosphines and SWNTs may be the fabrication of SWNT-FET devices and studying the effect of phosphine adsorption on individual SWNTs, as previously reported for amines [337]. This shall also help determine if phosphines show a preference for SWNTs of one electronic type over the other. Efforts in this direction are currently underway in the group.

3.3 Conclusion

SWNTs have been modified by tertiary phosphines (triphenyl- and trioctyl-phosphine) using a simple and robust solvent-free route. XPS data recorded in the P 2p region clearly shows that the phosphorous atoms present in the phosphine treated nanotube material are in a different chemical environment than found in pure phosphine indicating that charge transfer between the electron donating phosphorous atom and the carbon nanotube may have taken place. Modification with phosphines resulted in significant de-bundling of the SWNTs allowing stable dispersions in common organic solvents to be prepared. Although the modified material disperses readily the electronic properties of the nanotube are not perturbed and the surface of the nanotube is thought to be still accessible as the degree of functionalization is low (ca. 1 atomic *per cent*). The

effect of the tertiary phosphines on the electrical conductivity of SWNTs is currently under investigation.

4. COVALENT MODIFICATION OF SWNTs VIA REDUCTION FOLLOWED BY ELECTROPHILIC SUBSTITUTION

4.1 Introduction

A wide range of applications of immense technological importance have been proposed for CNTs, including nanoelectronics [66-69], sensors and detectors [79-83], and polymer composites with dramatically enhanced mechanical [84-87], thermal [88, 89] and electrical properties [89]. However, major challenges must be overcome before these applications can be realised on a large commercial scale. CNTs tend to aggregate into bundles owing to strong van der Waals forces of interaction between their smooth graphitic walls [100]. Consequently, they have extremely low affinity for other materials, and show very poor solubility in common solvents or dispersion in polymers. This is a serious drawback for industrial-scale handling and processing. Besides, amenability to solution processing is convenient and inexpensive, and will greatly reduce production costs. Also, many applications require individually dispersed CNTs. As described in Section 1.5.4, the true potential of CNTs for producing high-performance polymer composites can be realised only if individual nanotubes can be dispersed in the polymer matrices. For applications such as CNT based electronic devices like field effect transistors (FETs), not only will individual CNTs be required, but they also need to be separated by electronic type. Currently used synthesis methods yield mixtures of metallic and semiconducting SWNTs, and there is no known method for exclusively producing one type of SWNTs.

Chemical modification of CNT surfaces will be necessary to improve the solubility of CNTs and improve their affinity for other materials such as polymers. Several strategies for non-covalent as well as covalent modification of CNTs have been developed towards this end, which are reviewed in Chapter 1, Sections 1.6.3-1.6.5. Covalent modification can lead to the perturbation of the intrinsic electronic structure of

pristine nanotubes [103, 104, 163, 178, 188, 192-194, 204, 208, 224], which may lead to a loss of their interesting properties. Non-covalent methods for the modification of CNT surfaces result in relatively lesser disruption of the CNT electronic structure. However, most of the CNT surface may be rendered inaccessible owing to extensive coverage by the modifying agent, which may prove to be a disadvantage for applications like nanoelectronics. Non-covalent modification is generally easily reversible, although this may prove to be a disadvantage. For example, modification of CNTs by polymer wrapping can be reversed by changing the solvent [114]. Similarly, the adsorption of amines on CNTs also cannot withstand multiple processing steps or even slightly elevated temperatures or vacuum [228, 260, 337-339]. Covalent modification is more durable, and requires annealing at temperatures of 300°C or higher for reversal. Thus, covalent modification routes which significantly improve the solubility and dispersibility of CNTs, while not significantly compromising their electronic structure, would be very advantageous.

Yet another disadvantage of the covalent modification routes reported to date is that they are not very versatile. Some reactions also require long processing times, such as the *1,3*-dipolar cycloaddition which occurs over several days [208, 209]. The most commonly used route for the covalent modification of CNTs is carboxylation, followed by subsequent amidation / esterification (see Chapter 1, Section 1.6.5.1 and references therein). However, the process of carboxylating CNTs can cause considerable damage to the nanotubes, such as burning away of small diameter (and hence, more reactive) tubes [149, 262, 326-329], opening of end-caps [151, 155-157, 229-231, 259, 262, 289, 305, 311, 314, 315, 319, 320, 322], shortening [108, 143, 158, 289, 297], rupturing the CNT walls [323], and generation of amorphous carbon which may remain as a coating on the nanotubes if not removed, potentially hindering subsequent chemistry that aims to attach functional molecules to the CNT walls [263, 264].

One route for the covalent modification that has not received the attention it deserves is via the reduction of CNTs by nucleophiles such as alkali metals and organolithium reagents. Compared with the other reported routes, there are very few studies on this method of modifying CNTs (see references in Section 1.6.5.2.4). Similar to reactions such as fluorination and the Bingel reaction, reduction by alkali metals too has a precedent in the chemistry of graphite [215] and fullerenes [216]. The reduction of

fullerenes by alkyllithiums has also been demonstrated [222, 223]. For CNTs, reduction by alkyllithium reagents has only been used for grafting polymers directly onto the CNT walls [224, 225]. Hirsch and co-workers have reported a detailed spectroscopic study of the reduction of SWNTs by t-butyllithium [226]. They noted that the sequence of reduction of SWNTs by t-butyllithium could be repeated, leading to the species, $(t\text{-}Bu_n)_m$SWNT (where number of times the sequence is repeated, m = 1-3). The extent of functionalisation was around 2 atomic *per cent*. The charged species formed upon reduction spontaneously exfoliated in benzene; however, charged species would be stable only in an inert environment. Significantly, they also concluded from a Raman spectroscopic study that the reaction demonstrates a selectivity for metallic SWNTs, although their study had not included other nucleophiles.

Pénicaud and others showed the reduction of CNTs by alkali metal naphthalenides under an inert atmosphere [221]. The stoichiometry of the reduced species was found to be $C_{50}M$ (M = Li, Na, K), which is almost identical with that found by Hirsch and group for reduction of SWNTs with t-butyllithium [226]. Recently, Billups and co-workers reported the covalent modification of SWNTs by reduction with alkali metals (Na, K, Li) in ammonia, followed by electrophilic substitution with alkyl and aryl halides [218-220]. They obtained highly soluble SWNTs, with the extent of functionalisation ranging from one in every 17 to one in every 54 CNT carbon atoms, depending on the substituting group. This figure is much higher than that found by Hirsch and co-workers [226] and Pénicaud and co-workers [221].

The immense potential for extremely facile and versatile covalent modification of SWNTs by this route has independently also been the focus of our interest. However, unlike the work of Hirsch *et al.* [226] and Pénicaud *et al.* [221], our primary focus is the possibility to exploit the reduction of SWNTs by nucleophiles as a starting point for functionalisation via electrophilic substitution, according to the scheme shown in Figure 4-1. We show that this scheme can bring the great versatility of electrophilic substitution to the chemistry of SWNTs. Because of its enormous scope, this scheme could be used to tether a much wider range of functional moieties to CNTs than is possible with any of the previously reported routes. The functionalisation sequence can be repeated, and different moieties can be introduced in each cycle onto the same CNT backbone. Thus,

this scheme offers almost limitless possibilities in terms of the groups which can be attached to nanotubes, thereby opening the gateway to the tailoring of nanotube surfaces to suit various solvents and host matrices. We also report the first study to date by ultraviolet-visible-near infrared (UV-vis-NIR) spectroscopy of the effect of this modification route upon the electronic structure of the SWNTs. Importantly, it is observed that the extent of perturbation of the electronic bands of the SWNTs in one cycle of functionalisation is very small.
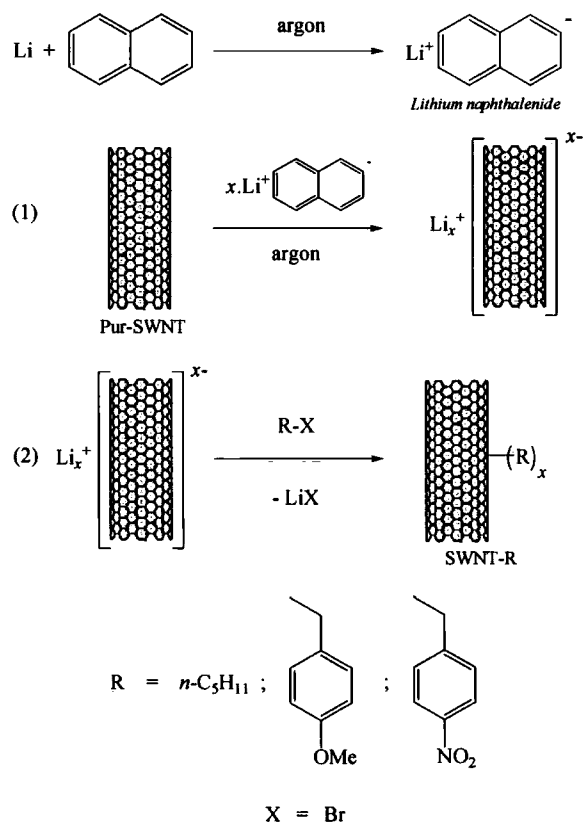
Figure 4-1

(i) Reaction scheme for the functionalisation of SWNTs via reduction with lithium naphthalenide, followed by electrophilic substitution.
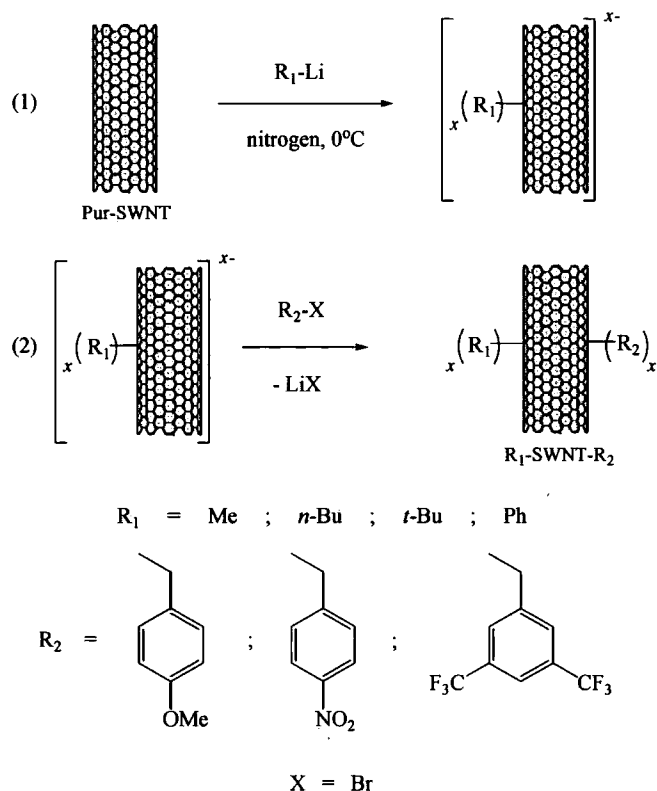
Figure 4-1

(ii) Reaction scheme for the functionalisation of SWNTs via reduction with organolithium reagents, followed by electrophilic substitution.

4.2 Results and discussion

4.2.1 Reduction by lithium naphthalenide

Purified SWNTs (Pur-SWNT) were obtained as described in Chapter 2, Section 2.2.1, and were modified by the reaction scheme shown in Figure 4-1*(i)*. Following the reduction with lithium naphthalenide (Step 1 in the scheme shown in Figure 4-1*(i)*), the reduced SWNTs were then covalently functionalised by electrophilic substitution with a range of alkyl halides RX (Step 2 in Figure 4-1*(i)*), where R = pentyl (Pe), 4-methoxybenzyl and 4-nitrobenzyl, and X = Br. The SWNTs thus modified are labelled as

SWNT-Pe, SWNT-OMe and SWNT-NO$_2$ respectively. The SWNTs were observed to spontaneously exfoliate upon modification, without the need for harsh ultrasonic treatment (Figure 4-2). The suspension shown in Figure 4-2 is not stable and settles within a few minutes. However, it is significant that a very uniform dispersion could be obtained merely by stirring, which was not possible for the pristine Pur-SWNTs (inset in Figure 4-2).

The modified SWNTs have been characterised by Raman spectroscopy, UV-visible-near infrared (UV-vis-NIR) spectroscopy, thermogravimetric analysis-mass spectrometry (TGA-MS) and cyclic voltammetry. TGA-MS has been used to estimate the degree of functionalisation.

Figure 4-2
Optical photograph showing the spontaneous exfoliation of 24 mg of Pur-SWNTs (inset, before reaction) upon modification to SWNT-NO$_2$ (after reaction) in ~20 mL dry THF.

To obtain preliminary evidence of chemical modification of the SWNTs, we employed cyclic voltammetry as a probe for the nitro- group in the SWNT-NO$_2$. Cyclic voltammetry has been used for detecting the nitro- group in the nitrophenyl group attached to CNTs via functionalisation with radicals generated from aryl diazonium

compounds [350, 351]. The reduction of the nitro- group follows the mechanism shown in Figure 4-3 using nitrobenzene as an example. CV was recorded on a film of SWNT-NO$_2$ drop cast from suspension onto a glassy carbon electrode and dried under a gentle stream of nitrogen, and the voltammograms are shown in Figure 4-4.
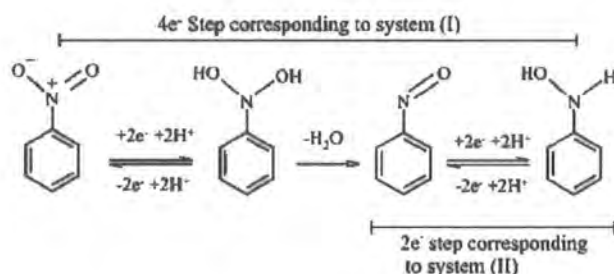
Figure 4-3

The mechanism for the electrochemical reduction of nitrobenzene.
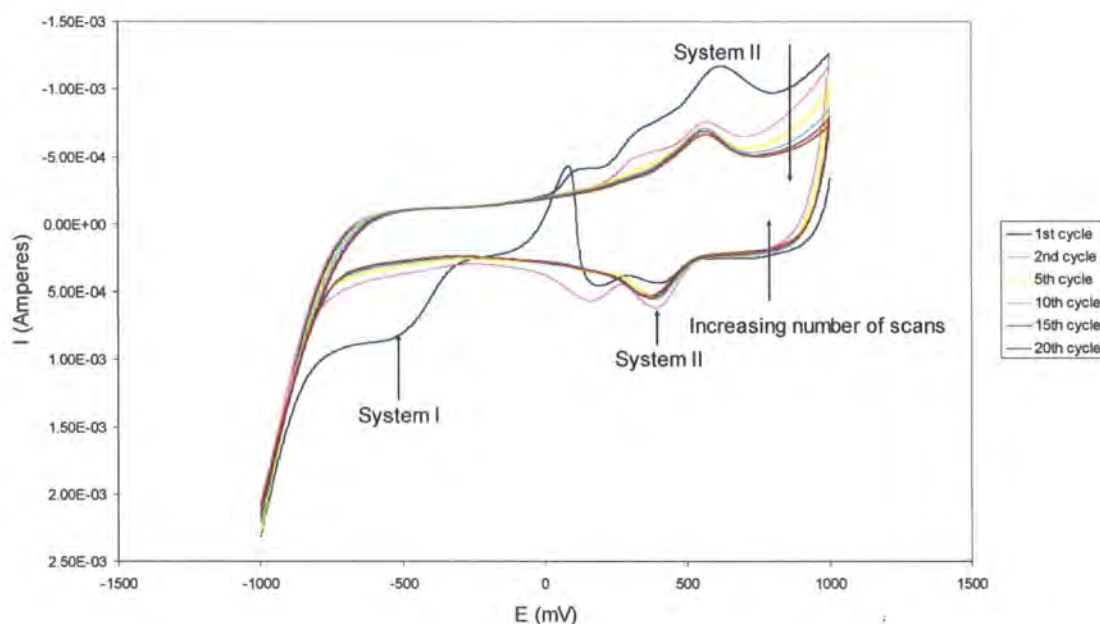
Figure 4-4

Cyclic voltammetry (CV) of SWNT-NB, showing the first, second, fifth, tenth, fifteenth and twentieth voltammograms.

In the first reductive scan (+1 to -1 V), a peak is observed at around -0.5 V, for which no corresponding peak was observed upon reversing the direction of the scan (-1 to +1 V). This peak corresponds to the 4-electron reduction of the nitro- group to hydroxylamine (System I in Figure 4-3). In the oxidative sweep, a new peak appears at around +0.6 V, for which there is a corresponding peak at around +0.4 V when the scanning direction is reversed. The intensities of these peaks reduce with increasing number of scans, as can be expected for a quasi-reversible reaction. These peaks correspond to the reduction of the nitroso- group to the hydroxylamine group (System II). Thus, we find that the voltammetric response of the SWNT-NO$_2$ is in line with what can be expected for an aromatic nitro- species [350, 351]. No such response was observed for a control sample comprising Pur-SWNTs that had been stirred with 4-nitrobenzyl bromide, followed by washing to remove any excess, physically adsorbed 4-nitrobenzyl bromide. This suggests that the 4-nitrobenzyl group may be covalently bound to the nanotube walls in the SWNT-NO$_2$.

Evidence that covalent functionalisation has been achieved is also provided by Raman spectroscopy. Upon functionalisation, some of the sp^2-hybridised carbon atoms of the SWNTs are converted into sp^3-hybridised ones by local puckering of the CNT walls. This increase in the proportion of sp^3-hybridised carbon atoms is reflected in the enhancement of the areal ratio of the intensity of the so-called disorder (D-) band, located at around 1340 cm^{-1}, to that of the tangential or graphitic (G-) band, located at around 1590 cm^{-1}. An increase in this ratio (I_D/I_G) is the most common indicator of covalent modification of CNTs in the literature [104, 163, 168, 182, 188, 190, 198, 218, 224]. In Figure 4-5, the Raman spectra of three modified samples, SWNT-Pe, SWNT-NO$_2$ and SWNT-OMe, are compared with that of the pristine Pur-SWNTs, and the I_D/I_G ratios for these samples are given in Table 4-1.
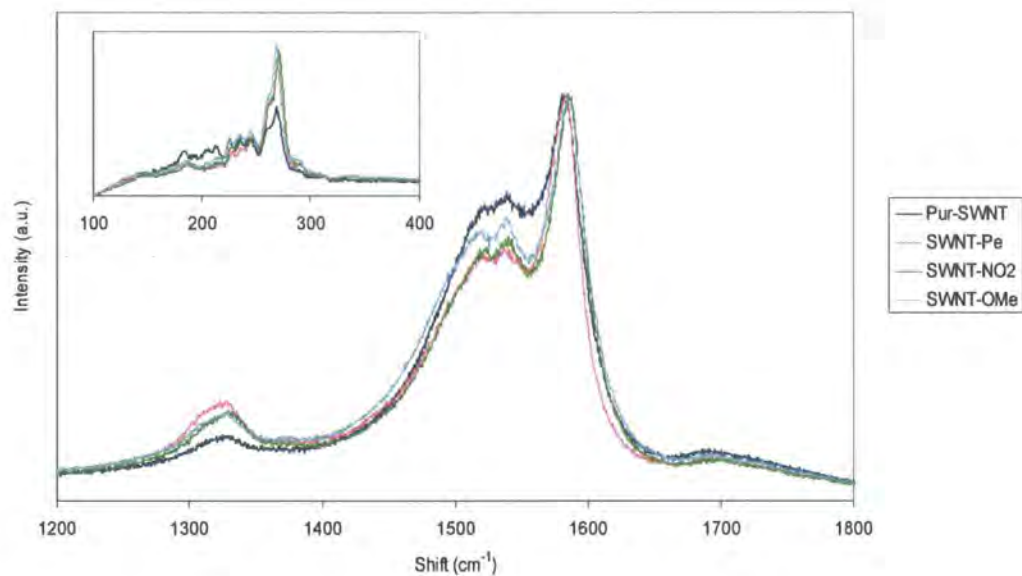
Figure 4-5

Raman spectra of pristine (Pur-SWNT) and three modified samples, SWNT-Pe, SWNT-NO$_2$ and SWNT-OMe and obtained using an excitation wavelength of 532 nm (normalised to have the same maximum intensity of the G-band). Inset: radial breathing modes (RBMs).

Sample	I_D/I_G
Pur-SWNTs	0.03
SWNT-Pe	0.092
SWNT-NO$_2$	0.062
SWNT-OMe	0.077

Table 4-1

The areal ratios (I_D/I_G) of the intensities of the disorder (D-) band to the graphitic tangential (G-) band of the SWNT samples for the Raman spectra in Figure 4-5.

Covalent functionalisation is suggested by a clear enhancement of the D-band intensities for the modified samples. It is also important to note that the enhancement in the I_D/I_G ratios is small relative to other reports [218-220], suggesting that the degree of functionalisation may be low. This qualitative observation is further supported by UV-vis-NIR spectroscopy, and confirmed by quantitative estimates from TGA-MS (see below). There is a noticeable change in the line shape of the G-band of the modified samples compared with that of the pristine Pur-SWNTs, which is suggestive of a change in the electronic structure [195]. Further, it can be seen that there are some changes in the low-energy radial breathing modes (RBMs) (inset in Figure 4-5), and the intensities of the RBMs of the modified samples relative to the intensity of the G-band are also different from that of the pristine Pur-SWNTs, which may be as a result of the modification of the electronic properties of the SWNTs by functionalisation [192, 194, 220, 226].

The electronic transitions between the densities of states (DOS) in SWNTs can be observed as absorption bands in optical spectroscopy in the ultraviolet-visible-near infrared range (UV-vis-NIR), of films or suspensions of the nanotubes [47]. These bands are suppressed as a result of the disruption of the native electronic structure of SWNTs by chemical modification, and the extent of the suppression of these bands provides a qualitative estimate of the degree of functionalisation [103, 104, 163, 178, 188, 192-194, 204, 208, 224]. UV-vis-NIR (not shown here) showed virtually no suppression of the absorption bands in the modified samples relative to those of the pristine Pur-SWNTs. However, this could be the result of the superimposition of two opposing phenomena: if the degree of functionalisation is low, the extent of suppression of the absorption bands will be low; on the other hand, functionalisation may result in a higher solubility for the modified SWNTs, owing to which their absorption bands may become more pronounced [199]. Thus, if a low level of functionalisation has led to enhancement in the solubility of the SWNTs, chemical modification may not be apparent in the UV-vis-NIR spectra of the SWNTs.

Thermogravimetric analysis-mass spectrometry (TGA-MS) was employed to follow the thermal evolution of the groups attached to the modified SWNTs. The TGA-MS profile under helium for SWNT-OMe is shown in Figure 4-6. The evolution of the groups from the thermal fragmentation of the moieties from the SWNTs occurs in two

distinct regions: in the temperature range around 200-400°C, and around 460-500°C. The high evolution temperatures suggest that the moieties are covalently attached to, and not physically adsorbed on, the SWNTs. This has been further confirmed by carrying out the TGA-MS analysis on control samples comprising Pur-SWNTs which had been merely stirred with the species, RX, followed by washing to remove physically adsorbed material, whereupon no evolution of groups could be detected in the analysis. From the weight loss of the modified samples, we estimate the degree of functionalisation to be around 2 atomic *per cent*.
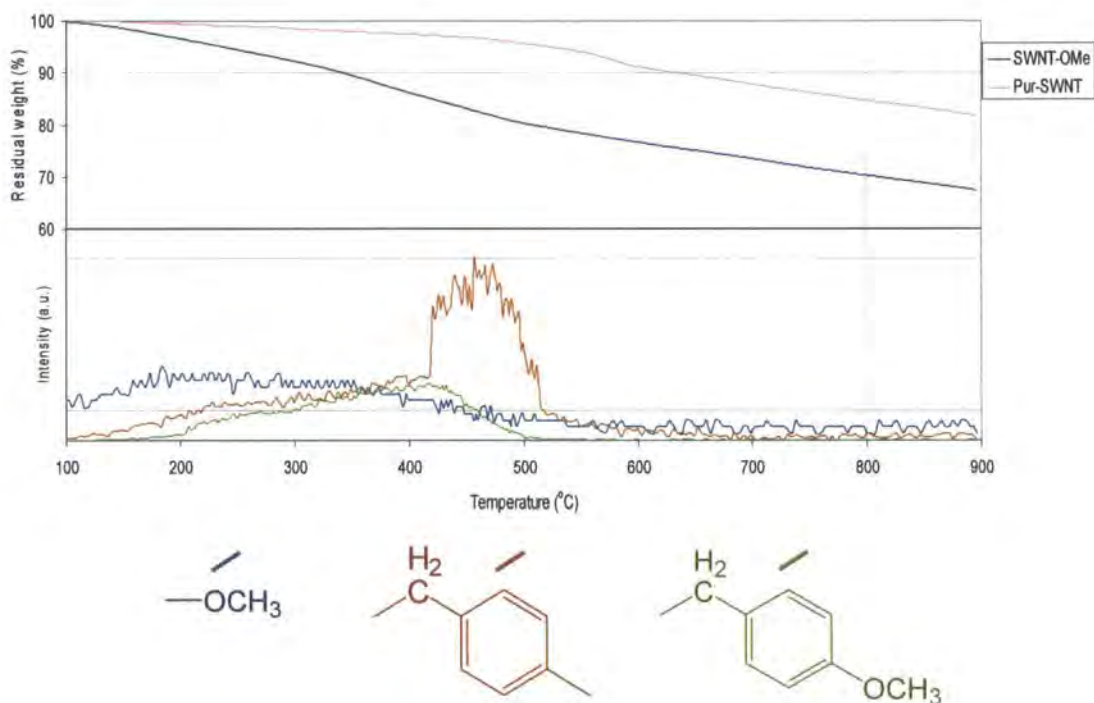
Figure 4-6

(Above) TGA in helium and (below) the corresponding mass spectrometry data for the thermal evolution of the indicated fragments for purified SWNT-OMe.

Thus, TGA-MS supports the evidence from Raman and UV-vis-NIR spectroscopy that the degree of functionalisation is low. This may prove to be a major advantage of this method of functionalisation over other routes reported to date, as it confers very high dispersibility without any significant disruption of the electronic structure of the SWNTs.

4.2.2 Reduction by organolithium reagents

It is more facile to carry out the reduction of SWNTs using organolithium reagents as compared with alkali metal naphthalenides. In order to explore the possibility of functionalising SWNTs by using organolithium reagents for the initial reduction step, purified Pur-SWNTs were subjected to the reaction scheme shown in Figure 4-1*(ii)*. Additionally, this variation of the functionalisation scheme has the advantage that two different moieties, R_1 and R_2, can be introduced on to the SWNTs, whereas the reduction by lithium naphthalenide allows only one moiety, R, to be attached to the SWNT walls. Thus, there shall be greater scope for tailoring the SWNT surface.

The Pur-SWNTs were reduced (Step 1 in Figure 4-1*(ii)*) by four nucleophiles, R_1Li, where R_1 = methyl (Me), *n*-butyl (*n*Bu), *t*-butyl (*t*Bu), and phenyl (Ph). The reduced SWNTs were then covalently functionalised by electrophilic substitution with a range of alkyl halides R_2X (Step 2 in Figure 4-1*(ii)*), where R_2 = *4*-methoxybenzyl (OMe), *4*-nitrobenzyl (NO$_2$), *3,5-bis*(trifluoromethyl)benzyl (CF$_3$), or pentyl (Pe), and X = Br. SWNTs thus modified are labelled as R_1-SWNT-R_2. As in the case of reduction with lithium naphthlenide, the SWNTs were observed to spontaneously exfoliate even when the reduction was carried out with organolithium reagents.

Raman spectroscopy provides evidence of covalent modification of the SWNTs, as was evident from an enhancement in the I_D/I_G ratios for the treated samples (Figure 4-7).
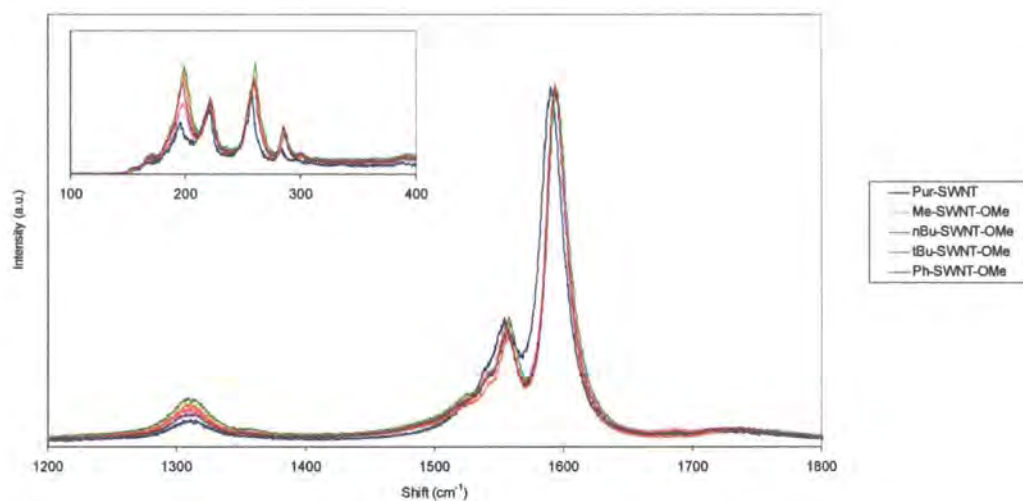
Figure 4-7

Raman spectra of pristine Pur- and four modified samples, R_1-SWNT-OMe (R_1 = Me, nBu, tBu, Ph) obtained using an excitation wavelength of 633 nm.

Sample	I_D/I_G
SWNT-Pur	0.079
Me-SWNT-OMe	0.121
nBu-SWNT-OMe	0.165
tBu-SWNT-OMe	0.142
Ph-SWNT-OMe	0.104

Table 4-2

The areal ratios (I_D/I_G) of the intensities of the disorder (D-) band to the graphitic tangential (G-) band of the SWNT samples, for which the Raman spectra are shown in Figure 4-7.

UV-vis-NIR spectroscopy (Figure 4-8) corroborates the Raman evidence that this method of functionalisation achieves a low degree of functionalisation, as it can be seen that the suppression of bands in the UV-vis-NIR absorption spectra of the modified SWNTs relative to the pristine sample is very low. More importantly, this fact is true regardless of the nucleophile employed for the initial reduction step.
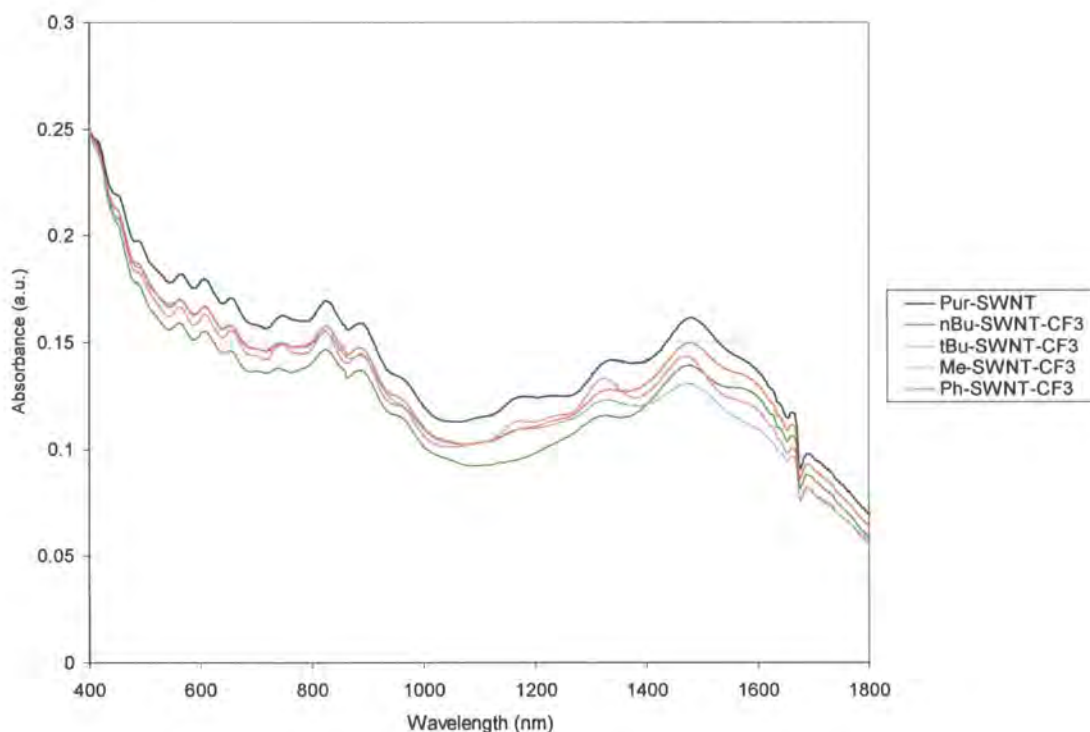
Figure 4-8

UV-vis-NIR spectra in DMF suspension of the pristine Pur-SWNTs, and four chemically modified samples, R1-SWNT-CF$_3$ (R$_1$ = Me, nBu, tBu or Ph). The spectra have been normalised to have an absorbance of 0.25 units at 400 nm.

Thermogravimetric analysis-mass spectrometry (TGA-MS) was employed to follow the thermal evolution of the groups attached to the modified SWNTs. The TGA-MS profile under helium for Me-SWNT-OMe is shown in Figure 4-9. The evolution of the groups from the thermal fragmentation of the moieties from the SWNTs occurs in two

distinct regions: in the temperature range around 200-400°C, and around 460-500°C. We postulate that the two distinct temperature ranges may correspond to different chemical environments at which the groups are attached to the SWNTs, such as the end-caps and the side-walls. The high evolution temperatures suggest that the moieties are covalently attached to, and not physically adsorbed on, the SWNTs. This has been further confirmed by carrying out the TGA-MS analysis on control samples comprising SWNTs which had been merely stirred with the species, R_2X, followed by washing to remove physically adsorbed material, whereupon no evolution of groups could be detected in the analysis.
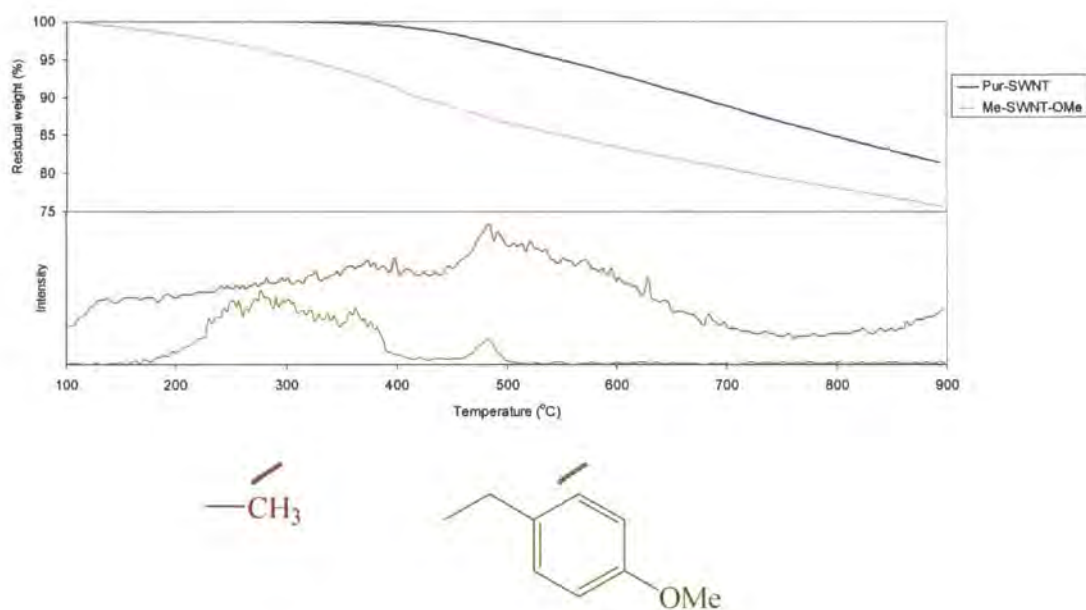
Figure 4-9

(Above) TGA in helium and (below) the corresponding mass spectrometry data for the thermal evolution of the indicated fragments for purified Me-SWNT-OMe.

The degree of functionalisation for all these samples is estimated to be approximately 2 atomic *per cent* from the weight losses. This also seems to agree with the evidence from Raman and UV-vis-NIR spectroscopy that the degree of functionalisation achieved by this route is both low and, viewed in conjunction with the degree of functionalisation reported for the modified SWNTs obtained via reduction with lithium naphthalenide (Section 4.2.1), independent of the nucleophile used for the initial reduction step. In order to conclusively establish if such is indeed the case, Pur-SWNTs were treated with a very vast excess of *n*-BuLi as in Step 1, Figure 4-1*(ii)*, after which they were quenched with water. The Raman spectrum (Figure 4-10) shows that the I_D/I_G ratio of this sample is virtually the same as that of the *n*Bu-SWNT-OMe. This confirms the finding of Pénicaud *et al*[221] that reduction is limited by the charge that can be held on the SWNTs, and is not influenced either by the nature or the amount of the nucleophile used.
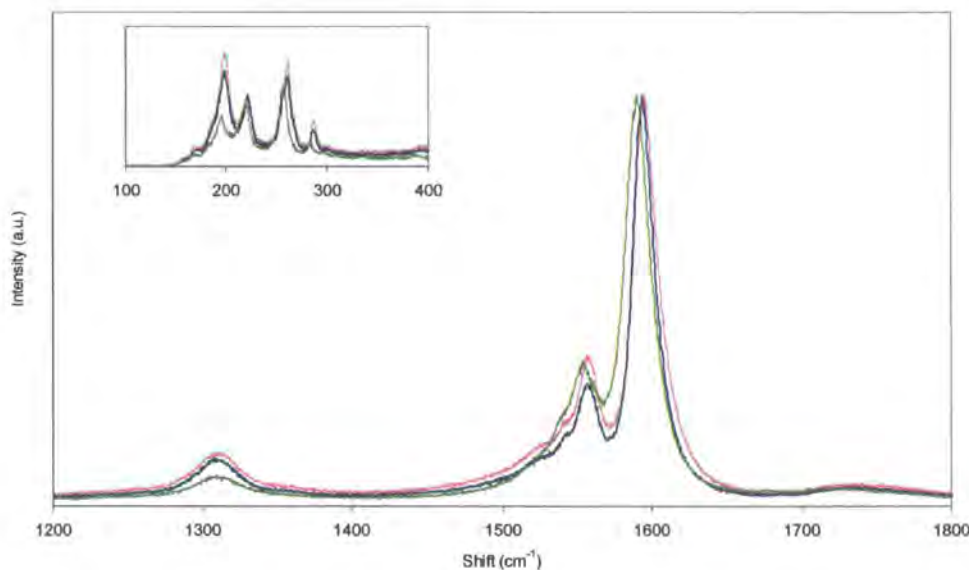
Figure 4-10

Raman spectra of Pur-SWNTs treated with *t*-BuLi such that the molar ratio of the carbon in the SWNTs to the nucleophile was 2:1 (blue line), and Pur-SWNTs treated with a very vast excess of *t*-BuLi, followed by quenching with water (red line). The I_D/I_G ratios for the samples are 0.141 and 0.142, as compared with 0.079 for the pristine Pur-SWNTs (green line). The inset shows the radial breathing modes (RBMs). The excitation wavelength used for recording the spectrum was 633 nm.

4.2.3 Multiple functionalisation sequences

The sequence of steps shown in Figure 4-1 *(ii)* can be repeated, and the same or different moieties R_1 and R_2 can be introduced on the same CNT backbone, as shown in Figure 4-11.
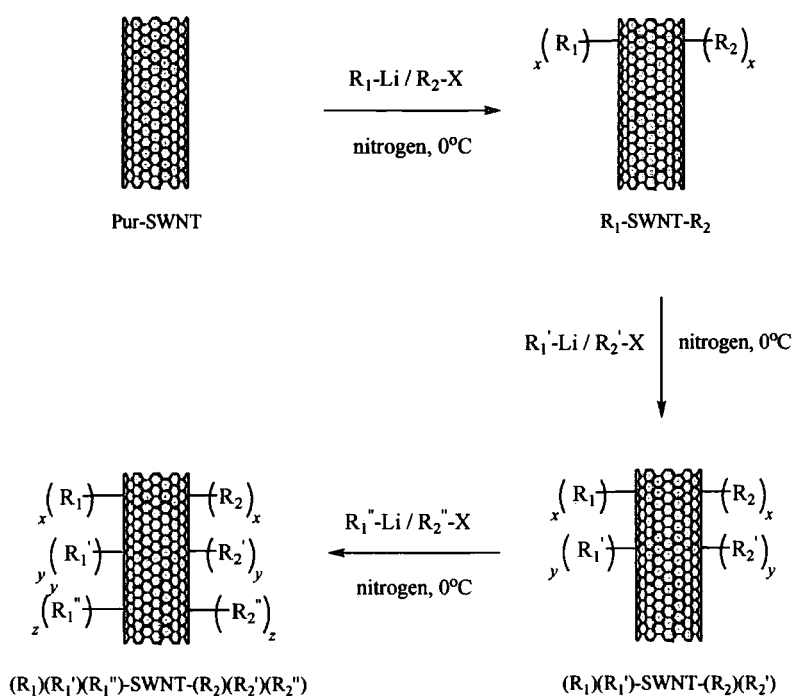
Figure 4-11

Reaction scheme for multiple sequences for the reduction / electrophilic substitution of SWNTs.

Pur-SWNTs were subjected to two and three functionalisation sequences. The nucleophiles used were $R_1 = R_1' = R_1'' = n\text{-Bu}$, and the electrophilic substituent moieties were $R_2 = 4$-methoxybenzyl (OMe), $R_2' = 4$-nitrobenzyl (NO$_2$), $R_2'' = 3,5$-*bis*(trifluoromethyl)benzyl (CF$_3$). It should, however, be noted that even the moieties R_1, R_1' and R_1'' can be different from each other. Although we have chosen n-BuLi itself as the nucleophile for the reduction, this step too can be exploited for introducing a range of

moieties onto the CNT walls. The two- and three-sequence functionalised SWNTs have been labelled as $(R_1)(R_1')$-SWNT-$(R_2)(R_2')$ and $(R_1)(R_1')(R_1''')$-SWNT-$(R_2)(R_2')(R_2'')$.

The Raman spectra of the two- and three-sequence modified SWNTs are shown in Figure 4-12. It can be seen that the I_D/I_G ratio increases in the order of pristine (I_D/I_G ratio = 0.03), one-sequence (0.036), two-sequence (0.048) and three-sequence functionalised SWNTs (0.084), suggesting incremental enhancement in the degree of functionalisation with each functionalisation sequence.
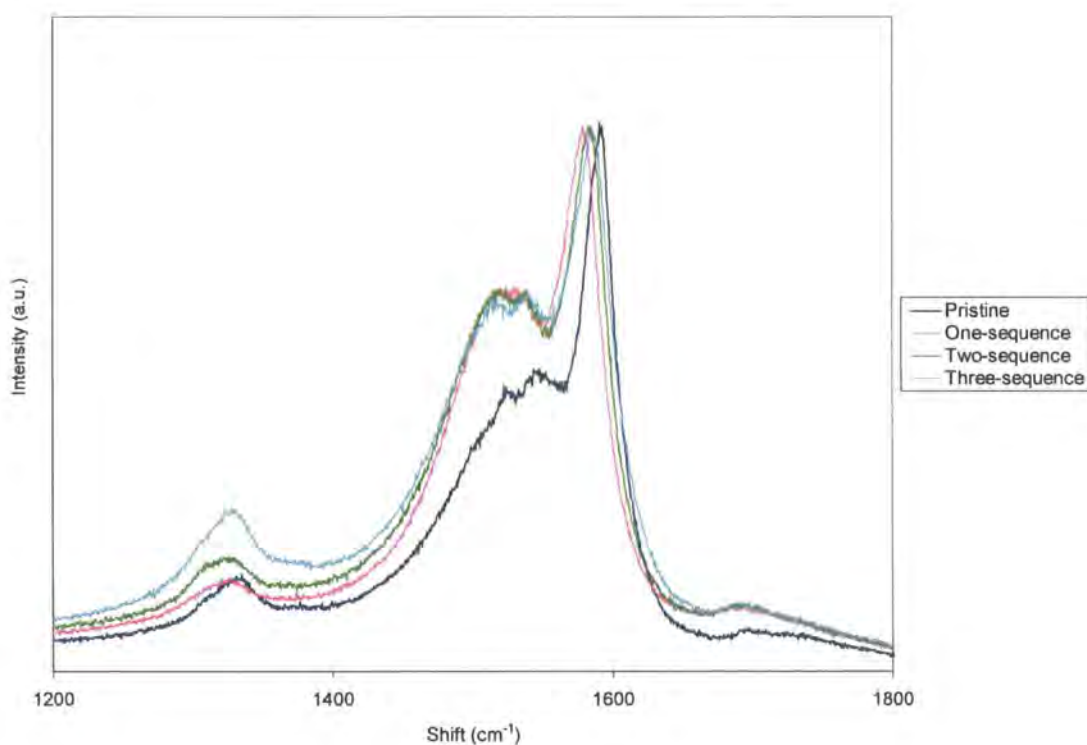
Figure 4-12

Raman spectra obtained at an excitation wavelength of 532 nm of pristine (2B-SWNTs) and SWNTs modified by one, two and three sequences as shown in Figure 4-11.

The groups attached to the SWNT-$(R_1)(R_1')$-$(R_2)(R_2')$ and SWNT-$(R_1)(R_1')(R_1''')$-$(R_2)(R_2')(R_2'')$ have also been detected by TGA-MS (Figure 4-13). Owing to the low extent of functionalisation, the heterogeneity of the samples and the error in

measurement, it was not possible to make an exact estimate of the degree of functionalisation in the second and third sequences, although it was in the region of 2 atomic *per cent* in each sequence.
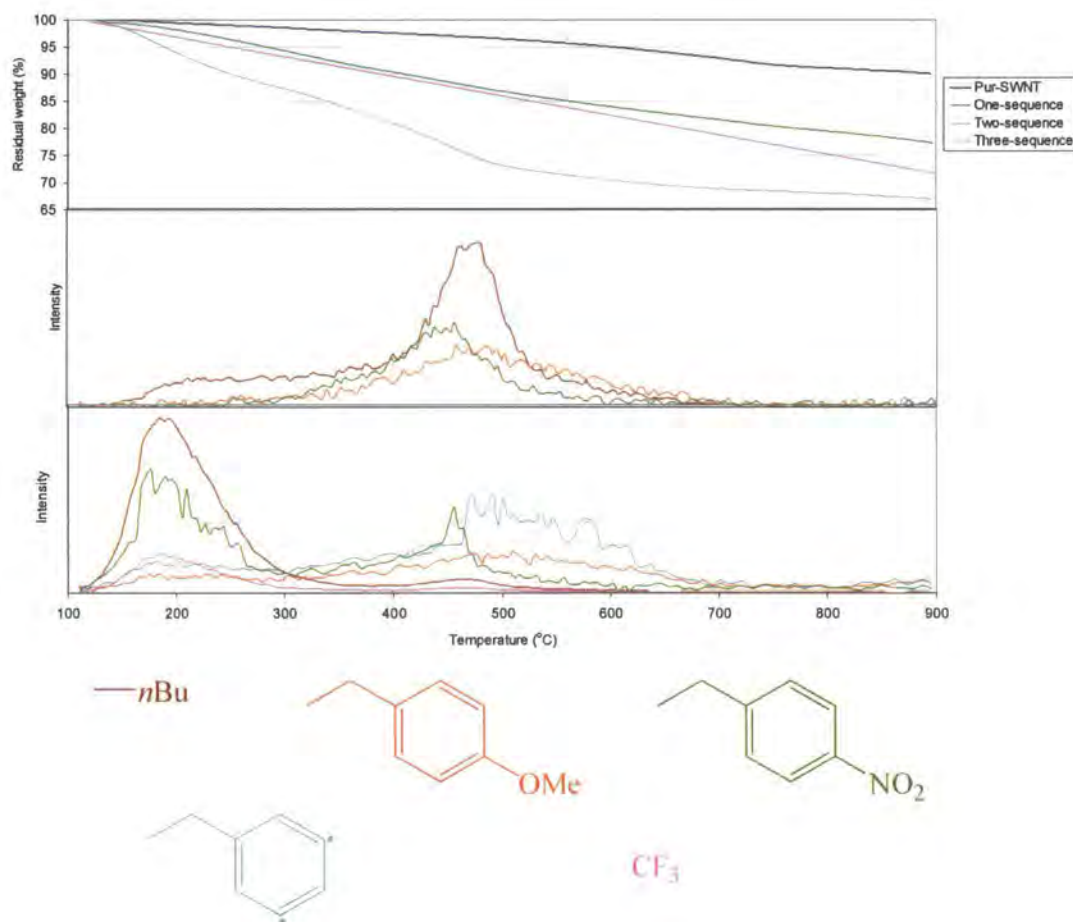
Figure 4-13

(Above) TGA in helium of Pur-SWNT and SWNTs subjected to one, two and three sequences of functionalisation as in Figure 4-11 [where $R_1 = R_1' = R_1'' = n$-Bu, and the electrophilic substituent moieties were $R_2 = 4$-methoxybenzyl (OMe), $R_2' = 4$-nitrobenzyl (NO$_2$), $R_2'' = 3,5$-bis(trifluoromethyl)benzyl (CF$_3$)] and the corresponding mass spectrometry data for the thermal evolution of the indicated fragments for SWNTs subjected to two (middle panel) and three (bottom panel) functionalisation sequences.

105

4.2.4 Possible specificity towards metallic SWNTs

Raman spectroscopy suggests that the reduction / electrophilic substitution reaction may show specificity towards metallic over semiconducting SWNTs. The line shape of the tangential, graphitic or G-band at around 1590 cm^{-1} is the superimposition of a higher frequency feature with a Lorentzian line shape owing to semiconducting tubes, and a lower frequency feature with a Breit-Wigner-Fano (BWF) line shape owing to metallic tubes [352]. Changes in the shape of the G-band have been reported previously for reactions that show chemoselectivity for SWNTs of one electronic type over the other. Notably the functionalisation by radicals derived from aryl diazonium salts [195] resulted in a broadening of the G-band and appearance of a low-frequency shoulder owing to the modification in the electronic structure of the metallic tubes by the functionalisation. When an excitation wavelength of 532 nm is used, we find that the G-band in the Raman spectrum of modified SWNTs is considerably broader than that of the pristine SWNTs (Figure 4-14(i)), and the formation of an additional shoulder is also observed. A slight broadening is also noticed when the Raman spectra are recorded at an excitation wavelength of 633 nm (Figure 4-14(ii)). This is significant as the 532 nm excitation wavelength is more sensitive to metallic than semiconducting SWNTs [196]. Additionally, it can be seen that there are noticeable changes in the low-frequency radial breathing mode (RBM) features (inset in Figure 4-14(i)) such as the appearance of new peaks at 231.8 and 240.0 cm^{-1}. Such changes are not observed in the Raman spectrum recorded at 633 nm (inset in Figure 4-14(ii)). However, there is a slight shift in the positions of the RBM features of the modified SWNTs, which can be attributed to the change in the state of aggregation of the nanotubes upon modification [206].
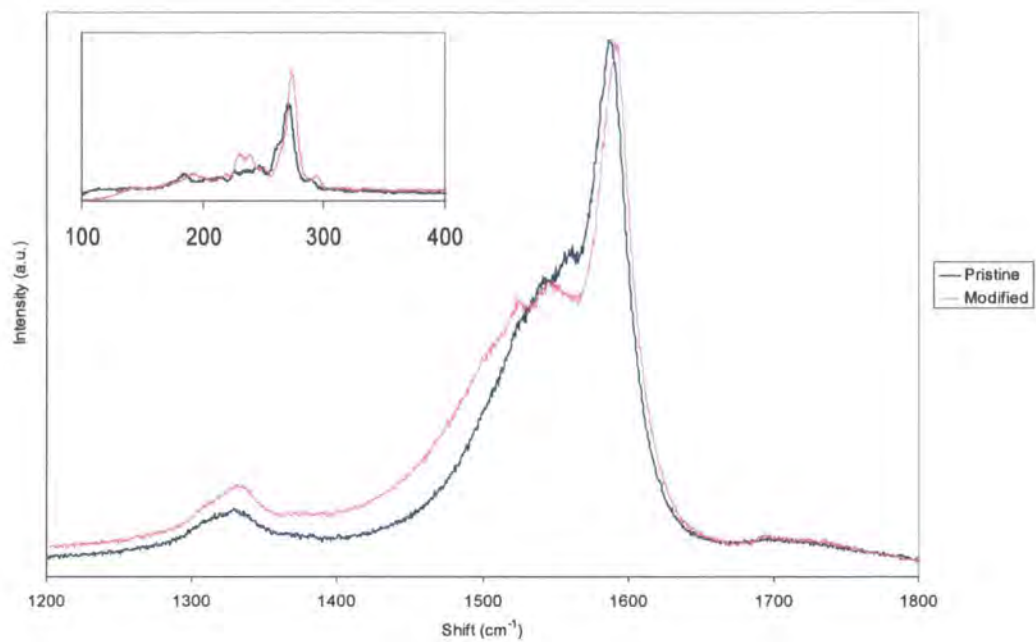
Figure 4-14

(i) Raman spectrum obtained with an excitation wavelength of 532 nm for pristine 1B-SWNT and modified *t*Bu-SWNT-MB. The inset shows the radial breathing modes (RBMs).
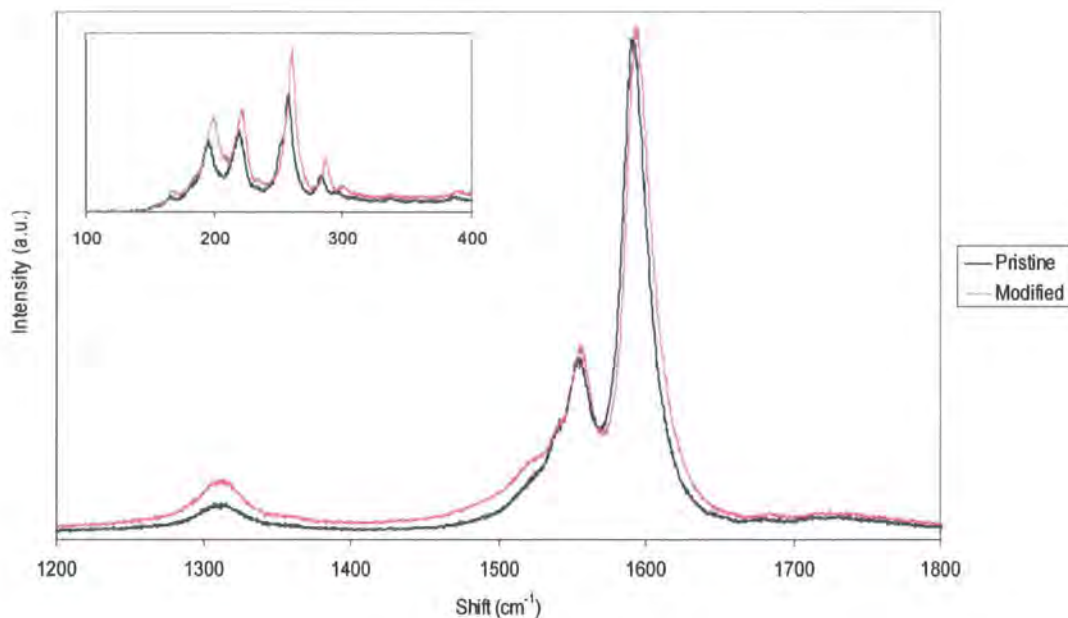
Figure 4-14

(ii) Raman spectrum obtained with an excitation wavelength of 633 nm for pristine 1B-SWNT and modified SWNT-*t*Bu-MB. The inset shows the radial breathing modes (RBMs).

Further work needs to be done before the chemoselectivity of this method of functionalisation of SWNTs can be conclusively determined. Work is underway to probe the reaction by UV-vis-NIR spectroscopy [195], and it is also proposed to study this reaction theoretically. If these studies corroborate our preliminary hypothesis that the reaction shows specificity for metallic SWNTs, then it could be exploited for the facile separation of nanotubes by electronic type [197].

4.3 Conclusion

We have demonstrated a new, extremely facile route for the covalent functionalisation of SWNTs via reduction with nucleophiles, followed by electrophilic substitution. The major advantage of this route over those reported to date is versatility. Since this functionalisation route is based on electrophilic substitution, it may well afford

almost limitless possibilities for attaching functional moieties to CNTs. It is observed that the degree of functionalisation is limited by the charge that can be transferred to the SWNTs in the first, or reduction, step. Thus, regardless of the nucleophile used, the degree of functionalisation is always found to be approximately 2 atomic *per cent*. The extent of functionalisation, though low, is still observed to cause remarkable exfoliation of the SWNTs into organic solvents such as THF and alcohols. As can be expected for such a low degree of functionalisation, the perturbation of the electronic structure is minimal. Thus, this functionalisation scheme is able to produce highly solubilised SWNTs, while not compromising the intrinsic electronic properties of the nanotubes. Further, the reaction sequence can be repeated to attach an entirely different set of moieties to the same SWNT backbone, thus enabling the tailoring of the SWNT surface by attaching groups for multiple functionalities, or enhancing the affinity of the SWNTs for several solvent systems / matrices. Although it was not possible to estimate the degree of functionalisation in each of the multiple sequences owing to factors such as errors in the TGA-MS analysis, it is in the region of 2 atomic *per cent*. Changes in the line shape of the G-band in the Raman spectra also seem to suggest that the reaction may be showing a preference for metallic SWNTs over semiconducting ones, although much further work needs to be done to establish if this is the case. If this reaction is indeed found to show specificity towards SWNTs of one electronic type, it may be possible that the reaction can be exploited for the separation of metallic and semiconducting SWNTs, which is of great importance for applications such as nanoelectronics.

5. FORMYLATION OF SINGLE-WALL CARBON NANOTUBES

5.1 INTRODUCTION

The covalent chemistry of CNTs is very closely related to, but not as rich as that of fullerenes, although several routes for the chemical modification of CNTs have been reported since the work of Liu *et al* [108]. Liu and co-workers [108] had demonstrated that treatment of SWNTs with oxidising acids could shorten or inflict defects or ruptures in the CNT walls, and result in the creation of oxygen-containing functional groups, predominantly carboxylic acid, at these defects or shortened ends. The carboxylic acid groups thus created could be exploited for the further covalent derivatisation of CNTs via amidation / esterification [163, 164, 166, 167, 169-173]. Many other routes have also been reported, which are described in Chapter 1, Section 1.6.5. However, the reported routes for the covalent modification of CNTs are not very versatile and severely restricted in terms of the groups / molecules that can be attached to the CNTs, although several attempts have been made to tether functional molecules to CNTs via these routes including polymers for composites [174, 201-203], biomolecules for sensing and detection [171, 175-177, 210], and dyes for light-harvesting applications [137]. Attaching formyl groups to CNTs could confer great advantage in terms of the wide range of modification reactions that become available. The aldehyde group can be subjected to numerous C–C and C–N coupling reactions, reductions and other transformations.

Aromatic aldehydes are traditionally synthesised by formylations reactions such as the Gatterman, Gatterman-Koch, Reimer-Tiemann, Vilsmeier and the Duff reactions. As CNTs are electron-deficient species, these reactions are not suitable candidates for the formylation of CNTs. Another possible route for formylation is the carboxylation of CNTs, reduction of the carboxylic acid groups to alcohols, followed by the selective oxidation of the hydroxyl group to the formyl [353]. However, firstly, it is a resort to defect-based chemistry, and would involve multiple steps. Secondly, there is the problem

of selectivity. Once again, such routes produce considerable quantities of, often solid, side-products.

N-formylpiperidine has been used for extremely facile formyl transfer to organolithium and Grignard reagents, resulting in formation of formylated molecules in very high yields [354]. It has been demonstrated that SWNTs can be lithiated by lithium naphthalenide [221] and lithium in ammonia [218-220], resulting in the formation of the salt, [(SWNT)x^-.Lix^+]. The SWNT salt can be subjected to nucleophilic substitution, akin to organolithium species. Therefore, it is not unreasonable to explore if, in a similar way, formyl transfer to the SWNT salt could be achieved by *N*-formylpiperidine, according to the proposed reaction scheme shown in Figure 5-1 *(i)*.
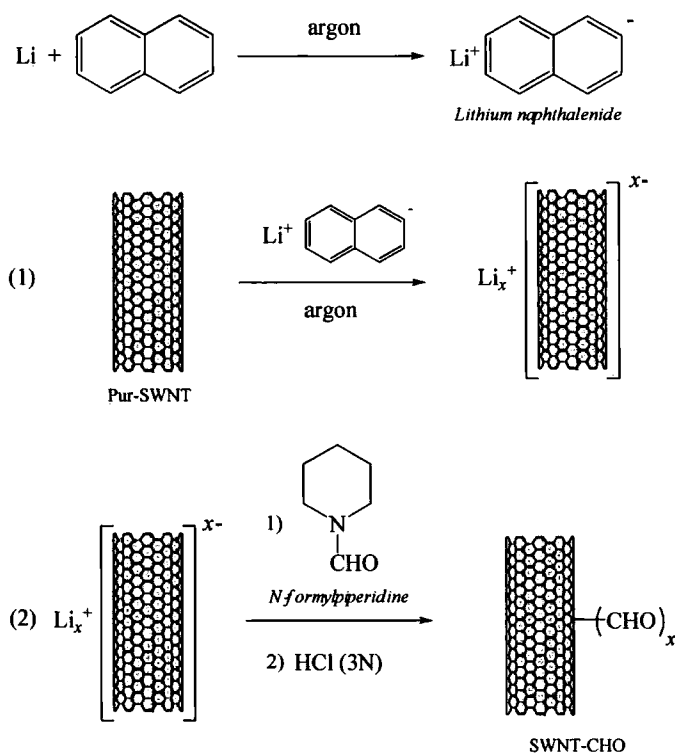
Figure 5-1

(i) Reaction scheme for the formylation of SWNTs.

111
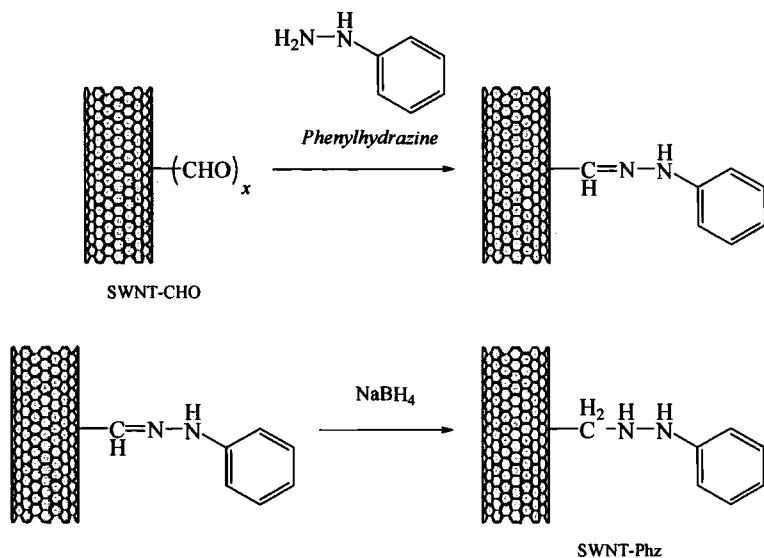
Figure 5-1

(ii) Reaction scheme for the tagging of the formylated SWNTs with phenylhydrazine.

5.2. Results and discussion

Single-wall carbon nanotubes were purified as described in Chapter 2. The purified SWNTs (Pur–SWNT) were subjected to the reaction scheme in Figure 5-1*(i)* (SWNT-CHO). The formylated SWNTs (SWNT-CHO) were characterised by Raman spectroscopy, UV-visible-near infrared (NIR) spectroscopy and thermogravimetric analysis-mass spectrometry (TGA-MS). It has been pointed out in Chapter 4 that the degree of functionalisation that is achieved via reduction with nucleophiles is low (~ 2 atomic *per cent*), although the modified SWNTs were found to be highly soluble. Owing to this, it was not possible to detect the formyl groups on the SWNT walls by mid-infrared spectroscopy. However, the formyl group was detected by tagging with phenylhydrazine via a hydrazone linkage (Figure 5-1*(ii)*). The SWNT-CHO tagged with phenylhydrazine (SWNT-Phz) were studied by Raman spectroscopy and TGA-MS. As a control, pristine SWNTs were simply stirred with *N*-formylpiperidine and washed to remove excess *N*-formylpiperidine (SWNT-CHO'), and these were also similarly treated with phenylhydrazine, followed by NaBH₄ (SWNT/Phz). Unlike the modified SWNTs

described in Chapter 4, it was observed that the SWNT-CHO and the SWNT-Phz show considerable ease of exfoliation not only in common organic solvents but also water.

The Raman spectra, recorded at an excitation wavelength of 532 nm, of the Pur-SWNT, SWNT-CHO, SWNT-Phz and SWNT/Phz are shown in Figure 5-2. Covalent functionalisation of CNTs may lead to an increase in the proportion of sp^3-hybridised carbon, resulting in an enhancement of the intensity of the D-band (I_D) relative to the G-band (I_G). The ratios of the intensities of the D-band to that of the G-band (I_D/I_G) for the various samples are summarised in Table 5-1. There is a small change in the I_D/I_G ratio for the SWNT-CHO (0.034) over that for the pristine Pur-SWNTs (0.03), although the increase is small and cannot be taken to be conclusive proof of covalent functionalisation. At the same time, it can be seen from Figure 5-2 that there is a broadening in the shape of the G-band for the SWNT-CHO over that for the Pur-SWNTs, suggesting a change in the electronic properties of the SWNT-CHO, which may be as a result of chemical modification. Also, the broadening of the G-band may mask an increase in the relative intensity of the D-band [195]. Significantly, upon the reaction for tagging with phenylhydrazine, the I_D/I_G ratio increases considerably to 0.062 from the value of 0.034 for the SWNT-CHO. However, the I_D/I_G ratio of the control SWNT/Phz (0.031) is almost identical with that of the pristine Pur-SWNTs (0.03). The D-band is considerably sensitive to resonance enhancement, and its intensity may change with a conversion of the functional group [178]. Thus, the Raman spectra suggest that the SWNTs may indeed have been modified by the formylation reaction, and further that these formyl groups on the SWNTs may be undergoing a conversion to a hydrazone bond upon tagging with phenylhydrazine.
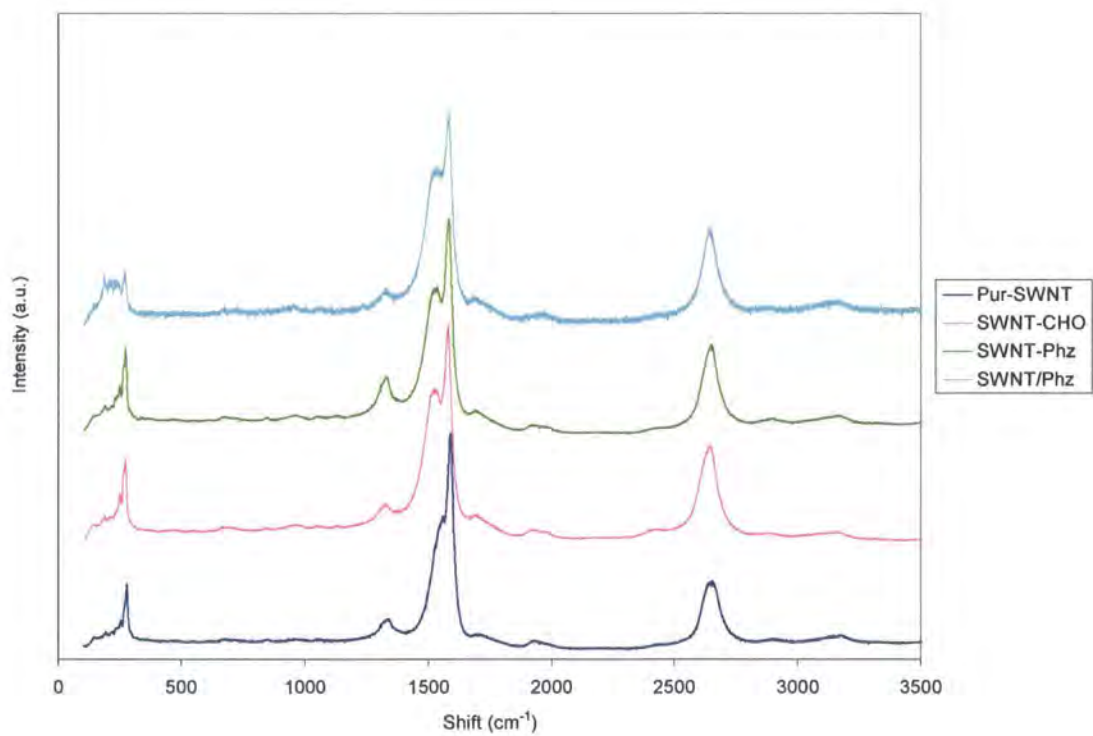
Figure 5-2

Raman spectra of pristine (Pur-SWNT) and formylated (SWNT-CHO) nanotubes, SWNT-CHO tagged with phenylhydrazine (SWNT-Phz), and a control sample (SWNT/Phz). The excitation wavelength is 532 nm. The spectra have been normalised to have identical maximum intensity of the G-band for ease of comparison.

Sample	I_D/I_G
Pur-SWNT	0.03
SWNT-CHO	0.034
SWNT-Phz	0.062
SWNT/Phz	0.031

Table 5-1

The areal ratios (I_D/I_G) of the intensities of the disorder (D-) band to the graphitic tangential (G-) band of the SWNT samples for which the Raman spectra are shown in Figure 5-2.

Further evidence of the modification of the SWNTs is provided by UV-vis-NIR spectroscopy. The transitions between the electronic densities of state in SWNTs can be observed as bands in the UV-vis-NIR spectra of the SWNTs [47]. Perturbation of the electronic structure of SWNTs by chemical modification leads to a suppression of the bands, and the extent of suppression provides a qualitative measure of the degree of functionalisation of the SWNTs [103, 104, 163, 178, 188, 192-194, 204, 208, 224]. The UV-vis-NIR spectra of the pristine Pur-SWNTs and the modified SWNT-CHO are shown in Figure 5-3. A weak suppression of the bands is observed for the SWNT-CHO, indicating that there has been a modification of the SWNTs, although the degree of functionalisation is low. This may prove to be a major advantage as the intrinsic electronic properties of the SWNTs are not modified by the formylation. It is worth pointing out that this observation is similar to that in Chapter 4, for SWNTs covalently modified via the reduction / electrophilic substitution route.
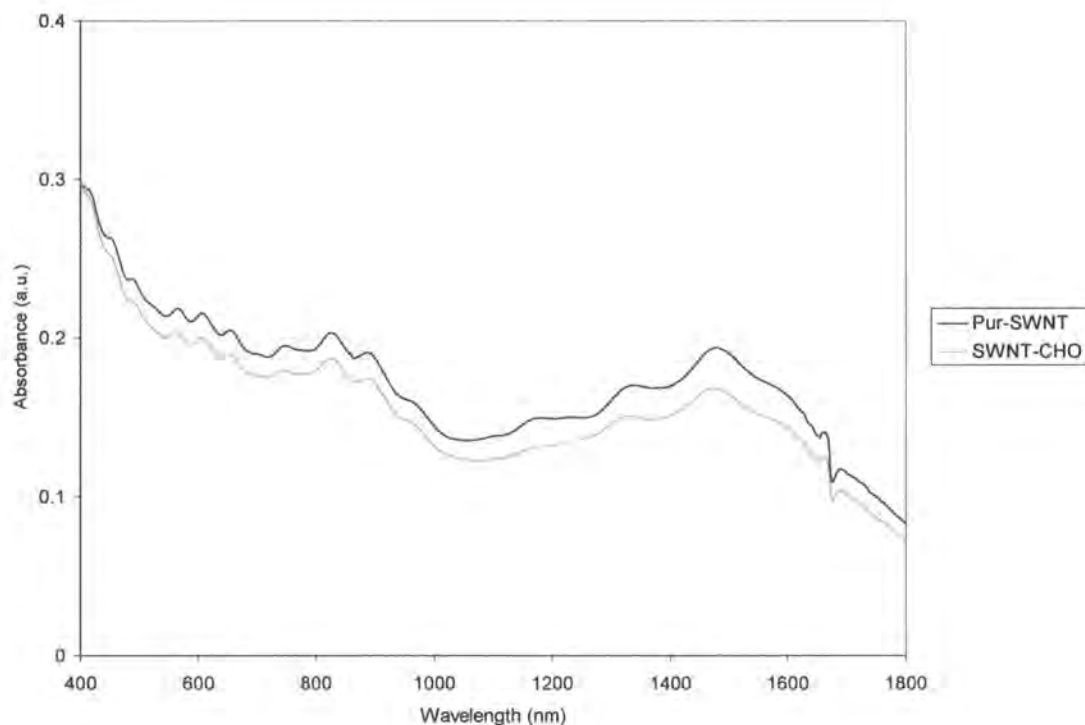
Figure 5-3

UV-vis-NIR spectra in DMF of Pur-SWNT and SWNT-CHO. The spectra have been normalised to have an absorbance of 0.3 units at 400 nm.

TGA-MS in helium of the SWNT-CHO (Figure 5-4*(i)*) shows the evolution of a fragment of weight 29.018 amu (corresponding to –CHO) in two regions: in the temperature range 100-180°C, and in the range 320-360°C. No such thermal defragmentation was observed for the control SWNT-CHO'. The evolution of the fragment at a temperature as high as 320-360°C suggests that it is covalently attached to the CNT framework, rather than physically adsorbed on the CNTs. It can be observed that the TGA curve has a steeper decline in the temperature range of 320-360°C than in the range 100-180°C. Also, the weight loss is greater in the higher temperature range than the lower range. Therefore, it may be reasonable to believe that the evolution of the –CHO group at the lower temperature range 100-180°C corresponds to the formyl groups that were attached to the amorphous carbon, which is considerably more reactive than the

SWNTs. Amorphous carbon present in raw SWNT material cannot be practically eliminated in entirety, and a very small amount of amorphous carbon can invariably be expected to be present in the starting Pur-SWNTs, even after the purification process. The weight loss in the higher temperature range 320-360°C corresponds to the thermal defragmentation of the –CHO groups that are attached directly to the SWNT walls.
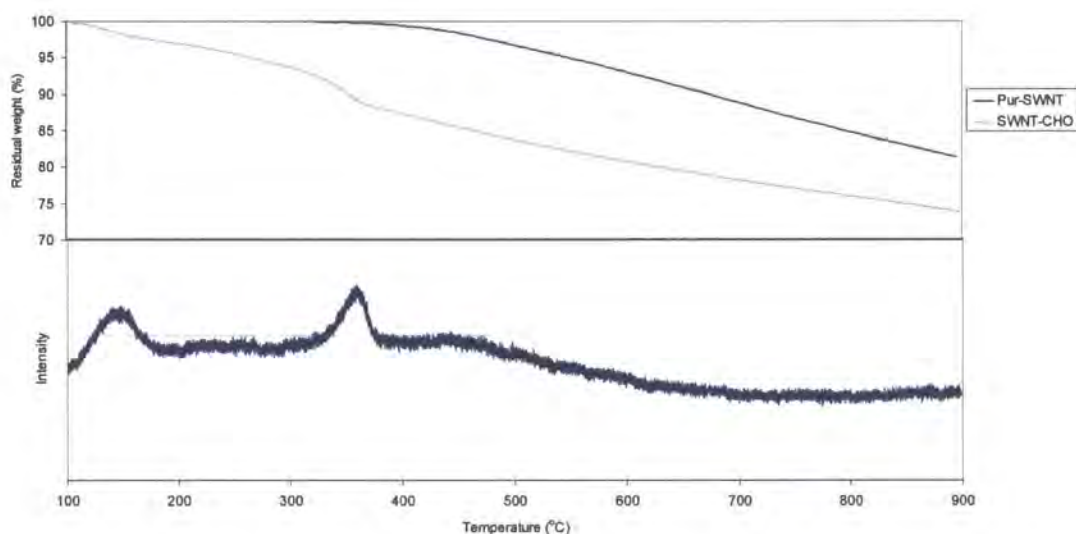
Figure 5-4

(i) (Above) TGA in helium for Pur-SWNT and SWNT-CHO and (below) the corresponding mass spectrometry data for the thermal evolution of –CHO (29.018 amu) for SWNT-CHO.
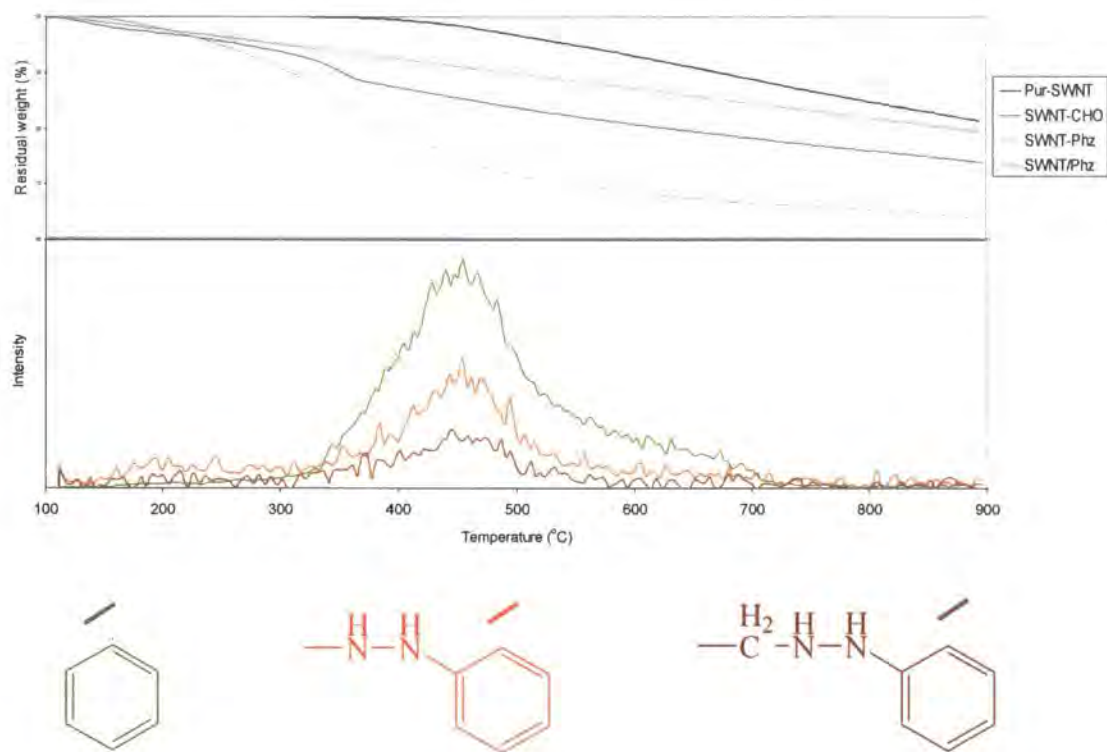
Figure 5-4

(ii) (Above) TGA in helium for Pur-SWNT, SWNT-CHO, SWNT-Phz and SWNT/Phz (control) and (below) the corresponding mass spectrometry data for the thermal evolution of the indicated fragments for SWNT-Phz.

The TGA-MS of the phenylhydrazine-tagged SWNT-Phz (Figure 5-4*(ii)*) shows a higher weight loss as compared to the SWNT-CHO. Also, the evolution of the fragments from the phenylhydrazide can be observed in the temperature range 350-500°C. The control SWNT/Phz does not show the evolution of these fragments. Additionally, the weight loss for the SWNT-Phz is higher than that for the control SWNT/Phz, which is almost identical with that for the pristine Pur-SWNTs. Thus, this demonstrates that there was indeed a covalent tagging of phenylhydrazine to the formyl groups on the SWNT-CHO.

From the TGA data of the SWNT-Phz, we estimate that the degree of formylation is approximately 2 atomic *per cent*. However, it must be cautioned that it is difficult to estimate the degree of functionalisation accurately from the TGA data of the SWNT-Phz,

as the percentage conversion of the formyl groups into hydrazone bonds is not exactly known. It is reasonable to believe that it should be quite similar to the degree of functionalisation achieved in the reduction / electrophilic substitution route described in Chapter 4, *i.e.* around 2 atomic *per cent*.

5.3 Conclusion

We have demonstrated a simple and elegant route for the formylation of SWNTs. Formylation of aromatic molecules is traditionally accomplished by reactions such as the Gatterman, Gatterman-Koch, Reimer-Tiemann, Vilsmeier and the Duff; however, these are electrophilic substitution reactions and cannot be readily extended to electron-deficient SWNTs. We have devised a route based on the reduction chemistry of SWNTs described in Chapter 4, followed by formyl transfer from *N*-formylpiperidine [354] to the reduced intermediate.

As can be expected for functionalisation via reduction of SWNTs, the degree of formylation is low. Owing to the low molecular weight of the formyl (–CHO) group, it was not possible to quantitatively estimate the degree of formylation from thermogravimetric analysis-mass spectrometry (TGA-MS). For this reason, the formyl groups could not be detected by mid-IR spectroscopy. However, TGA-MS showed the thermal evolution of the –CHO group at temperatures high enough (320-360°C) as to suggest that they were covalently attached to the SWNTs. For proving the covalent attachment of formyl groups on the SWNT, the formylated SWNTs were tagged with phenylhydrazine via a hydrazone linkage, and the tagged SWNTs were characterised by TGA-MS.

The available routes for the chemical modification of SWNTs are limited in scope, and do not offer great variety in terms of the moieties that can be attached to the nanotubes. The formyl group can potentially open the gateway for a wide range of C–C and C–N coupling reactions, reductions and other transformations, thus considerably enriching the chemistry of carbon nanotubes.

6. FUTURE WORK

1. Probing the electronic interaction between tertiary phosphines and SWNTs

Efforts are underway in the group to study the exact nature of the interaction between tertiary phosphines and SWNTs (Chapter 3). X-ray photoelectron spectroscopy (XPS) and measurement of the bulk electrical transport properties of SWNTs modified by tertiary phosphines suggest that there may be an interaction via the lone pair of electrons on the phosphorus atom in the phosphines. The electronic properties of SWNTs are sensitive to chemical species, as is evident from the chemical gating of semiconducting SWNTs upon exposure to electron-donating molecues such as ammonia [79] and amines [337], and electron-accepting ones such as O_2 [347] and NO_2 [79]. Thus, a suitable way for probing the charge-transfer interaction between tertiary phosphines and SWNTs may be studying the changes in the transport properties of field-effect transistors (FETs) fabricated from individual semiconducting SWNTs. Similarly, it is also proposed to use scanning tunnelling spectroscopy (STS) for studying the changes in the densities of state [347] induced by exposure to phosphines.

It is reasonable to compare the non-covalent modification of SWNTs by phosphines with that by amines [228, 260, 337-339], as both molecules have a lone pair of electrons (on the phosphorus and nitrogen atoms respectively). It has recently been suggested that amines may interact selectively with semiconducting SWNTs as compared with metallic ones, thus raising the possibility that modification by amines may be exploited for the enrichment of SWNTs of one electronic type based on differences in solubility [338]. Electrical property measurements on individual SWNT-based FET devices and STS studies may help in determining if a similar selective interaction exists for phosphines also, which may be used for the separation of nanotubes by electronic type.

2. Chemical modification of SWNTs for polymer composites

The true potential of CNT-based polymer composites is far from realised, thanks to the poor affinity of CNTs for, and poor dispersion in, polymer matrices [90-92], which has to be addressed by suitable chemical modification of the CNT surfaces. A major drawback of the reported routes for the chemical modification of CNTs is their lack of versatility. We have developed a facile route for the chemical modification of SWNTs by reduction with nucleophiles, followed by electrophilic substitution (Chapter 4), which shall considerably enrich the chemistry of SWNTs. The solubility of the SWNTs is considerably enhanced, and a wide range of moieties can be covalently attached to SWNTs, while the disruption of the intrinsic electronic structure of the nanotubes is minimal, thereby ensuring that the interesting properties of the nanotubes are not compromised. At the same time, we have also demonstrated an elegant reaction for the formylation of SWNTs (Chapter 5). The formyl (–CHO) group makes possible numerous coupling and transformation reactions, which shall enable the tethering of a wide range of molecules to SWNTs.

We propose to exploit these functionalisation routes for tailoring the surfaces of SWNTs for interaction with a wide range of polymers. The modified SWNTs shall be used as reinforcements in polymer composites, and their mechanical, thermal and electrical properties studied. It is hoped that the gap between the potential and currently achieved enhancement levels in the performance of CNT-polymer composites, can be substantially bridged.

7. EXPERIMENTAL

7.1 Purification

The SWNTs used in these studies were produced by the High-Pressure Carbon Monoxide (HiPCO) process [24], and obtained from Carbon Nanotechnologies, Inc. (CNI), Houston TX (USA). The average nanotube diameter is given by the supplier as 1.2 nm. Two batches of SWNTs, Batch 1 (#P0289) and Batch 2 (#P0323) have been used. The as-received SWNTs from these batches have been referred to herein as 1A- and 2A-SWNTs respectively.

7.1.1 Preparation of 1B-, 2B-, 2B'-, 2B''- and 2C-SWNTs

1B- and 2B-SWNTs: 100 mg of 1A-SWNTs were heated at 350°C for 1 h. They were then soaked in 400 mL 6M HCl for 8h at room temperature. The SWNTs were then separated from this suspension by filtering over a Whatman Cyclopore polycarbonate membrane filter (pore size 0.2 μm, diameter 47 mm) and washed with copious amounts of high-purity (18.2Ω) water to remove the acid. 2B-SWNTs were obtained by subjecting the as-received 2A-SWNTs to an identical procedure.

2B'-SWNTs: 100 mg of 2A-SWNTs were heated at 350°C for 1h, and then refluxed in 400 mL 6M NaOH solution at 120°C for 12 h. The suspension of the SWNTs in the NaOH solution was diluted with plenty of water, the SWNTs were separated from the suspension by filtering over Whatman Cyclopore membrane filter as above and washed with plenty of high-purity water to remove excess alkali, then immediately suspended in 400 mL 6M HCl and stirred for 6 h at room temperature. The SWNTs were then filtered and washed. The procedure for obtaining 2B''-SWNTs is identical, but without the air oxidation step.

2C-SWNTs: 100 mg 2A-SWNTs were heated at 350°C for 2h, then soaked in 400 mL 6M HCl for 8h at room temperature. The SWNTs were separated from this

suspension by filtering over a polycarbonate membrane filter and washed with copious amounts of high-purity water to remove the acid.

7.1.2 Preparation of 1B-ox-, 1B-ox'-, and 1B-nox-SWNTs

1B-ox-SWNTs: 100 mg 1B-SWNTs were refluxed in 50 mL of a 3:1 volume mixture of 6M sulphuric and 6M nitric acids at 120°C for 3 h. This suspension was then diluted with high purity water, and filtered over a Cyclopore polycarbonate membrane filter and washed with copious amounts of high purity water to remove excess acid.

1B-ox'-SWNTs: 40 mg 1B-ox-SWNTs were refluxed in 100 mL 6M NaOH solution at 120°C for 48 h, after which the suspension was diluted, filtered and washed as above, whereupon a reddish-brown filtrate was obtained. This procedure was repeated, after which the NaOH-treated SWNTs were then immediately suspended in 6M HCl solution and stirred at room temperature for 12 h, then filtered and washed.

1B-nox-SWNTs: 40 mg 1B-SWNTs were treated with NaOH, then neutralised with HCl, as described for the 1B-ox'-SWNTs above.

7.2 Modification by phosphines

Ann-Pur-SWNT-PA: The Pur-SWNT were annealed under vacuum (< 0.2 mbar) at 900°C for 8 h.

SWNT-PPh₃: 20 mg Ann-Pur-SWNT were stirred with molten triphenylphosphine, PPh_3 (Lancaster, 99%) under nitrogen at 90°C for 48 h. After this, excess PPh_3 was removed by Soxhlet extraction with dichloromethane for 48 h.

SWNT-POc₃: 20 mg Ann-Pur-SWNT were stirred with tri-*n*-octylphosphine, POc_3 (Lancaster, technical grade, 90%) under nitrogen at 90°C for 48 h. After this, excess POc_3 was removed by Soxhlet extraction with dichloromethane for 48 h.

7.3 Functionalisation by reduction followed by electrophilic substitution

Lithium metal (99%, sticks, Fluka), methyllithium (1.6 M solution in diethyl ether, Aldrich), n-butyllithium (1.6 M solution in hexanes, Aldrich), t-butyllithium solution (1.7 M solution in pentane, Aldrich), phenyllithium (1.8 M solution in di-n-butyl ether), naphthalene (99%, Aldrich), 1-bromopentane (99%, Aldrich), 4-methoxybenzyl bromide (synthesis grade, Aldrich), 4-nitrobenzyl bromide (99%, Aldrich), $3,5$-bis(trifluoromethyl)benzyl bromide (97%, Aldrich), N-formylpiperidine (99%, Aldrich) and phenylhydrazine (97%, Aldrich) and sodium borohydride, $NaBH_4$ (98%, Aldrich) were used as received.

SWNT-Pe, SWNT-OMe and SWNT-NO₂: The synthesis of these modified SWNTs was carried out entirely in an argon atmosphere. 7 mg (1 mmol) lithium and 128 mg naphthalene (1 mmol) were transferred into a Schlenk. Dry THF (~ 20 mL) was cannulated into the Schlenk, and the contents were left to stir for 24 h under argon till all the metal had dissolved, to yield a green solution of lithium naphthalenide. The lithium naphthalenide was cannulated onto 12 mg Pur-SWNT taken in another Schlenk, and the contents were allowed to stir for 8 h at room temperature. After 8 h, the Schlenk was cooled to 0°C, and the reduced SWNTs were quenched by addition of 2 mmol of RX (302 mg of 1-bromopentane, 402 mg of 4-methoxybenzyl bromide or 432 mg of 4-nitrobenzyl bromide, respectively). The modified SWNTs were then washed by Soxhlet extraction with THF for 24 h, followed by absolute ethanol for a further 24 h to remove excess reactants and by-products. The modified SWNTs were filtered over a polycarbonate membrane filter.

R₁-SWNT-R₂: The synthesis of these modified SWNTs was carried out entirely in a nitrogen atmosphere. 12 mg Pur-SWNT were taken in a Schlenk and dry THF (~ 20 mL) was cannulated into it. The contents of the Schlenk were cooled to 0°C, after which 0.5 mmol of R₁-Li (R₁ = Me, nBu, tBu, Ph) were injected into the Schlenk, and the contents allowed to stir at 0°C for 8 h. The reduced SWNTs were then quenched under rapid stirring in an ice bath with 0.75 mmol of R₂X [R₂ = 4-methoxybenzyl, 4-nitrobenzyl, $3,5$-bis(trifluoromethyl)benzyl, and X = Br]. The modified SWNTs were

then subjected to Soxhlet extraction with THF followed by absolute ethanol as above, and were then filtered over a polycarbonate membrane filter.

(R₁)(R₁′)-SWNT-(R₂)(R₂′) and **(R₁) (R₁′)(R₁″)-SWNT-(R₂)(R₂′)(R₂″)**: The multiple sequences of functionalisation were carried out under nitrogen and at a temperature of 0°C throughout as follows [quenching with *3,5-bis*(trifluoromethyl)benzyl bromide was carried out after cooling the Schlenk to -44°C]:

1. addition of 0.5 mmol of R_1-Li, stirring for 8 h, followed by quenching with 0.75 mmol of R_2X;
2. addition of 0.5 mmol of R_1'-Li, stirring for 8 h, followed by quenching with 0.75 mmol of $R_2'X$;
3. addition of 0.5 mmol of R_1''-Li, stirring for 8 h, followed by quenching with 0.75 mmol of $R_2''X$.

The modified SWNT samples were washed as described above.

7.4 Formylation

SWNT-CHO: The synthesis is identical with that of SWNT-Pe, SWNT-OMe and SWNT-NO₂. After reduction of the Pur-SWNTs with lithium naphthalenide for 8 h, the reaction was quenched by addition of *N*-formylpiperidine, and allowed to stir for 1 h, and then worked up with 3N HCl till the solution turns acidic. The formylated SWNT samples were washed as above.

SWNT-Phz: 12 mg SWNT-CHO and 54 mg (0.5 mmol) phenylhydrazine were allowed to react for 24 h in 20 mL acetate buffer (pH = 5.0), at the end of which 19 mg NaBH₄ (0.5 mmol) was added to the suspension and allowed to stir for a further 2 h. The tagged SWNT-Phz were washed as above.

7.5 Characterisation

7.5.1 Raman spectroscopy

Raman spectra were recorded on solid samples taken on optically transparent glass sides, using a Jobin Yvon Horiba LabRAM spectrometer in a back scattered confocal configuration, using excitation wavelengths of 532.3 nm or 632.8 nm. All spectra were referenced to the silicon line at 520 cm^{-1}. In view of the heterogeneity of the samples, spectra were recorded at three different regions of the samples to ensure that the obtained spectra are truly representative of the sample. The ratios of the area of the D-band to that of the G-band (I_D/I_G) reported herein are the average values for all the spectra recorded for a particular sample.

7.5.2 Ultraviolet-visible-near infrared (UV-vis-NIR spectroscopy)

The UV-vis-NIR absorption spectra were recorded on a Perkin Elmer Lambda 900 spectrometer, on suspensions of the CNT samples taken in a quartz cell of optical path length 10 mm. The suspensions were prepared by dispersing the nanotube material in DMF (99%, Aldrich) or *1,2*-dichlorobenzene (Aldrich, 99%) to an initial concentration of 1 mg/mL using mild bath sonication (Ultrawave U50, 30–40 kHz) for 5 min, followed by filtration through cotton wool to remove particulates.

7.5.3 Thermogravimetric analysis-mass spectrometry (TGA-MS)

Thermogravimetric analysis (TGA) was carried out using a Perkin Elmer Pyris I system in a He environment. Samples were heated from room temperature to 900°C at a rate of 10°C/min. Mass spectrometry was carried out by a Hiden HPR-20 mass spectrometer coupled to the TGA system.

7.5.4 Atomic force microscopy (AFM)

Samples for AFM analysis were produced by drop deposition onto mica of the corresponding solution of SWNTs (concentration of 0.005 mg/ml) in DMF produced by sonication in an ultrasonic bath (Ultrawave U50, 30 – 40 kHz) for 15 minutes. Samples were dried in air before imaging in tapping mode using a Digital Instruments Multimode AFM with a Nanoscope IV controller.

7.5.5 X-ray photoelectron spectroscopy (XPS)

XPS studies were performed at NCESS, Daresbury laboratory using a Scienta ESCA 300 hemispherical analyser with a base pressure under 3×10^{-9} mbar. The analysis chamber was equipped with a monochromated Al K_α X-ray source ($h\nu = 1486.6$ eV). Charge compensation was achieved (if required) by supplying low energy (<3 eV) electrons to the samples. XPS data were referenced with respect to the corresponding C 1s binding energy of 284.5 eV which is typical for carbon nanotubes. Photoelectrons were collected at a 45 degree take-off angle, and the analyser pass energy was set to 150 eV giving an overall energy resolution of 0.4 eV.

7.5.6 Measurement of bulk electrical properties

The bulk electrical transport properties of the CNTs were measured at room temperature in air by a four-point contact apparatus, on thick films (roughly few tens of microns) of CNTs obtained by filtering a dispersion of nanotubes in absolute ethanol over a 0.22 µm pore-size, 25 mm cellulose acetate membrane, which was then dried in a vacuum oven at 60°C for 8h to remove the solvent. The 4- wire resistances of the samples were measured in a Van der Pauw geometry using a Keithley 2602 Source Measure Unit (SMU). A constant current (<5 mA) was applied between two adjacent terminals and the voltage across the opposite terminals was recorded.

7.5.7 Cyclic voltammetry

Measurements taken using a computer controlled potentiostat (Autolab PGSTAT12) with a standard three-electrode configuration. All experiments were carried out in a three-necked glass cell. Electrolyte solution consisted of 0.1M HCl (at pH of 1) and degassed with N_2 for 30 minutes before use. A glassy carbon electrode (BASi supplied) acted as a working electrode. CV was recorded on a film of SWNT sample drop cast from suspension onto the working electrode and dried under a gentle stream of nitrogen. The counter electrode consisted of a 0.5 mm diameter Pt wire (exposed length of 4 cm) and a Ag/AgCl electrode in 0.1M KCl solution acted as the reference electrode. Cyclic voltammagrams were recorded using a 2 mV step potential and scan rate of 100 mVs^{-1}.

APPENDIX

As an illustration, the estimation of the degree of functionalisation for the SWNT-OMe (Figure 4-6) is shown here. We consider the residual weights at 550°C (after the evolution of the organic groups is complete), and assume that the weight loss of pristine Pur-SWNTs is entirely owing to –COOH groups.

For the Pur-SWNTs, the percentage coverage of –COOH groups, a, is given by

$$\frac{12 \times (100 - a)}{12 \times (100 - a) + 45a} = 0.94$$

or $a = 1.7$

For the SWNT-OMe, the percentage coverage of the 4-methoxybenzyl groups, b, is given by

$$\frac{12 \times (100 - 1.7 - b)}{12 \times (100 - 1.7 - b) + 45 \times 1.7 + 133b} = 0.78$$

or $b = 1.9$

Thus, the degree of functionalisation is 1.9 *per cent.*

REFERENCES

1. Iijima S *Nature* **1991**, *354*, 56-58.

2. Boehm HP *Carbon* **1997**, *35*, 581-584.

3. Monthioux M, Kuznetsov VL *Carbon* **2006**, *44*, 1621-1623.

4. Radushkevich LV, Lukyanovich VM *Zurn. Phys. Chem.* **1952**, *26*, 88-95.

5. Kroto HW, Heath JR, O'Brien SC, Curl RF, Smalley RE *Nature* **1985**, *318*, 162-163.

6. Iijima S, Ichihashi T *Nature* **1993**, *363*, 603-605.

7. Bethune DS, Klang CH, de Vries MS, Gorman G, Savoy R, Vazquez J, Beyers R *Nature* **1993**, *363*, 605-607.

8. Peng HY, Wang N, Zheng YF, Lifshitz Y, Kulik J, Zhang RQ, Lee CS, Lee ST *Appl. Phys. Lett.* **2000**, *77*, 2831-2833.

9. Hayashi T, Kim YA, Matoba T, Esaka M, Nishimura K, Tsukada T, Endo M, Dresselhaus MS *Nano Lett.* **2003**, *3*, 887-889.

10. Krätschmer W, Lamb LD, Fostiropoulos K, Huffman DR *Nature* **1990**, *347*, 354-358.

11. Ebbesen TW, Ajayan PM *Nature* **1992**, *358*, 220-222.

12. Guo T, Nikolaev P, Thess A, Colbert DT, Smalley RE *Chem. Phys. Lett.* **1995**, *243*, 49-54.

13. Thess A, Lee R, Nikolaev P, Dai H, Petit P, Robert J, Xu C, Lee YH, Kim SG, Rinzler AG, Colbert DT, Scuseria GE, Tomanek D, Fischer JE, Smalley RE *Science* **1996**, *273*, 483-487.

14. Yudasaka M, Kikuchi R, Matsui T, Ohki Y, Yoshimura S, Etsuro O, *Appl. Phys. Lett.* **1995**, *67*, 2477-2479.

15. Peigney A, Laurent C, Dobigeon F, Rousset A *J. Mater. Res.* **1997**, *12*, 613-615.

16. Kong J, Cassell AM, Dai H *Chem. Phys. Lett.* **1998**, *292*, 567-574.

17. Dai H, Rinzler AG, Nikolaev P, Thess A, Colbert DT, Smalley RE *Chem. Phys. Lett.* **1996**, *260*, 471-475.

18. Hafner JH, Bronikowski MJ, Azamian BR, Nikolaev P, Rinzler AG, Colbert DT, Smith KA, Smalley RE *Chem. Phys. Lett.* **1998**, *296*, 195-202.

19. Nikolaev P, Bronikowski MJ, Bradley RK, Rohmund F, Colbert DT, Smith KA, Smalley RE *Chem. Phys. Lett.* **1999**, *313*, 91-97.

20. Mukhopadhyay K, Koshio A, Tanaka N, Shinohara H *Japan. J. Appl. Phys.* **1998**, *37*, L1257-L1259.

21. Murakami Y, Miyauchi Y, Chiashi S, Maruyama S *Chem. Phys. Lett.* **2003**, *374*, 53-58.

22. Zhang ZJ, Wei BQ, Ramanath G, Ajayan PM *Appl. Phys. Lett.* **2000**, *77*, 3764-3766.

23. Li Y-L, Kinloch IA, Windle AH *Science* **2004**, *304*, 276-278.

24. Kong J, Soh HT, Cassell AM, Quate CF, Dai H *Nature* **1998**, *395*, 878-881.

25. Wong SS, Joselevich E, Woolley AT, Cheung CL, Lieber CM *Nature* **1998**, *394*, 52-55.

26. Gamaly EG, Ebbesen TW *Phys. Rev. B* **1995**, *52*, 2083-2089.

27. de Heer WA, Poncharal P, Berger C, Gezo J, Song Z, Bettini J, Ugarte D *Science* **2005**, *307*, 907-910.

28. Harris PJF, Tsang SC, Claridge JB, Green MLH *J. Chem. Soc. Faraday Trans.* **1994**, *90*, 2799-2802.

29. Zhou D, Chow L *J. Appl. Phys.* **2003**, *93*, 9972-9976.

30. Huang JY, Chen S, Ren ZF, Chen G, Dresselhaus MS *Nano Lett.* **2006**, *6*, 1699-1705.

31. Harris PJF *Carbon* **2007**, *45*, 229-239.

32. Kroto HW *Science* **1988**, *242*, 1139-1145.

33. Buseck PR, Tsipursky SJ, Hettich R *Science* **1992**, *257*, 215-217.

34. Daly TK, Buseck PR, Williams P, Lewis CF *Science* **1993**, *259*, 1599-1601.

35. Heymann D, Chibante LPF, Brooks RR, Wolbach WS, Smalley RE *Science* **1994**, *265*, 645-647.

36. Becker L, Bada JL *Science* **1994**, *265*, 642-645.

37. Kawasaki S, Shinoda M, Shimada T, Okino F, Touhara H *Carbon* **2006**, *44*, 2139-2141.

38. Chen GY, Poa CHP, Henley SJ, Stolojan V, Silva SRP *Appl. Phys. Lett.* **2005**, *87*, 253115.

39. Takagi D, Homma Y, Hibino H, Suzuki S, Kobayashi Y *Nano Lett.* **2006**, *6*, 2642-2645.

40. Walter EC, Beetz T, Sfeir MY, Brus LE, Steigerwald ML *J. Am. Chem. Soc.* **2006**, *128*, 15590-15591.

41. Mintmire JW, Dunlap BI, White CT *Phys. Rev. Lett.* **1992**, *68*, 631-634.

42. Hamada N, Sawada S, Oshiyama A *Phys. Rev. Lett.* **1992**, *68*, 1579-1581.

43. Saito R, Fujita M, Dresselhaus G, Dresselhaus MS *Appl. Phys. Lett.* **1992**, *60*, 2204-2206.

44. Wildöer JWG, Venema LC, Rinzler AG, Smalley RE, Dekker C *Nature* **1998**, *391*, 59-62.

45. Odom TW, Huang J-L, Kim P, Lieber C *Nature* **1998**, *391*, 62-64.

46. Venema LC, Meunier V, Lambin Ph., Dekker C *Phys. Rev. B* **2000**, *61*, 2991-2996.

47. Kataura H, Kumazawa Y, Maniwa Y, Umezu I, Suzuki S, Ohtsuka Y, Achiba Y *Synth. Met.* **1999**, *103*, 2555-2558.

48. Jost O, Gorbunov AA, Pompe W, Pichler T, Friedlein R, Knupfer M, Reibold M, Bauer H-D, Dunsch L, Golden MS, Fink J *Appl. Phys. Lett.* **1999**, *75*, 2217-2219.

49. de Jonge N, Bonard J-M *Phil. Trans. R. Soc. Lond. A* **2004**, *362*, 2239-2266.

50. Tans SJ, Devoret MH, Dai H, Thess A, Smalley RE, Geerligs LJ, Dekker C *Nature* **1997**, *386*, 474-477.

51. Frank S, Poncharal P, Wang ZL, de Heer WA *Science* **1998**, *280*, 1744-1746.

52. Hone J, Whitney M, Zettl A *Synth. Met.* **1999**, *103*, 2498-2499.

53. Hone J, Llaguno MC, Biercuk MJ, Johnson AT, Batlogg B, Benes Z, Fischer JE *Appl. Phys. A* **2002**, *74*, 339-343.

54. Berber S, Kwon Y-K, Tománek D *Phys. Rev. Lett.* **2000**, *84*, 4613-4616.

55. Che J, Çağin T, Goddard WA III *Nanotechnol.* **2000**, *11*, 65-69.

56. Lu Q, Keskar G, Ciocan R, Rao R, Mathur RB, Rao AM, Larcom LL *J. Phys. Chem. B* **2006**, *110*, 24371-24376.

57. Treacy MMJ, Ebbesen TW, Gibson JM *Nature* **1996**, *381*, 678-680.

58. Krishnan A, Dujardin E, Ebbesen TW, Yianilos PN, Treacy MMJ *Phys. Rev. B* **1998**, *58*, 14013-14019.

59. Lu JP *Phys. Rev. Lett.* **1997**, *79*, 1297-1300.

60. Popov VN, Van Doren VE, Balkanski M *Phys. Rev. B* **2000**, *61*, 3078-3084.

61. Yu M-F, Lourie O, Dyer MJ, Moloni K, Kelly TF, Ruoff RS *Science* **2000**, *287*, 637-640.

62. Yu M-F, Files BS, Arepalli S, Ruoff RS *Phys. Rev. Lett.* **2000**, *84*, 5552-5555.

63. Li F, Cheng HM, Bai S, Su G, Dresselhaus MS *Appl. Phys. Lett.* **2000**, *77*, 3161-3163.

64. Baughman RH, Zakhidov AA, de Heer WA *Science* **2002**, *297*, 787-792.

65. Endo M, Hayashi T, Kim YA, Terrones M, Dresselhaus MS *Phil. Trans. R. Soc. Lond. A* **2004**, *362*, 2223-2238.

66. Tans SJ, Verschueren ARM, Dekker C *Nature* **1998**, *393*, 49-52.

67. Martel R, Schmidt T, Shea HR, Hertel T, Avouris Ph *Appl. Phys. Lett.* **1998**, *73*, 2447-2449.

68. Bachtold A, Hadley P, Nakanishi T, Dekker C *Science* **2001**, *294*, 1317-1320.

69. Johnston DE, Islam MF, Yodh AG, Johnson AT *Nature Mater.* **2005**, *4*, 589-592.

70. Chung D-S, Park SH, Lee HW, Choi JH, Cha SN, Kim JW, Jang JE, Min KW, Cho SH, Yoon MJ, Lee JS, Lee CK, Yoo JH, Kim J-M, Jung JE, Jin YW, Park YJ, You JB *Appl. Phys. Lett.* **2002**, *80*, 4045-4047.

71. Saito Y, Uemura S *Carbon* **2000**, *38*, 169-182.

72. Sugie H, Tanemura M, Filip V, Iwata K, Takahashi K, Okuyama F *Appl. Phys. Lett.* **2001**, *78*, 2578-2580.

73. Gao B, Kleinhammes A, Tang XP, Bower C, Fleming L, Wu Y, Zhou O *Chem. Phys. Lett.* **1999**, *307*, 153-157.

74. Che G, Lakshmi BB, Fisher ER, Martin CR *Nature* **1999**, *393*, 346-349.

75. Britto PJ, Santhanam KSV, Rubio A, Alonso JA, Ajayan PM *Adv. Mater.* **1999**, *11*, 154-157.

76. Niu C, Sichel EK, Hoch R, Moy D, Tennent H *Appl. Phys. Lett.* **1997**, *70*, 1480-1482.

77. An KH, Kim WS, Park YS, Moon J-M, Bae DJ, Lim SC, Lee YS, Lee YH *Adv. Funct. Mater.* **2001**, *11*, 387-392.

78. Baughman RH, Cui C, Zakhidov AA, Iqbal Z, Barisci JN, Spinks GM, Wallace GG, Mazzoldi A, De Rossi D, Rinzler AG, Jaschinski O, Roth S, Kertesz M *Science* **1999**, *284*, 1340-1344.

79. Kong J, Franklin NR, Zhou C, Chapline MG, Peng S, Cho K, Dai H *Science* **2000**, *287*, 622-625.

80. Varghese OK, Kichambre PD, Gong D, Ong KG, Dickey EC, Grimes CA *Sensors and Actuators B* **2001**, *81*, 32-41.

81. Chopra S, Pham A, Gaillard J, Parker A, Rao AM *Appl. Phys. Lett.* **2002**, *80*, 4632-4634.

82. Cai H, Cao X, Jiang Y, He P, Fang Y *Anal. Bioanal. Chem.* **2003**, *375*, 287-293.

83. Star A, Gabriel J-CP, Bradley K, Grüner G *Nano Lett.* **2003**, *3*, 459-463.

84. Qian D, Dickey EC, Andrews R, Rantell T *Appl. Phys. Lett.* **2000**, *76*, 2868-2870.

85. Haggenmueller R, Gommans HH, Rinzler AG, Fischer JE, Winey KI *Chem. Phys. Lett.* **2000**, *330*, 219-225.

86. Kumar S, Dang TD, Arnold FE, Bhattacharyya AR, Min BG, Zhang X, Vaia RA, Park C, Adams WW, Hauge RH, Smalley RE, Ramesh S, Willis PA *Macromol.* **2002**, *35*, 9039-9043.

87. Xu X, Thwe MM, Shearwood C, Liao K *Appl. Phys. Lett.* **2002**, *81*, 2833-2835.

88. Biercuk MJ, Llaguno MC, Radosavljevic M, Hyun JK, Johnson AT, Fischer JE *Appl. Phys. Lett.* **2002**, *80*, 2767-2769.

89. Choi ES, Brooks JS, Eaton DL, Al-Haik MS, Hussaini MY, Garmestani H, Li D, Dahmen K *J. Appl. Phys.* **2003**, *94*, 6034-6039.

90. Graff RA, Swanson JP, Barone PW, Baik S, Heller DA, Strano MS *Adv. Mater.* **2005**, *17*, 980-984.

91. Penumadu D, Dutta A, Pharr GM, Files B *J. Mater. Res.* **2003**, *18*, 1849-1853.

92. Ajayan PM, Schadler LS, Giannaris C, Rubio A *Adv. Mater.* **2000**, *12*, 750-753.

93. Qin Y, Liu L, Shi J, Wu W, Zhang J, Guo Z-X, Li Y, Zhu D *Chem. Mater.* **2003**, *15*, 3256-3260.

94. Eitan A, Jiang K, Dukes D, Andrews R, Schadler LS *Chem. Mater.* **2003**, *15*, 3198-3201.

95. Dyke CA, Tour JM *J. Phys. Chem. A* **2004**, *108*, 11151-11159.

96. Li S, Qin Y, Shi J, Guo Z-X, Li Y, Zhu D *Chem. Mater.* **2005**, *17*, 130-135.

97. Chen Y, Shaw DT, Bai XD, Wang EG, Lund C, Lu WM, Chung DDL *Appl. Phys. Lett.* **2001**, *78*, 2128-2130.

98. Tibbetts GG, Meisner GP, Olk CH *Carbon* **2001**, *39*, 2291-2301.

99. Shen K, Xu H, Jiang Y, Pietraß T *Carbon* **2004**, *42*, 2315-2322.

100. Girifalco LA, Hodak M, Lee RS *Phys. Rev. B* **2000**, *62*, 13104-13110.

101. Lu KL, Lago RM, Chen YK, Green MLH, Harris PJF, Tsang SC *Carbon* **1996**, *34*, 814-816.

102. Shelimov KB, Esenaliev RO, Rinzler AG, Huffman CB, Smalley RE *Chem. Phys. Lett.* **1998**, *282*, 429-434.

103. Kamaras K, Itkis ME, Hu H, Zhao B, Haddon RC *Science* **2003**, *301*, 1501.

104. Cai L, Bahr JL, Yao Y, Tour JM *Chem. Mater.* **2002**, *14*, 4235-4241.

105. Kadish KM, Ruoff RS (ed.) *Fullerenes: Chemistry, Physics and Technology*, Wiley-Interscience (New York), **2000**.

106. Haddon RC *Science* **1993**, *261*, 1545-1550.

107. Haddon RC *Acc. Chem. Res.* **1998**, *21*, 243-249.

108. Liu J, Rinzler AG, Dai H, Hafner JH, Bradley RK, Boul PJ, Lu A, Iverson T, Shelimov K, Huffman CB, Rodriguez-Macias F, Shon Y-S, Lee TR, Colbert DT, Smalley RE *Science* **1998**, *280*, 1253-1256.

109. Duesberg GS, Burghard M, Muster J, Philipp G, Roth S *Chem. Commun.* **1998**, 435-436.

110. Islam MF, Rojas E, Bergey DM, Johnson AT, Yodh AG *Nano Lett.* **2003**, *3*, 269-273.

111. Matarredona O, Rhoads H, Li Z, Harwell JH, Balzano L, Resasco DE *J. Phys. Chem. B* **2003**, *107*, 13357-13367.

112. Bandow S, Rao AM, Williams KA, Thess A, Smalley RE, Eklund PC *J. Phys. Chem. B* **1997**, *101*, 8839-8842.

113. Moore VC, Strano MS, Haroz EH, Hauge RH, Smalley RE *Nano Lett.* **2003**, *3*, 1379-1382.

114. O'Connell MJ, Boul P, Ericson LM, Huffman C, Yang W, Haroz E, Kuper C, Tour J, Ausman KD, Smalley RE *Chem. Phys. Lett.* **2001**, *342*, 265-271.

115. Zou Y, Feng Y, Wang L, Liu X *Carbon* **2004**, *42*, 271-277.

116. Baskaran D, Mays JW, Bratcher MS *Chem. Mater.* **2005**, *17*, 3389-3397.

117. Liu A, Honma I, Ichihara M, Zhou H *Nanotechnol.* **2006**, *17*, 2845-2849.

118. Bandyopadhyaya R, Nativ-Roth E, Regev O, Yerushalmi-Rozen R *Nano Lett.* **2002**, *2*, 25-28.

119. Star A, Steuerman DW, Heath JR, Stoddart JF *Angew. Chem. Int. Ed.* **2002**, *41*, 2508-2512.

120. Curran SA, Ajayan PM, Blau WJ, Carroll DL, Coleman JN, Dalton AB, Davey AP, Drury A, McCarthy B, Maier S, Strevens A *Adv. Mater.* **1998**, *10*, 1091-1093.

121. Curran S, Davey AP, Coleman JN, Dalton AB, McCarthy B, Maier S, Drury A, Gray D, Brennan M, Ryder K, Lamy de la Chapelle M, Journet C, Bernier P, Byrne HJ, Carroll D, Ajayan PM, Lefrant S, Blau W *Synth. Met.* **1999**, *103*, 2559-2562.

122. Coleman JN, Dalton AB, Curran S, Rubio A, Davey AP, Drury A, McCarthy B, Lahr B, Ajayan PM, Roth S, Barklie RC, Blau WJ *Adv. Mater.* **2000**, *12*, 213-216.

123. Dalton AB, Blau WJ, Chambers G, Coleman JN, Henderson K, Lefrant S, McCarthy B, Stephan C, Byrne HJ *Synth. Met.* **2001**, *121*, 1217-1218.

124. Star A, Stoddart JF, Steuerman D, Diehl M, Boukai A, Wong EW, Yang X, Chung S-W, Choi H, Heath JR *Angew. Chem. Int. Ed.* **2001**, *40*, 1721-1725.

125. Star A, Liu Y, Grant K, Ridvan L, Stoddart JF, Steuerman DW, Diehl MR, Boukai A, Heath JR *Macromol.* **2003**, *36*, 553-560.

126. Tang BZ, Xu H *Macromol.* **1999**, *32*, 2569-2576.

127. Steuerman DW, Star A, Narizzano R, Choi H, Ries RS, Nicolini C, Stoddart JF, Heath JR *J. Phys. Chem. B* **2002**, *106*, 3124-3130.

128. Huang J-W, Bai SH *Nanotechnol.* **2005**, *16*, 1406-1410.

129. Tsang SC, Guo Z, Chen YK, Green MLH, Hill HAO, Hambley TW, Sadler PJ *Angew. Chem. Int. Ed.* **1997**, *36*, 2198-2200.

130. Guo Z, Sadler PJ, Tsang SC *Adv. Mater.* **1998**, *10*, 701-703.

131. Azamian BR, Davis JJ, Coleman KS, Bagshaw CB, Green MLH *J. Am. Chem. Soc.* **2002**, *124*, 12664-12665.

132. Davis JJ, Coleman KS, Azamian BR, Bagshaw CB, Green MLH *Chem. Eur. J.* **2003**, *9*, 3732-3739.

133. Balavoine F, Schultz P, Richard C, Mallouh V, Ebbesen TW, Mioskowski C *Angew. Chem. Int. Ed.* **1999**, *38*, 1912-1915.

134. Zheng M, Jagota A, Strano MS, Santos AP, Barone P, Chou SG, Diner BA, Dresselhaus MS, Mclean RS, Onoa GB, Samsonidze GG, Semke ED, Usrey M, Walls DJ *Science* **2003**, *302*, 1545-1548.

135. Zheng M, Jagota A, Semke ED, Diner BA, Mclean RS, Lustig SR, Richardson RE, Tassi NG *Nature Mater.* **2003**, *2*, 338-342.

136. Chen RJ, Zhang Y, Wang D, Dai H *J. Am. Chem. Soc.* **2001**, *123*, 3838-3839.

137. Tagmatarchis N, Prato M, Guldi DM *Physica E* **2005**, *29*, 546-550.

138. Paloniemi H, Ääritalo T, Laiho T, Liuke H, Kocharova N, Haapakka K, Terzi F, Seeber R, Lukkari J *J. Phys. Chem. B* **2005**, *109*, 8634-8642.

139. Yuan WZ, Sun JZ, Dong Y, Häussler M, Yang F, Xu HP, Qin A, Lam JWY, Zheng Q, Tang BZ *Macromol.* **2006**, *39*, 8011-8020.

140. Tomonari Y, Murakami H, Nakashima N *Chem. Eur. J.* **2006**, *12*, 4027-4034.

141. Rinzler AG, Liu J, Dai H, Nikolaev P, Huffman CB, Rodríguez-Macías FJ, Boul PJ, Lu AH, Heymann D, Colbert DT, Lee RS, Fischer JE, Rao AM, Eklund PC, Smalley RE *Appl. Phys. A* **1998**, *67*, 29-37.

142. Dujardin E, Ebbesen TW, Krishnan A, Treacy MMJ *Adv. Mater.* **1998**, *10*, 611-613.

143. Dillon AC, Gennett T, Jones KM, Alleman JL, Parilla PA, Heben MJ *Adv. Mater.* **1999**, *11*, 1354-1358.

144. Vaccarini L, Goze C, Aznar R, Micholet V, Journet C, Bernier P *Synth. Met.* **1999**, *103*, 2492-2493.

145. Zhang M, Yudasaka M, Koshio A, Iijima S *Chem. Phys. Lett.* **2001**, *349*, 25-30.

146. Chen XH, Chen CS, Chen Q, Cheng FQ, Zhang G, Chen ZZ *Mater. Lett.* **2002**, *57*, 734-738.

147. Kajiura H, Tsutsui S, Huang H, Murakami Y *Chem. Phys. Lett.* **2002**, *364*, 586-592.

148. Martínez MT, Callejas MA, Benito AM, Cochet M, Seeger T, Ansón A, Schreiber J, Gordon C, Marhic C, Chauvet O, Maser WK *Nanotechnol.* **2003**, *14*, 691-695.

149. Li Y, Zhang X, Luo J, Huang W, Cheng J, Luo Z, Li T, Liu F, Xu G, Ke X, Li L, Geise HJ *Nanotechnol.* **2004**, *15*, 1645-1649.

150. Shen K, Xu H, Jiang Y, Pietraß T *Carbon* **2004**, *42*, 2315-2322.

151. Vivekchand SRC, Govindaraj A, Seikh MM, Rao CNR *J. Phys. Chem. B* **2004**, *108*, 6935-6937.

152. Johnston DE, Islam MF, Yodh AG, Johnson AT *Nature Mater.* **2005**, *4*, 589-592.

153. Wang Y, Gao L, Sun J, Liu Y, Zheng S, Kajiura H, Li Y, Noda K *Chem. Phys. Lett.* **2006**, *432*, 205-209.

154. Wang Y, Liu Y-Q, Wei D-C, Cao L-C, Fu L, Li X-L, Kajiura H, Li Y-M, Noda K *J. Mater. Chem.* **2007**, *17*, 357-363.

155. Porro S, Musso S, Vinante M, Vanzetti L, Anderle M, Trotta F, Tagliaferro A *Physica E* **2007**, *37*, 58-61.

156. Hiura H, Ebbesen TW, Tanigaki K *Adv. Mater.* **1995**, *7*, 275-276.

157. Colomer J-F, Piedigrosso P, Fonseca A, Nagy JB *Synth. Met.* **1999**, *103*, 2482-2483.

158. Aitchison TJ, Ginic-Markovic M, Matisons JG, Simon GP, Fredericks PM *J. Phys. Chem. C* **2007**, *111*, 2440-2446.

159. Zhao X, Ohkohchi M, Inoue S, Suzuki T, Kadoya T, Ando Y *Diamond Related Mater.* **2006**, *15*, 1098-1102.

160. Montoro LM, Rosolen JM *Carbon* **2006**, *44*, 3293-3301.

161. Suzuki T, Suhama K, Zhao X, Inoue S, Nishikawa N, Ando Y *Diamond Related Mater.* **2007**, *16*, 1116-1120.

162. Wang Y, Shan H, Hauge RH, Pasquali M, Smalley RE *J. Phys. Chem. B* **2007**, *111*, 1249-1252.

163. Chen J, Hamon MA, Hu H, Chen Y, Rao AM, Eklund PC, Haddon RC *Science* **1998**, *282*, 95-98.

164. Hamon MA, Chen J, Hu H, Chen Y, Itkis ME, Rao AM, Eklund PC, Haddon RC *Adv. Mater.* **1999**, *11*, 834-840.

165. Mawhinney DB, Naumenko V, Kuznetsova A, Yates Jr. JT *J. Am. Chem. Soc.* **2000**, *122*, 2383-2384.

166. Hamon MA, Hui H, Bhowmik P, Itkis HME, Haddon RC *Appl. Phys. A* **2002**, *74*, 333-338.

167. Gao J, Zhao B, Itkis ME, Bekyarova E, Hu H, Kranak V, Yu A, Haddon RC *J. Am. Chem. Soc.* **2006**, *128*, 7492-7496.

168. Banerjee S, Wong SS *J. Phys. Chem. B* **2002**, *106*, 12144-12151.

169. Riggs JE, Guo Z, Carroll DL, Sun Y-P *J. Am. Chem. Soc.* **2000**, *122*, 5879-5880.

170. Sun Y-P, Huang W, Lin Y, Fu K, Kitaygorodskiy A, Riddle LA, Yu YJ, Carroll DL *Chem. Mater.* **2001**, *13*, 2864-2869.

171. Huang W, Taylor S, Fu K, Lin Y, Zhang D, Hanks TW, Rao AM, Sun Y-P *Nano Lett.* **2002**, *2*, 311-314.

172. Jiang K, Schadler LS, Siegel RW, Zhang X, Zhang H, Terrones M *J. Mater. Chem.* **2004**, *14*, 37-39.

173. Peng H, Alemany LB, Margrave JL, Khabasheshku *J. Am. Chem. Soc.* **2003**, *125*, 15174-15182.

174. Sano M, Kamino A, Okamura J, Shinkai S *Langmuir* **2001**, *17*, 5125-5128.

175. Pompeo F, Resasco DE *Nano Lett.* **2002**, *2*, 369-372.

176. Zhang Y-B, Kanungo M, Ho AJ, Freimuth P, van der Lelie D, Chen M, Khamis SM, Datta SS, Johnson ATC, Misewich JA, Wong SS *Nano Lett.* **2007**, *7*, 3086-3091.

177. Li C, Curreli M, Lin H, Lei B, Ishikawa FN, Datar R, Cote RJ, Thompson ME, Zhou C *J. Am. Chem. Soc.* **2005**, *127*, 12484-12485.

178. Coleman KS, Chakraborty AK, Bailey SR, Sloan J, Alexander M *Chem. Mater.* **2007**, *19*, 1076-1081.

179. Lagow RJ, Badachhape RB, Wood JL, Margrave JL *J. Chem. Soc., Dalton Trans.* **1974**, *12*, 1268-1273.

180. Holloway JH, Hope EG, Taylor R, Langley GJ, Avent AG, Dennis TJ, Hare JP, Kroto HW, Walton DRM *J. Chem. Soc., Chem. Commun.* **1991**, 966-969.

181. Hamwi A, Alvergnat H, Bonnamy S, Béguin F *Carbon* **1997**, *35*, 723-728.

182. Mickelson ET, Huffman CB, Rinzler AG, Smalley RE, Hauge RH, Margrave JL *Chem. Phys. Lett.* **1998**, *296*, 188-194.

183. Zhao W, Song C, Zheng B, Liu J, Viswanathan T *J. Phys. Chem. B* **2002**, *106*, 293-296.

184. Pehrsson PE, Zhao W, Baldwin JW, Song C, Liu J, Kooi S, Zheng B *J. Phys. Chem. B* **2003**, *107*, 5690-5695.

185. Mickelson ET, Chiang IW, Zimmerman JL, Boul PJ, Lozano J, Liu J, Smalley RE, Hauge RH, Margrave JL *J. Phys. Chem. B* **1999**, *103*, 4318-4322.

186. Geng H, Rosen R, Zheng B, Shimoda H, Fleming L, Liu J, Zhou O *Adv. Mater.* **2002**, *14*, 1387-1390.

187. Boul PJ, Liu J, Mickelson ET, Huffman CB, Ericson LM, Chiang IW, Smith KA, Colbert DT, Hauge RH, Margrave JL, Smalley RE *Chem. Phys. Lett.* **1999**, *310*, 367-372.

188. Stevens JL, Huang AY, Peng H, Chiang IW, Khabasheshku VN, Margrave JL *Nano Lett.* **2003**, *3*, 331-336.

189. Peng H, Reverdy P, Khabasheshku VN, Margrave JL *Chem. Commun.* **2003**, 362-363.

190. Plank NOV, Jiang L, Cheung R *Appl. Phys. Lett.* **2003**, *83*, 2426-2428.

191. Plank NOV, Forrest GA, Cheung R, Alexander AJ *J. Phys. Chem. B* **2005**, *109*, 22096-22101.

192. Bahr JL, Yang J, Kosynkin DV, Bronikowski MJ, Smalley RE, Tour JM *J. Am. Chem. Soc.* **2001**, *123*, 6536-6542.

193. Bahr JL, Tour JM *Chem. Mater.* **2001**, *13*, 3823-3824.

194. Dyke CA, Tour JM *Nano Lett.* **2003**, *3*, 1215-1218.

195. Strano MS, Dyke CA, Usrey ML, Barone PW, Allen MJ, Shan H, Kittrell C, Hauge RH, Tour JM, Smalley RE *Science* **2003**, *301*, 1519-1522.

196. Strano MS *J. Am. Chem. Soc.* **2003**, *125*, 16148-16153.

197. Kim W-J, Usrey ML, Strano MS *Chem. Mater.* **2007**, *19*, 1571-1576.

198. Ying Y, Saini RK, Liang F, Sadana AK, Billups WE *Org. Lett.* **2003**, *5*, 1471-1473.

199. Holzinger M, Vostrowsky O, Hirsch A, Hennrich F, Kappes M, Weiss R, Jellen F *Angew. Chem. Int. Ed.* **2001**, *40*, 4002-4005.

200. Plank NOV, Cheung R, Andrews RJ *Appl. Phys. Lett.* **2004**, *85*, 3229-3231.

201. Shaffer MSP, Koziol K *Chem. Commun.* **2002**, 2074-2075.

202. Sung JH, Kim HS, Jin H-J, Choi HJ, Chin I-J *Macromol.* **2004**, *37*, 9899-9902.

203. Qin S, Qin D, Ford WT, Herrera JE, Resasco DE *Macromol.* **2004**, *37*, 9963-9967.

204. Hu H, Zhao B, Hamon MA, Kamaras K, Itkis ME, Haddon RC *J. Am. Chem. Soc.* **2003**, *125*, 14893-14900.

205. Holzinger M, Abraham J, Whelan P, Graupner R, Ley L, Hennrich F, Kappes M, Hirsch A *J. Am. Chem. Soc.* **2003**, *125*, 8566-8580.

206. Holzinger M, Steinmetz J, Samaille D, Glerup M, Paillet M, Bernier P, Ley L, Graupner R *Carbon* **2004**, *42*, 941-947.

207. Maggini M, Scorrano G, Prato M *J. Am. Chem. Soc.* **1993**, *115*, 9798-9799.

208. Georgakilas V, Kordatos K, Prato M, Guldi DM, Holzinger M, Hirsch A *J. Am. Chem. Soc.* **2002**, *124*, 760-761.

209. Tagmatarchis N, Prato M *J. Mater. Chem.* **2004**, *14*, 437-439.

210. Georgakilas V, Tagmatarchis N, Pantarotto D, Bianco A, Briand J-P, Prato M *Chem. Commun.* **2002**, 3050-3051.

211. Camps X, Hirsch A *J. Chem. Soc., Perkin Trans. 1* **1997**, 1595-1596 and references therein.

212. Coleman KS, Bailey SR, Fogden S, Green MLH *J. Am. Chem. Soc.* **2003**, *125*, 8722-8723.

213. Haufler RE, Conceicao J, Chibante LPF, Chai Y, Byrne NE, Flanagan S, Haley MM, O'Brien SC, Pan C, Xiao Z, Billups WE, Ciufolini MA, Hauge RH, Margrave JL, Wilson LJ, Curl RF, Smalley RE *J. Phys. Chem.* **1990**, *94*, 8634-8636.

214. Pekker S, Salvetat J-P, Jakab E, Bonard J-M, Forró L *J. Phys. Chem. B* **2001**, *105*, 7938-7943.

215. Bergbrieter DE, Killough JM *J. Am. Chem. Soc.* **1978**, *100*, 2126-2134.

216. Buffinger DR, Zieberth RP, Stenger VR, Recchia C, Pennington CH *J. Am. Chem. Soc.* **1993**, *115*, 9267-9270.

217. Bower C, Suzuki S, Tanigaki K, Zhou O *Appl. Phys. A* **1998**, *67*, 47-52.

218. Liang F, Sadana AK, Peera A, Chattopadhyay J, Gu Z, Hauge RH, Billups WE *Nano Lett.* **2004**, *4*, 1257-1260.

219. Chattopadhyay J, Sadana AK, Liang F, Beach JM, Xiao Y, Hauge RH, Billups WE *Org. Lett.* **2005**, *7*, 4067-4069.

220. Liang F, Alemany LB, Beach JM, Billups WE *J. Am. Chem. Soc.* **2005**, *127*, 13941-13948.

221. Pénicaud A, Poulin P, Derré A, Anglaret E, Petit P *J. Am. Chem. Soc.* **2005**, *127*, 8-9.

222. Hirsch A, Soi A, Karfunkel HR *Angew. Chem. Int. Ed. Eng.* **1992**, *31*, 766-768.

223. Fagan PJ, Krusic PJ, Evans DH, Lerke SA, Johnston E *J. Am. Chem. Soc.* **1992**, *114*, 9697-9699.

224. Viswanathan G, Chakrapani N, Yang H, Wei B, Chung H, Cho K, Ryu CY, Ajayan PM *J. Am. Chem. Soc.* **2003**, *125*, 9258-9259.

225. Blake R, Gun'ko YK, Coleman J, Cadek M, Fonseca A, Nagy JB, Blau WJ *J. Am. Chem. Soc.* **2004**, *126*, 10226-10227.

226. Graupner R, Abraham J, Wunderlich D, Vencelová A, Lauffer P, Röhrl J, Hundhausen M, Ley L, Hirsch A *J. Am. Chem. Soc.* **2006**, *128*, 6683-6689.

227. Rao AM, Richter E, Bandow S, Chase B, Eklund PC, Williams KA, Fang S, Subbaswamy KR, Menon M, Thess A, Smalley RE, Dresselhaus G, Dresselhaus MS *Science* **1997**, *275*, 187-191.

228. Choi N, Kimura M, Kataura H, Suzuki S, Achiba Y, Mizutani W, Tokumoto H *Japan. J. Appl. Phys.* **2002**, *41*, 6264-6266.

229. Ajayan PM, Iijima S *Nature* **1993**, *361*, 333-334.

230. Ajayan PM, Ebbsen TW, Ichihashi T, Iijima S, Tanigaki K, Hiura H *Nature* **1993**, *362*, 522-525.

231. Tsang SC, Chen YK, Harris PJF, Green MLH *Nature* **1994**, *372*, 159-162.

232. Sloan J, Hammer J, Zwiefka-Sibley M, Green MLH *Chem. Commun.* **1998**, 347-348.

233. Ajayan PM, Stephan O, Redlich Ph., Colliex C *Nature* **1995**, *375*, 564-567.

234. Chen YK, Green MLH, Tsang SC *Chem. Commun.* **1996**, 2489-2490.

235. Sloan J, Wright DM, Woo H-G, Bailey S, Brown G, York APE, Coleman KS, Hutchison JL, Green MLH *Chem. Commun.* **1999**, 699-700.

236. Sloan J, Grosvenor SJ, Friedrichs S, Kirkland AI, Hutchison JL, Green MLH *Angew. Chem. Int. Ed.* **2002**, *41*, 1156-1159.

237. Sloan J, Terrones M, Nufer S, Friedrichs S, Bailey SR, Woo H-G, Rühle M, Hutchison JL, Green MLH *J. Am. Chem. Soc.* **2002**, *124*, 2116-2117.

238. Sloan J, Kirkland AI, Hutchison JL, Green MLH *Chem. Commun.* **2002**, 1319-1332.

239. Smith BW, Monthioux M, Luzzi DE *Nature* **1998**, *396*, 323-324.

240. Smith BW, Luzzi DE *Chem. Phys. Lett.* **2000**, *321*, 169-174.

241. Hirahara K, Suenaga K, Bandow S, Kato H, Okazaki T, Shinohara H, Iijima S *Phys. Rev. Lett.* **2000**, *85*, 5384-5387.

242. Britz DA, Khlobystov AN, Wang J, O'Neil AS, Poliakoff M, Ardavan A, Briggs GAD *Chem. Commun.* **2004**, 176-177.

243. Chamberlain TW, Camenisch A, Champness NR, Briggs GAD, Benjamin SC, Ardavan A, Khlobystov AN *J. Am. Chem. Soc.* **2007**, *129*, 8609-8614.

244. Britz DA, Khlobystov AN, Porfyrakis K, Ardavan A, Briggs GAD *Chem. Commun.* **2005**, 37-39.

245. Tsang SC, Davis JJ, Green MLH, Hill HAO, Leung YC, Sadler PJ *J. Chem. Soc., Chem. Commun.* **1995**, 1803-1804.

246. Davis JJ, Green MLH, Hill HAO, Leung YC, Sadler PJ, Sloan J, Xavier AV, Tsang SC *Inorg. Chim. Acta* **1998**, *272*, 261-266.

247. Monthioux M *Carbon* **2002**, *40*, 1809-1823.

248. Monthioux M, Smith BW, Burteaux B, Claye A, Fischer JE, Luzzi DE *Carbon* **2001**, *39*, 1251-1272.

249. Liu Y, Wang Y, Liu Y, Li W, Zhou W, Wei F *Nanotechnol.* **2007**, *18*, 175704.

250. Yu A, Bekyarova E, Itkis ME, Fakhrutdinov D, Webster R, Haddon RC *J. Am. Chem. Soc.* **2006**, *128*, 9902-9908.

251. Takahashi T, Tsunoda K, Yajima H, Ishii T *Japan. J. Appl. Phys.* **2004**, *43*, 1227-1230.

252. Zhao X, Inoue S, Jinno M, Suzuki T, Ando Y *Chem. Phys. Lett.* **2003**, *373*, 266-271.

253. Harutyunyan AR, Pradhan BK, Chang J, Chen G, Eklund PC *J. Phys. Chem. B* **2002**, *106*, 8671-8675.

254. Kim Y, Luzzi DE *J. Phys. Chem. B* **2005**, *109*, 16636-16643.

255. Takahashi T, Tsunoda K, Yajima H, Ishii T *Jap. J. Appl. Phys.* **2004**, *43*, 3636-3639.

256. Zhang H, Sun CH, Li F, Li HX, Cheng HM *J. Phys. Chem. B* **2006**, *110*, 9477-9481.

257. Thiên-Nga L, Hernadi K, Ljubović E, Garaj S, Fórró L *Nano Lett.* **2002**, *2*, 1349-1352.

258. Fang H-T, Liu C-G, Liu C, Li F, Liu M, Cheng H-M *Chem. Mater.* **2004**, *16*, 5744-5750.

259. Chen C-M, Chen M, Peng Y-W, Yu H-W, Chen C-F *Thin Solid Films* **2006**, *498*, 202-205.

260. Basiuk EV, Basiuk VA, Bañuelos J-G, Saniger-Blesa JM, Pokrovskiy VA, Gromovoy TY, Mischanchuk AV, Mischanchuk BG *J. Phys. Chem. B* **2002**, *106*, 1588-1597.

261. Hu H, Zhao B, Itkis ME, Haddon RC *J. Phys. Chem. B* **2003**, *107*, 13838-13842.

262. Zhang J, Zou H, Qing Q, Yang Y, Li Q, Liu Z, Guo X, Du Z *J. Phys. Chem. B* **2003**, *107*, 3712-3718.

263. Verdejo R, Lamoriniere S, Cottam B, Bismarck A, Shaffer M *Chem. Commun.* **2007**, 513-515.

264. Salzmann CG, Llewellyn SA, Tobias G, Ward MAH, Huh Y, Green MLH *Adv. Mater.* **2007**, *19*, 883-887.

265. Martinez MT, Callejas MA, Benito AM, Cochet M, Seeger T, Anson A, Schreiber J, Gordon C, Marhic C, Chauvet O, Fierro JLG, Maser WK *Carbon* **2003**, *41*, 2247-2256.

266. Hamon MA, Itkis ME, Niyogi S, Alvaraez T, Kuper C, Menon M, Haddon RC *J. Am. Chem. Soc* **2001**, *123*, 11292-11293.

267. Kuznetsova A, Mawhinney DB, Naumenko V, Yates Jr. JT, Liu J, Smalley RE *Chem. Phys. Lett.* **2000**, *321*, 292-296.

268. Li J, Zhang Y *Physica E* **2005**, *28*, 309-312.

269. Yudasaka M, Zhang M, Jabs C, Iijima S *Appl. Phys. A* **2000**, *71*, 449-451.

270. Murphy R, Coleman JN, Cadek M, McCarthy B, Bent M, Drury A, Barklie RC, Blau WJ *J. Phys. Chem. B* **2002**, *106*, 3087-3091.

271. Huang X, Mclean RS, Zheng M *Anal. Chem.* **2005**, *77*, 6225-6228.

272. Bonard J-M, Stora T, Salvetat J-P, Maier F, Stöckli T, Duschl C, Forró L, de Heer WA, Châtelain A *Adv. Mater.* **1997**, *9*, 827-831.

273. Yamamoto K, Akita S, Nakayama Y *Jpn. J. Appl. Phys.* **1996**, *35*, L917-L918.

274. Bubke K, Gnewuch H, Hempstead M, Hammer J, Green MLH *Appl. Phys. Lett.* **1997**, *71*, 1906-1908.

275. Chen XQ, Saito T, Yamada H, Matsushige K *Appl. Phys. Lett.* **2001**, *78*, 3714-3716.

276. Liu X, Spencer JL, Kaiser AB, Arnold WM *Curr. Appl. Phys.* **2006**, *6*, 427-431.

277. Yamamoto K, Akita S, Nakayama Y *J. Phys. D: Appl. Phys.* **1998**, *31*, L34-L36.

278. Duesberg GS, Muster J, Krstic V, Burghard M, Roth S *Appl. Phys. A* **1998**, *67*, 117-119.

279. Duesberg GS, Blau W, Byrne HJ, Muster J, Burghard M, Roth S *Synth. Met.* **1999**, *103*, 2484-2485.

280. Yang Y, Xie L, Chen Z, Liu M, Zhu T, Liu Z *Synth. Met.* **2005**, *155*, 455-460.

281. Niyogi S, Hu H, Hamon MA, Bhowmik P, Zhao B, Rozenzhak SM, Chen J, Itkis ME, Meier MS, Haddon RC *J. Am. Chem. Soc.* **2001**, *123*, 733-734.

282. Xu X, Ray R, Gu Y, Ploehn HJ, Gearheart L, Raker K, Scrivens WA *J. Am. Chem. Soc.* **2004**, *126*, 12736-12737.

283. Zhao B, Hu H, Niyogi S, Itkis ME, Hamon MA, Bhowmik P, Meier MS, Haddon RC *J. Am. Chem. Soc.* **2001**, *123*, 11673-11677.

284. Holzinger M, Hirsch A, Bernier P, Duesberg GS, Burghard M *Appl. Phys A* **2000**, *70*, 599-602.

285. Bai X, Li D, Du D, Zhang H, Chen L, Liang J *Carbon* **2004**, *42*, 2113-2130.

286. Huang SM, Dai LM *J. Phys. Chem. B* **2002**, *106*, 3543-3545.

287. Zheng B, Li Y, Liu J *Appl. Phys. A* **2002**, *74*, 345-348.

288. Igarashi H, Murakami H, Murakami Y, Maruyama S, Nakashima N *Chem. Phys. Lett.* **2004**, *392*, 529-532.

289. Raymundo-Piñero E, Cacciaguerra T, Simon P, Béguin F *Chem. Phys. Lett.* **2005**, *412*, 184-189.

290. Engel-Herbert R, Pforte P, Hesjedal T *Mater. Lett.* **2007**, *61*, 2589-2593.

291. Okubo S, Sekine T, Suzuki S, Achiba Y, Tsukagoshi K, Aoyagi Y, Kataura H, *Jap. J. Appl. Phys.* **2004**, *43*, L396.

292. Ramesh P, Okazaki T, Sugai T, Kimura J, Kishi N, Sato K, Ozeki Y, Shinohara H *Chem. Phys. Lett.* **2006**, *418*, 408-412.

293. Bandow S, Asaka S, Zhao X, Ando Y *Appl. Phys. A* **1998**, *67*, 23-27.

294. Li F, Cheng HM, Xing YT, Tan PH, Su G *Carbon* **2000**, *38*, 2041-2045.

295. Ebbesen TW, Ajayan PM, Hiura H, Tanigaki K *Nature* **1994**, *367*, 519.

296. Shi Z, Lian Y, Liao F, Zhou X, Gu Z, Zhang Y, Iijima S *Solid State Commun.* **1999**, *112*, 35-37.

297. Moon J-M, An KH, Lee YH, Park YS, Bae DJ, Park G-S *J. Phys. Chem. B* **2001**, *105*, 5677-5681.

298. Ohkohchi M, Zhao X, Inoue S, Ando Y *Japan. J. Appl. Phys.* **2004**, *43*, 8365-8368.

299. Ando Y, Zhao X, Inoue S, Suzuki T, Kadoya T *Diamond Related Mater.* **2005**, *14*, 729-732.

300. Xu Y-Q, Peng H, Hauge RH, Smalley RE *Nano Lett.* **2005**, *5*, 163-168.

301. Chiang IW, Brinson BE, Smalley RE, Margrave JL, Hauge RH *J. Phys. Chem. B* **2001**, *105*, 1157-1161.

302. Strong KL, Anderson DP, Lafdi K, Kuhn JN *Carbon* **2003**, *41*, 1477-1488.

303. Vázquez E, Georgakilas V, Prato M *Chem. Commun.* **2002**, 2308-2309.

304. Dailly A, Yim JWL, Ahn CC, Miura E, Yazami R, Fultz B *Appl. Phys. A* **2005**, *80*, 717-722.

305. Tran NE, Lambrakos SG *Nanotechnol.* **2005**, *16*, 639-646.

306. Huang W, Wang Y, Luo G, Wei F *Carbon* **2003**, *41*, 2585-2590.

307. Mathur RB, Seth S, Lal C, Rao R, Singh BP, Dhami TL, Rao AM *Carbon* **2007**, *45*, 132-140.

308. Min Y-S, Bae EJ, Park W *J. Am. Chem. Soc.* **2005**, *127*, 8300-8301.

309. Mizoguti E, Nihey F, Yudasaka M, Iijima S, Ichihashi T, Nakamura K *Chem. Phys. Lett.* **2000**, *321*, 297-301.

310. Martínez MT, Callejas MA, Benito AM, Maser WK, Cochet M, Andrés JM, Schreiber J, Chauvet O, Fierro JLG *Chem. Commun.* **2002**, 1000-1001.

311. Chen C-M, Chen M, Leu F-C, Hsu S-Y, Wang S-C, Shi S-C, Chen C-F *Diamond Related Mater.* **2004**, *13*, 1182-1186.

312. Ko C-J, Lee C-Y, Ko F-H, Chen H-L, Chu T-C *Microelectron. Eng.* **2004**, *73-74*, 570-577.

313. Ko F-H, Lee C-Y, Ko C-J, Chu T-C *Carbon* **2005**, *43*, 727-733.

314. Chen C-M, Chen M, Peng Y-W, Lin C-H, Chang L-W, Chen C-F *Diamond Related Mater.* **2005**, *14*, 798-803.

315. Tobias G, Shao L, Salzmann CG, Huh Y, Green MLH *J. Phys. Chem. B* **2006**, *110*, 22318-22322.

316. Hata K, Futaba DN, Mizuno K, Namai T, Yumura M, Iijima S *Science* **2004**, *306*, 1362-1364.

317. Zhu L, Xiu Y, Hess DW, Wong C-P *Nano Lett.* **2005**, *5*, 2641-2645.

318. Ikazaki F, Ohshima S, Uchida K, Kuriki Y, Hayakawa H, Yumura M, Takahashi K, Tojima K *Carbon* **1994**, *32*, 1539-1542.

319. Hou PX, Bai S, Yang QH, Liu C, Cheng HM *Carbon* **2002**, *40*, 81-85.

320. Fan Y-Y, Kaufman A, Mukasyan A, Varma A *Carbon* **2006**, *44*, 2160-2170.

321. Chen YK, Green MLH, Griffin JL, Hammer J, Lago RM, Tsang SC *Adv. Mater.* **1996**, *8*, 1012-1015.

322. Skowroński JM, Scharff P, Pfänder N, Cui S *Adv. Mater.* **2003**, *15*, 55-57.

323. Bulusheva LG, Okotrub AV, Dettlaff-Weglikowska U, Roth S, Heggie MI *Carbon* **2004**, *42*, 1095-1098.

324. Kuznetsova A, Yates Jr. JT, Liu J, Smalley RE *J. Chem. Phys.* **2000**, *112*, 9590-9598.

325. Unger E, Graham A, Kreupl F, Liebau M, Hoenlein W *Curr. Appl. Phys.* **2002**, *2*, 107-111.

326. Yang Y, Zou H, Wu B, Li Q, Zhang J, Liu Z, Guo X, Du Z *J. Phys. Chem. B* **2002**, *106*, 7160-7162.

327. Nagasawa S, Yudasaka M, Hirahara K, Ichihashi T, Iijima S *Chem. Phys. Lett.* **2000**, *328*, 374-380.

328. Wiltshire JG, Khlobystov AN, Li LJ, Lyapin SG, Briggs GAD, Nicholas RJ *Chem. Phys. Lett.* **2004**, *386*, 239-243.

329. Shen K, Curran S, Xu H, Rogelj S, Jiang Y, Dewald J, Pietrass T *J. Phys. Chem. B* **2005**, *109*, 4455-4463.

330. Chattopadhyay D, Galeska I, Papadimitrakopoulos F *Carbon* **2002**, *40*, 985-988.

331. Geng HZ, Zhang XB, Mao SH, Kleinhammes A, Shimoda H, Wu Y, Zhou O *Chem. Phys. Lett.* **2004**, *399*, 109-113.

332. Shao L, Tobias G, Huh Y, Green MLH *Carbon* **2006**, *44*, 2855-2858.

333. Andrews R, Jacques D, Qian D, Dickey EC *Carbon* **2001**, *39*, 1681-1687.

334. Yudasaka M, Ichihashi T, Kasuya D, Kataura H, Iijima S *Carbon* **2003**, *41*, 1273-1280.

335. Métérnier K, Bonnamy S, Béguin F, Journet C, Bernier P, Lamy de la Chapelle M, Chauvet O, Lefrant S *Carbon* **2002**, *40*, 1765-1773.

336. Terrones M, Terrones H, Banhart F, Charlier J-C, Ajayan PM *Science* **2000**, *288*, 1226-1229.

337. Kong J, Dai H *J. Phys. Chem. B* **2001**, *105*, 2890-2893.

338. Chattopadhyay D, Galeska I, Papadimitrakopoulos F *J. Am. Chem. Soc.* **2003**, *125*, 3370-3375.

339. Basiuk EV, Monroy-Peláez M, Punte-Lee I, Basiuk VA *Nano Lett.* **2004**, *4*, 863-866.

340. Hoste S, van de Vandel DF, van der Kelen GP *J. Electron. Spectrosc. Relat. Phenom.* **1979**, *17*, 191-195.

341. Moulder JF, Stickle WF, Soble PE, Bomben KD *Handbook of X-ray Photoelectron Spectroscopy*, Physical Electronics Inc.: Minnesota, USA, 1995.

342. Dresselhaus MS, Eklund PC *Advances in Physics* **2000**, *49*, 705-814.

343. Zhou C, Kong J, Dai H *Appl. Phys. Lett.* **2000**, *76*, 1597-1599.

344. Derycke V, Martel R, Appenzeller J, Avouris Ph. *Nano Lett.* **2001**, *1*, 453-456.

345. Derycke V, Martel R, Appenzeller J, Avouris Ph. *Appl. Phys. Lett.* **2002**, *80*, 2773-2775.

346. Itkis ME *et al. Nano Lett.* **2002**, *2*, 155-159.

347. Collins PG, Bradley K, Ishigami M, Zettl A *Science* **2000**, *287*, 1801-1804.

348. Chen J, Rao AM, Lyuksyutov S, Itkis ME, Hamon MA, Hu H, Cohn RW, Eklund PC, Colbert DT, Smalley RE, Haddon RC *J. Phys. Chem. B* **2001**, *105*, 2525-2528.

349. Hirsch A, Li Q, Wudl F *Angew. Chem. Int. Ed. Eng.* **1991**, *30*, 1309-1310.

350. Heald CGR, Wildgoose GG, Jiang L, Jones TGJ, Compton RG *ChemPhysChem* **2004**, *5*, 1794-1799.

351. Wildgoose GG, Wilkins SJ, Williams GR, France RR, Carnahan DL, Jiang L, Jones TGJ, Compton RG *ChemPhysChem* **2005**, *6*, 352-362.

352. Brown SDM, Jorio A, Corio P, Dresselhaus MS, Dresselhaus G, Saito R, Kneipp K *Phys. Rev. B* **2001**, *63*, 155414.

353. Cornforth RH, Cornforth JW, Popjak G *Tetrahedron* **1962**, *18*, 1351-1354.; Corey EJ, Suggs W *Tetrahedron Lett.* **1975**, *16*, 2647-2650.

354. Olah GA, Arvanaghi M *Angew. Chem. Int. Ed. Engl.* **1981**, *20*, 878-879.

355. Bandow S, Asaka S, Saito Y, Rao AM, Grigorian L, Richter E, Eklund PC *Phys. Rev. Lett.* **1998**, *80*, 3779-3782.

356. Suri A, Chakraborty AK, Coleman KS *Chem. Mater.* (accepted).